FRONTS IN THE ATMOSPHERE

LECTURE ONE - Historical perspective

1. Introduction

In the context of this series of lectures on the topic of "Fronts in the atmosphere", the term "front" refers to a narrow (sloping) zone of transition between two air masses of differing properties, the gradient of properties across the front being much greater than the gradients within each air mass. In association with this zone of transition there generally exists a vertical circulation (essentially in the vertical plane perpendicular to the front) which not only determines the weather accompanying the front but which is also an essential factor in the development of the front and its maintenance against dissipative effects.

The series of lectures of which this is the first will deal mainly with frontal systems associated with synoptic-scale mid-latitude depressions, but other atmospheric features which assume the dynamical characteristics of fronts referred to above, such as sea breeze fronts and squall lines, are also covered.

Attempts to predict the weather, albeit for very short periods ahead, by making use of current observations (either from a single location or from a network of sites) allied with some methodology superior to pure folk-lore, can be traced back to the late 18th century; a "potted history" of some important events in the development of the understanding of atmospheric processes is included, in a necessarily abbreviated form, in section 2. The interested reader is referred to Bergeron's (1959) fascinating historical critique for a much more complete and learned account. In many ways the history reads like a catalogue of missed opportunities with only painfully slow progress being made during the latter half of the 19th century, despite the occasional contributions of far-sighted individuals with ideas well ahead of their time, ideas which failed all too frequently to be capitalised on. The most significant progress had to await the valuable work of the Bergen School during the years immediately following World War I. This work, mainly involving the painstakingly detailed analysis of as dense a network of surface observations as possible together with a very limited number of upper air soundings, led to the emergence of the Polar Front Theory and ideas on the life cycle of depressions, clearly a turning point in the development of the science of meteorology. The resumé in Section 2 covers the period from the beginning of the 19th century up to about 1950. On the apparent lack of progress in the development of weather forecasting, particularly during the second half of the 19th century, Bergeron (1959) comments wryly "progress is impeded by want of meteorological knowledge on the part of theoreticians and by too poor mathematical training of weather men".

2. Important historical events

The dates in parentheses, following the names of various individuals, usually refer to the year in which their major work appeared in published form.

Brandes (1820). He formalised his proposed method, the so-called "synoptic" method of analysing weather observations and subsequently attempting to predict the weather sequence for a short time ahead. The synoptic method, which was to persist basically unchanged for many decades, relied essentially on the apparent association of clouds and precipitation with centres of low pressure. The concept of air masses

found no place in the "structure models" of depressions and their associated weather.

Howard (1820, 1833). In his publications on "Climate of London" he gave striking descriptions of weather situations and developments in terms of cold and warm air masses alternatingly moving across the observation site at the surface and aloft.

Dove (1837). His early ideas contained the gist of the concept of air masses and the association of active weather systems with air mass boundaries. In later years he failed to capitalise on his early ideas, in the face of the increasingly entrenched synoptic method.

Espy (1841) was largely responsible for the so-called "convectional" hypothesis of cyclones. From the association of depressions with precipitation it was inferred that low-pressure centres comprised regions of ascending motion. Cyclones were regarded as heat engines driven by the supposedly warm ascending air in their centres, the heat being derived from the release of latent heat of condensation; heating and vertical expansion led to a raising of the upper isobaric surfaces in the central portion causing a lateral outflow aloft, and, with the removal of air from the central column, a pressure fall occurred at low levels resulting in an inrush of air down the pressure gradient. Espy attached no significance to the rotation of air currents, although this was known at the time.

Ferrel (1856) introduced the idea that the circulation of air around cyclones was due to the deflection of currents approaching the low-pressure centre, induced by the earth's rotation. Coriolis, in his earlier general treatment of this problem, did not mention its application to the atmosphere.

Buys Ballot (1857) formulated the rule that "winds always blow, in the northern hemisphere, with high pressure to the right and low pressure to the left of the direction in which they blow".

Fitz Roy (1863). First Chief of Meteorological Office, London, presented a strikingly realistic picture of the structure of surface air currents in extra tropical depressions and anticyclones (Fig 1). Unfortunately he died shortly afterwards in 1865. Essentially Fitz Roy's model incorporated the recognition that depressions form at the zone of interaction of air masses having different properties, originating in subtropical or polar regions. His contribution to meteorology had relatively little influence on practising meteorologists in succeeding decades, partly due to the lack of routine observations necessary for day to day analysis.

Sir Francis Galton (1863). A cousin of Charles Darwin, his work "Meteorographica" contains 3 European maps a day for the month of December 1861 with pictorial symbols for the winds and main hydrometeors; temperature, wet bulb depression and pressure were also included (he based his analyses on about 300 reporting stations in northwest Europe). Galton unfortunately relinquished active work in meteorology in 1870 and his extensive attempts to understand the weather by the detailed analysis of all available observations were not followed up. It was to be another 40 years or so before anybody in Europe took the trouble to perform synoptic analysis work of similar intensity, although attempts to predict weather sequences using the "synoptic" method based on relatively few observations and inadequate structure models persisted. In the 1860s the Meteorological Office, London supplied seven Observatories in the British Isles with automatic recording instruments (meteorograms) for pressure, temperature, humidity (indirectly), precipitation and wind (Fig 2). The data recorded appeared regularly in every

detail in the Quarterly Weather Report of the Meteorological Office (London) from 1869 to 1880 (see Fig 3). The series terminated due apparently to the lack of comprehension of its great value, and, probably, to lack of funds and personnel.

Blasius (1875), Helmholtz (1888, 1889), Bigelow (1904). All contributed notably to the understanding of the evolution of weather systems, recognising in particular the importance of enhanced horizontal temperature gradients to the development of cyclones.

Abercromby (1887). Attempted to stress the great value of the type of data routinely collected using meteorograms (with continuous traces) in supplementing the limited information available for constructing synoptic maps. In particular he pointed out that the nature of apparent discontinuities ("troughs" in particular) could be better understood through the use of continuous traces. However he failed in subsequent years to follow up these ideas.

Koppen (1879, 1882, 1914), Durand-Gréville (1892). Koppen had seen indications of what we now call the cold front and eventually came to the conclusion that it consisted of a cold-air wedge invading warmer air, but he gave it a very modest depth (600 m). Durand-Gréville undertook some detailed synoptic analyses in which he demonstrated the progress across northwest Europe of discontinuities in the surface wind field. Fig 4 shows the progress of a "ligne de grain" or "squall line", identified by Durand-Gréville (with the assistance of barogram traces from numerous sites). He was however a synoptic meteorologist with only a vague notion of the dynamics of weather systems and failed to follow up his findings as thoroughly as he might have done. Indeed, the relative stagnation of the study of weather continued into the first decade of the 20th century.

Rotch (1898) Assmann (1900), Teisserenc de Bort (1902). In the last years of the 19th century and the early years of the 20th century, these individuals were responsible, among others, for the first regular investigations of the vertical structure of the atmosphere using instruments attached to balloons and kites. These revealed the general lapse of temperature with height, the existence of inversions and the presence of the near-isothermal layer of the stratosphere (the International Aerological Commission was established in 1900).

Hann (1901). As early as 1875 Hann had criticised the "convectional" theory of Espy, and proposed an alternative dynamical hypothesis in which cyclones and anticyclones originate as eddies in the general strong westerly flow of mid-latitudes, feeding off the energy of the basic current.

Ekholm (1891), V Bjerknes (1898, 1902). The precise formulation of the circulation theorem by V Bjerknes, together with Margules' work on energy transformations provided much of the theoretical background and inspiration for later hypotheses concerning atmospheric disturbances. Apparently V Bjerknes was inspired to applying his circulation theorem to the atmosphere following discussions with Ekholm who had (from 1891) constructed some synoptic maps which included isopycnics.

Margules (1901, 1905) was the first to provide a thorough theoretical analysis which showed that the kinetic energy of disturbances is derived from the available potential energy associated with horizontal temperature contrasts. He also demonstrated that, in a rotating framework, a sloping discontinuity between air masses of different temperature can exist in equilibrium provided that there existed a cyclonic wind shear across the discontinuity. He derived the formula for the equilibrium slope ($\tan\theta$) of a surface of (density) discontinuity:-

$$\tan\theta \approx \frac{f T_m}{g}\left(\frac{v_1 - v_2}{T_2 - T_1}\right)$$

where v_1 and v_2 are the geostrophic wind components parallel to the front, T_1 and T_2 the temperatures in the cold and warm air masses respectively, T_m the mean of T_1 and T_2, f is the Coriolis parameter and g the gravitational acceleration. (Typical slopes of frontal surfaces are about 1 in 100 and generally differ appreciably from the equilibrium values obtained by Margules formula, mainly because the winds in the vicinity of the front are ageostrophic; in addition atmospheric fronts can rarely be considered to be in an "equilibrium" state).

Lempfert and Shaw (1906) demonstrated the way in which air at the surface spirals inward towards depression centres and outward from anticyclones. Back-trajectories of air parcels within the cyclones were found to originate in widely different regions.

Lempfert and Corless (1910). Described wind shifts and temperature contrasts associated with cold fronts which they referred to as "line squalls" or "linear fronts" (see Fig 5); they demonstrated their regular progression by use of isochrone charts (Fig 6), discussing also the cyclonic shift of the geostrophic wind and the character of the associated vertical circulation.

Shaw (1911). Drawing on some results of earlier work (Lempfert and Shaw, 1906), Shaw proposed a simple model of cyclone structure which incorporated some of the essential features of the later Norwegian cyclone models, but in a less definitive form, but again, this work was not properly followed up.

V Bjerknes, Devik and Hesselberg (1910, 1911). Published the two classical volumes: Vol I - Statics (1910) and Vol II - Kinematics (1911). When established at Leipzig in 1913-17 V Bjerknes tried to complete this great undertaking by editing a Vol III - Dynamics, but this was never accomplished, due partly to the outbreak of World War I which scattered the scientists of the Leipzig School.

Dines (1912, 1919, 1925), Schedler (1921). During the early years of the 20th century Dines and Schedler were responsible for an extensive series of upper air observations, and for some very thorough analyses. A result which was considered remarkable by some was the discovery that low pressure centres were, on average, considerably colder aloft (and high pressure centres considerably warmer aloft) than the average of all soundings. It did not become evident until much later that the thermal structure of a cyclone changed quite considerably during its life cycle, and that this variation and the thermal asymmetry of cyclones were both obscured by the statistical methods of analysis of the data. Based on correlations between pressure and temperature at various levels, Dines noted that the relatively low tropospheric temperature of the cyclone and the relatively high temperature of the anticyclone were due to dynamically forced ascent and descent in the respective regions.

J Bjerknes and Solberg (1921). Thorough utilization of all available north-west European weather reports, improvements to the surface observational network in Norway and the application of the method of "indirect aerology" (use of surface reports as clues to conditions aloft) all contributed to the great success of the Bergen School in the years immediately following the First War. The so-called Polar Front Theory became established, in which the importance of fronts and the life cycle of depressions was recognised (see Figs 7 and 8). (Fig 9 shows an early example of one of the Bergen surface analyses, using streamlines). In the course of analysis of depressions, it was realised that these entered the west

coast of Europe in series, often in fairly quick succession, and that the structure of an individual cyclone varied according to its place in the series; from this experience it was deduced that depressions usually occur in "families" (as in Fig 10, for example). Individual depressions were viewed as forming on the Polar Front which separated air masses of polar origin from warmer air masses of subtropical or tropical origin, and moving generally north-eastward while developing according to the sequence in Fig 8; successive depressions then formed on the trailing cold fronts. In the hemispherical context it was recognised that the depressions played a crucial role in the process of heat exchange between tropical and polar regions, necessary to balance the net radiative gain of heat in low latitudes and net loss of heat in high latitudes.

The Norwegian model envisaged three types of front:

(a) Warm front, characterised by steady upgliding of the warm air above the cold air; at any place there would be a steady thickening and lowering of the cloud, with increasing precipitation, as the front approached. The main mass of cloud is in the warm air but, where precipitation is fairly heavy, evaporation below the frontal surface leads to saturation and stratus formation in the cold air.

(b) Cold front, with cold air undercutting the warm air, leading to more vigorous ascent than at the warm front but over a more limited area. The cloud, again mainly in the warm air mass, is often convective in character.

(c) Occluded front, where the cold front has overtaken the surface warm front and warm air is no longer present at the surface.

Richardson (1922). Following the fundamental lines of thought of V Bjerknes, Richardson postulated that "if the initial state of the atmosphere were completely described, it would then be possible to make a prognosis of the future states by use of the fundamental laws of hydrodynamics and thermodynamics". His attempt at a 6-hr numerical forecast for Central Europe was doomed to failure, due mainly to the use of unmodified (or non-initialized) observations (with the inevitable inplied imbalance between the mass and wind fields) and to computational instabilities of the numerical schemes used.

Rossby and collaborators (1937, 1939), from the "Chicago School", systematically tackled the problem of the interaction between several weather systems, the role of weather systems in the general circulation, and the predictability of atmospheric motions beyond 24 hours. Rossby introduced the concept of isentropic analysis.

In the 20 years following the publication of the Norwegian work in the 1920s, ideas on the nature of fronts changed little, but knowledge of the 3-dimensional structure of the atmosphere and its evolution in time improved steadily over the period with the development of aircraft and the necessity for routine upper air soundings (the first regular radiosonde ascents started just before World War II). During the same period refinements of ideas on the development of surface features and the associated upper air evolution, in particular on the forecasting of low level developments from the upper flow pattern, were forthcoming (eg Brunt (1930), Scherhag (1934) J Bjerknes (1937), Sutcliffe (1939, 1940).

In Sutcliffe's (1947) development theory an expression for the difference between the horizontal divergence at two levels is derived (applying a series of approximations) and criteria for the implied vertical motion can be obtained.

Charney (1947), Eady (1949) developed theories on baroclinic instability; the quasi-geostrophic theory that they used has played a central role in modern dynamical meteorology. The so-called Omega equation, a diagnostic equation for vertical velocity, emanates from the quasi-geostrophic system of equations (see for example Holton (1972)).

Particular attention during the decade following World War II was paid to the 3-dimensional structure of depressions and their associated fronts, and our knowledge of the distribution of temperature, wind, humidity and cloud associated with fronts was considerably enhanced during this period (eg Sawyer (1955, 1958), Freeman (1961)).

Some important early work on the transverse circulation in the vicinity of fronts by Sawyer (1956), complemented and extended by Eliassen (1959, 1962), is described briefly in the next section.

3. Frontogenetic processes

In discussion of the amplification of wave-like disturbances in a baroclinic current (ie baroclinic instability leading to cyclogenesis) many text-book accounts (eg Holton (1972) of the phenomenon, often in a basic two-level model, assume the mean thermal wind to be independent of the N-S coordinate (usually the y-coordinate); this assumption is necessary to obtain a mathematically simple model which allows the easy illustration of the instability mechanism. We know however that in the real atmosphere the baroclinicity is not uniformly distributed, the temperature gradients tending to be concentrated in narrow frontal zones associated with the tropospheric jet streams, and this latitudinal dependence of the thermal wind must obviously be included in any complete theory of baroclinic wave development. The fact that the simplified perturbation theory is able to qualitatively reproduce the essential synoptic-scale features of developing baroclinic waves indicates that the fundamental process of mid-latitude cyclogenesis is the (baroclinic) instability due to the vertical wind shear, not the lateral shear across the jet stream, although this undoubtedly influences, inter alia, the rate of development of the perturbation. The energetics of baroclinic waves require that the developing waves remove available potential energy from the basic zonal flow, this tending to weaken the mean meridional temperature gradient; the mean pole-to-equator temperature gradient is of course continually replenished by differential solar heating. In order to explain the observed persistence, over quite lengthy periods, of mid-latitude fronts, some dynamic process is required which can continuously maintain strong gradients characteristic of the frontal zone - such a process is referred to as frontogenesis.

Given the situation in Fig 11, it can be seen that the velocity field, defined by the streamfunction $\psi = -Cxy$ (C is constant), will tend to advect the temperature field so that the isotherms are concentrated along the axis of dilatation (x-axis), provided that the initial temperature field has a finite gradient along the axis of contraction (y-axis). The velocity field here is a pure deformation field, with zero vorticity and divergence; a parcel of air within the flow will merely have its shape changed, with no change in horizontal area. If a component of mean zonal flow is added to the field, a confluent flow will result in the region near the origin. In a homogeneous (baratropic) incompressible fluid a confluent flow such as in Fig 12a would be non-divergent, but in a

baroclinic atmosphere the increase in concentration of the isotherms along the jet implies an increase in the thermal wind along the jet. As a consequence the cyclonic (positive) vorticity north of the jet core and the anticyclonic (negative) vorticity to the south must both increase in magnitude, and in order to produce these vorticity changes a secondary tranverse circulation such as that shown in Fig 12b must exist (the relationship between vorticity changes and the vertical motion can be more easily understood by reference to the quasi-geostrophic vorticity equation).

Sawyer (1956) explored the suggestion that a front should be considered as a region into which active confluence of air currents of contrasting temperatures is taking place (not simply as a stable sloping discontinuity between two air masses with different densities and velocities which, according to simple dynamical theory, can be shown to exist without vertical movement of either air mass). Sawyer states "There are several processes - friction, turbulence and the vertical motion - which can be expected to destroy the sharp temperature contrast within a day or so of its formation, so it would not be surprising if clearly defined fronts were found only where active frontogenesis is in progress, namely in areas where horizontal air movements are such as to intensify the horizontal temperature gradients. There is some observational evidence for this point of view, and it will be demonstrated that the frontogenetic process is necessarily accompanied by a vertical circulation system which can explain several characteristic features of the structure of fronts". Sawyer carried out calculations of the tranverse (cross front X vertical) circulation associated with a zone of confluence under the assumption that the flow (u) along the direction of the isotherms in Fig 12a is geostrophic; an ageostophic v-component (necessary for geostrophic adjustment of the u-component) was allowed. A constant rate of confluence ($\partial u/\partial x \simeq 3$ ms^{-1} per 100 km) and various density distributions, similar to that implied in Fig 12, were also assumed. The resultant tranverse circulation is derived through the solution of a second order differential equation relating stream function ψ (defining the wind velocity field in the y-p plane) to the known density and horizontal wind fields, as follows:

$$f\left(f - \frac{\partial u}{\partial y}\right)\frac{\partial^2 \psi}{\partial p^2} + 2\frac{\partial \alpha}{\partial y}\frac{\partial^2 \psi}{\partial p \partial y} - \frac{\partial \alpha}{\partial p}\frac{\partial^2 \psi}{\partial y^2} = 2\frac{\partial u}{\partial x}\frac{\partial \alpha}{\partial y}$$

where α is specific volume ($= 1/\text{density}$) and f is the Coriolis parameter).

Sawyer solved this equation numerically, using suitable boundary conditions, to obtain the tranverse circulations which would be expected to accompany the various specified fields of u and α . He presented several solutions, two of which are shown in Fig 13. In both cases a direct solenoidal circulation is evident (as anticipated). In Fig 13a no condensation was allowed for, and both vertical motions and ageostrophic lateral motions are fairly small. Fig 13b illustrates a case where diabatic heating due to condensation was permitted to occur (the area above and to the left of the thick sloping line was assumed to be saturated with water vapour; the remaining area was assumed dry). In addition the horizontal density gradient assumed for this latter case was appreciably greater than that for Fig 13a; consequently both the vertical and the horizontal branches of the tranverse circulation are much stronger. The ascending (saturated) branch is also more intense than the descending branch.

References

For the sake of brevity, only a selection of the references mentioned in the text, for the period 1820-1940, are listed here; the interested reader should have no difficulty in tracing the omitted references, although many are in German, French or other European languages. The following are in order of appearance in the text.

BERGERON, T. 1959 Methods in scientific weather analysis and forecasting. An outline in the history of ideas and hints at a program. In "The atmosphere and the sea in motion" (B. Bolin, ed) pp 440-474 Rockefeller Inst. Press, N.Y.

HOWARD, L. 1820 The climate of London, deduced from meteorological observations, made at different places in the neighbourhood of the Metropolis. Vol II. London.

ESPY, J.P. 1841 Philosophy of storms. Boston.

FERREL, W. 1856 An essay on the winds and the currents of the ocean. Nashville J. Med. and Surgery, 12, No. 4 & 5.

FITZROY, R. 1863 The weather book. A manual of practical meteorology. 2nd Ed., London.

GALTON, F. 1863 Meteorographica, or methods of mapping the weather. Macmillan & Co, London and Cambridge.

BLASIUS, W. 1875 Storms, their nature, classification and laws. Philadelphia.

BIGELOW, F.H. 1904 The mechanism of countercurrents of different temperatures in cyclones and anticyclones. Mon. Wea. Rev., 31, p 72.

ABERCROMBY, R. 1887 Weather, a popular exposition of the nature of weather changes from day to day. Inter. Sci. Series, 59, K. Paul Trench and Co Ltd. London.

KOPPEN, W. 1879 Beitrage zur Kenntris der Böen und Gewitterstürme. Ann. Hydr. u. marit. Met., 7, p 324.

DURAND-GREVILLE, E. 1892 Les grains et les orages. Ann. Bur. Centr. Met. de France, 1, p 249.

ROTCH, L.A. 1898 The exploration of the free air by means of kites, at Blue Hill Observatory, Mass., USA. Q.J.R. Met. Soc., 24, p 250.

HANN, J. von 1901 Lehrbuch der Meteorologie. I. Aufl. Leipzig.

BJERKNES, V. 1902 Zirkulatron relativ zur Erde. Met. Z., 19, p 97.

LEMPFERT, R.G.K. SHAW, W.N.	1906	Life history of surface air currents. Met. Committee, M.O. 174, London.
LEMPFERT, R.G.K. CORLESS, R.	1910	Line squalls and associated phenomenon. Q.J.R. Met. Soc., 36, p 135-170.
SHAW, W.N.	1911	Forecasting Weather. Constable and Co., London.
DINES, W.H.	1912	Total and partial correlation coefficients between sundry variables of the upper air. Geophys. Memo., 1, No. 2.
BJERKNES, J. SOLBERG, H.	1921	Meteorological conditions for the formation of rain. Geof. Publ., 2, No. 3.
	1922	Life cycle of cyclones and the Polar Front Theory of atmospheric circulation. Geof. Publ., 3, No. 1.
RICHARDSON L.F.	1922	Weather prediction by numerical process. Cambridge.
ROSSBY C.G. and collaborators	1937	Isentropic analysis. Bull. Am. Met. Soc., 18, p 201.
	1939	Relation between variations in the intensity of the zonal circulation of the atmosphere and the displacements of the semi-permanent centres of action. J. Mar. Res., 2, p 38.
BRUNT, D.	1930	Some problems of modern meteorology: I. The present position of theories on the origin of cyclonic depressions. Q.J.R. Met. Soc., 56, pp 345-350.
SUTCLIFFE, R.C.	1939	Cyclonic and anticyclonic development. Q.J.R. Met. Soc., 65, p 518.
	1947	A contribution to the problem of development. Q.J.R. Met. Soc., 73, p 370.
CHARNEY, J.G.	1947	The dynamics of long waves in a baroclinic westerly current. J. Met., 4, pp 135-163.
EADY, E.T.	1949	Long waves and cyclone waves. Tellus, 1, pp 33-52.
HOLTON, J.R.	1972	An introduction to dynamic meteorology. Int. Geoph. Series. Academic Press, N.Y. and London.
SAWYER, J.S.	1955	The free atmosphere in the vicinity of fronts. Geophys. Mem., London, 12, No 96.
	1956	The vertical circulation at meteorological fronts and its relation to frontogenesis. Proc. Royal Society, A, 234, pp 346-362.

SAWYER, J.S. 1958 Temperature, humidity and cloud near fronts in the middle and upper troposphere. Q.J.R. Met. Soc., 84, pp 375-388.

ELIASSEN, A. 1959 On the formation of fronts in the atmosphere. In "The atmosphere and the sea in motion" (B. Bolin, ed) pp 277-287. Rockefeller Inst. Press, N.Y.

1962 On the vertical circulation in frontal zones Geof. Publikasjoner, 24 (Bjerknes Memorial Vol).

PALMEN, E. NEWTON, C.W. 1969 Atmospheric circulation systems. Int. Geophys. Series, 13, Academic Press, N.Y.

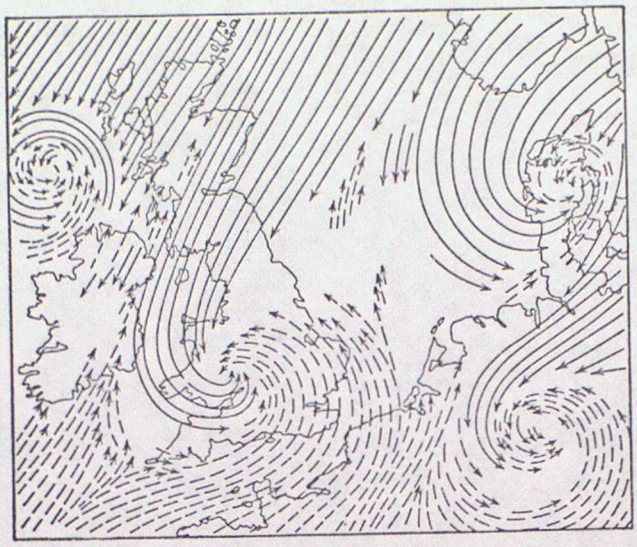

Fig. 1. FitzRoy's air mass concept
(after FitzRoy, 1863)

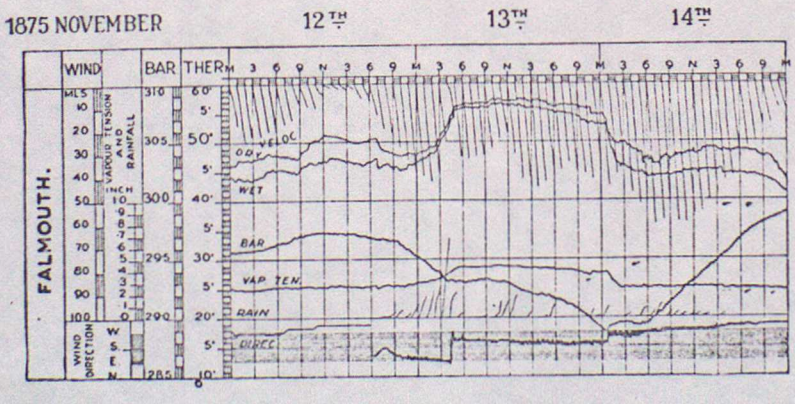

Un secteur chaud idéal.
(Reproduction à échelle originale du météogramme de Falmouth le 12 au 14 novembre 1875.)

Fig. 2. Meteorogram sample (after Bergeron, 1935)

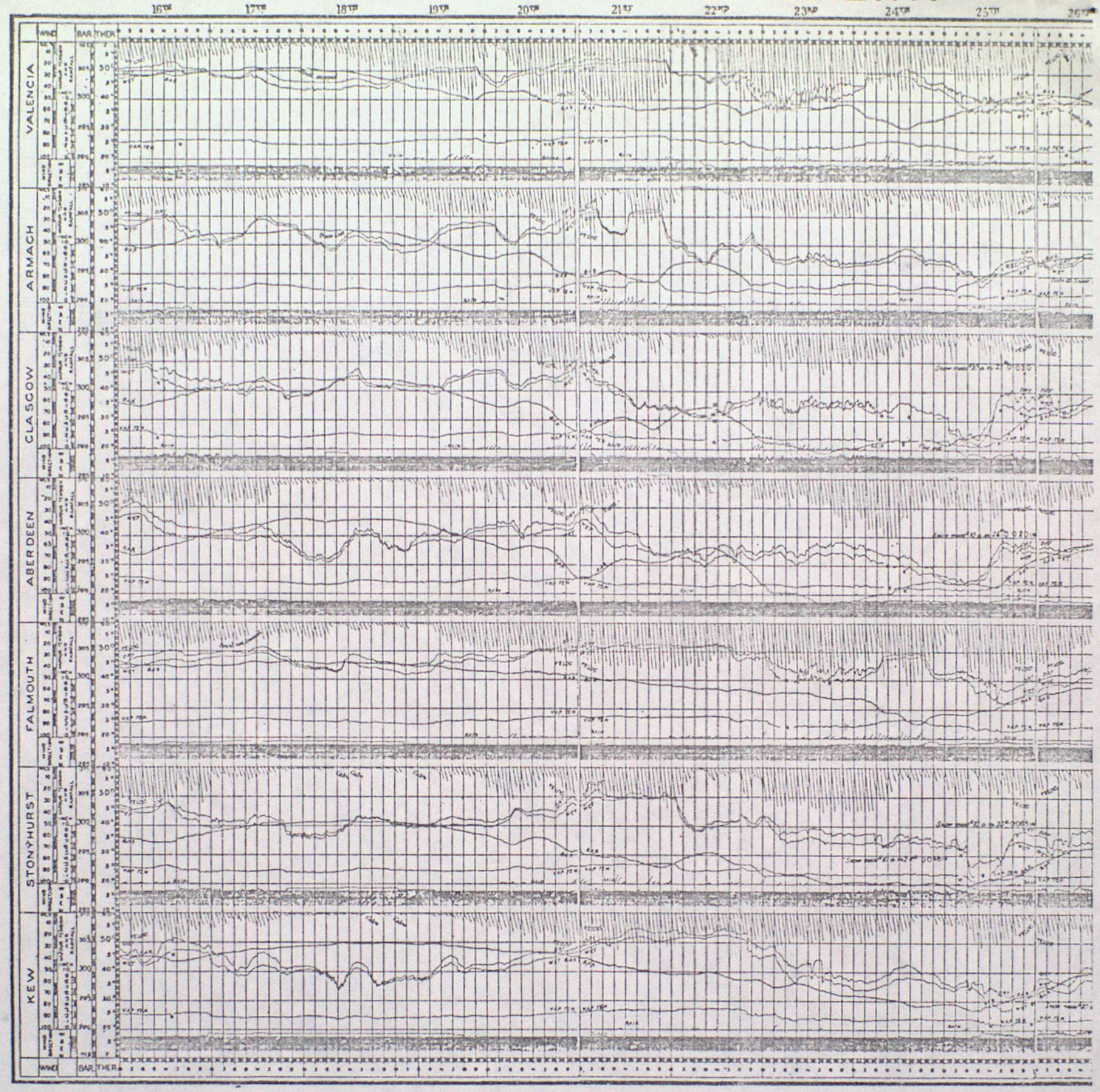

Fig. 3.

The seven meteorograms from the Quarterly Weather Report, 16–25 Jan 1878.

(after Bergeron, 1935)

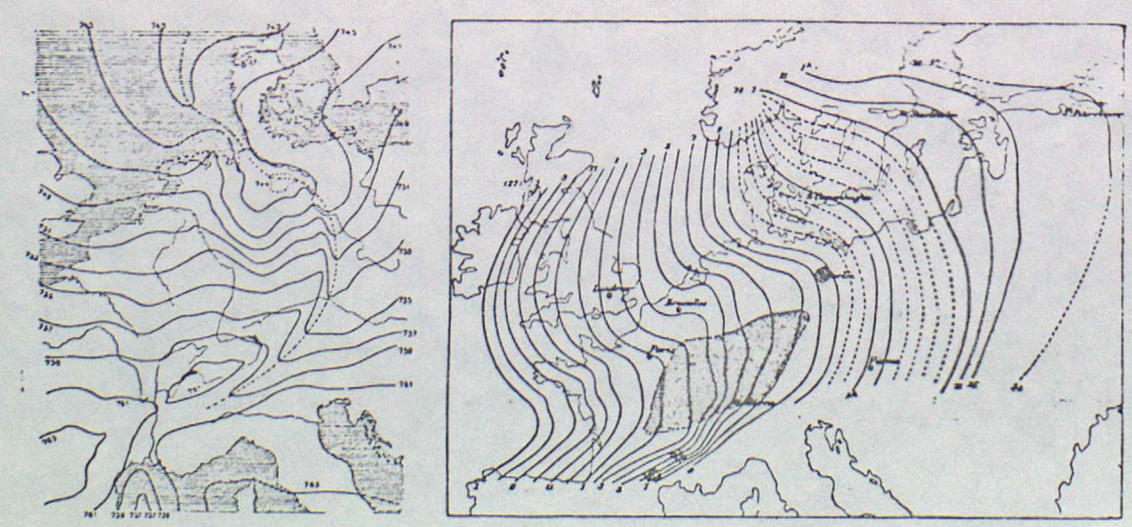

a. Isobars and front of 27. VIII., 21h GMT. b. Isochrones of front. Area of thunder at front-passage.

Fig. 4. –E. DURAND-GRÉVILLE's analysis of the cold-front of 27.—28. VIII. 1890.

(after Bergeron, 1959)

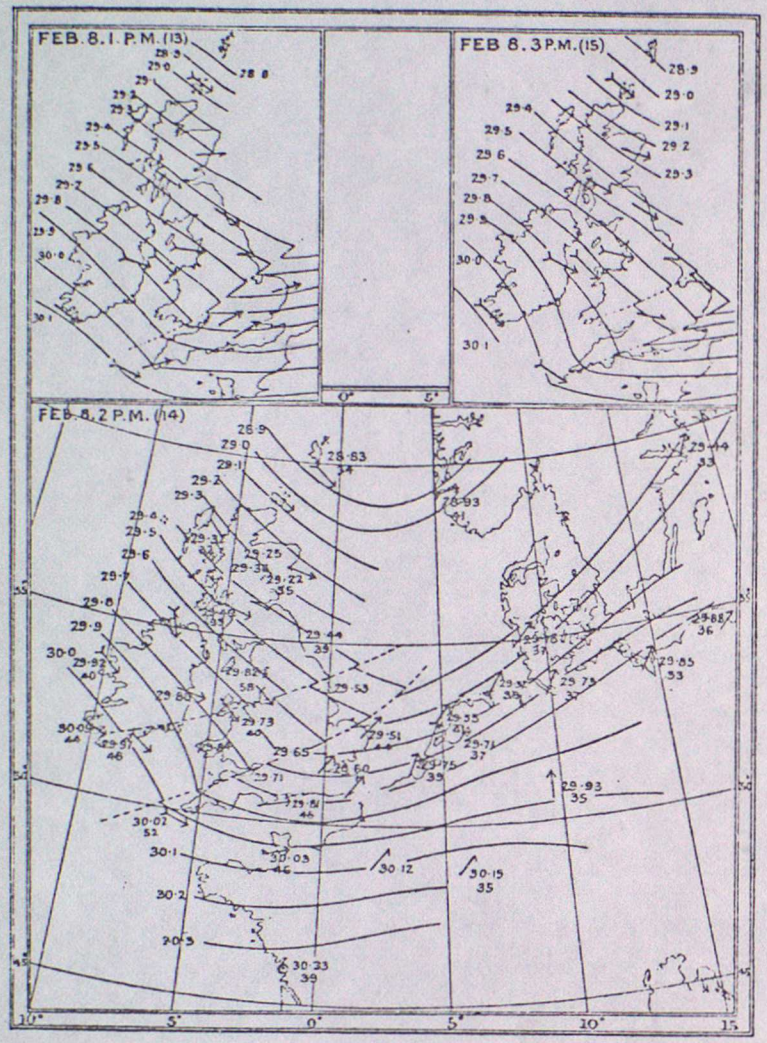

Fig. 5. Surface pressure analyses showing the 'line squall' of 8 February 1906.

(after Shaw, 1911)

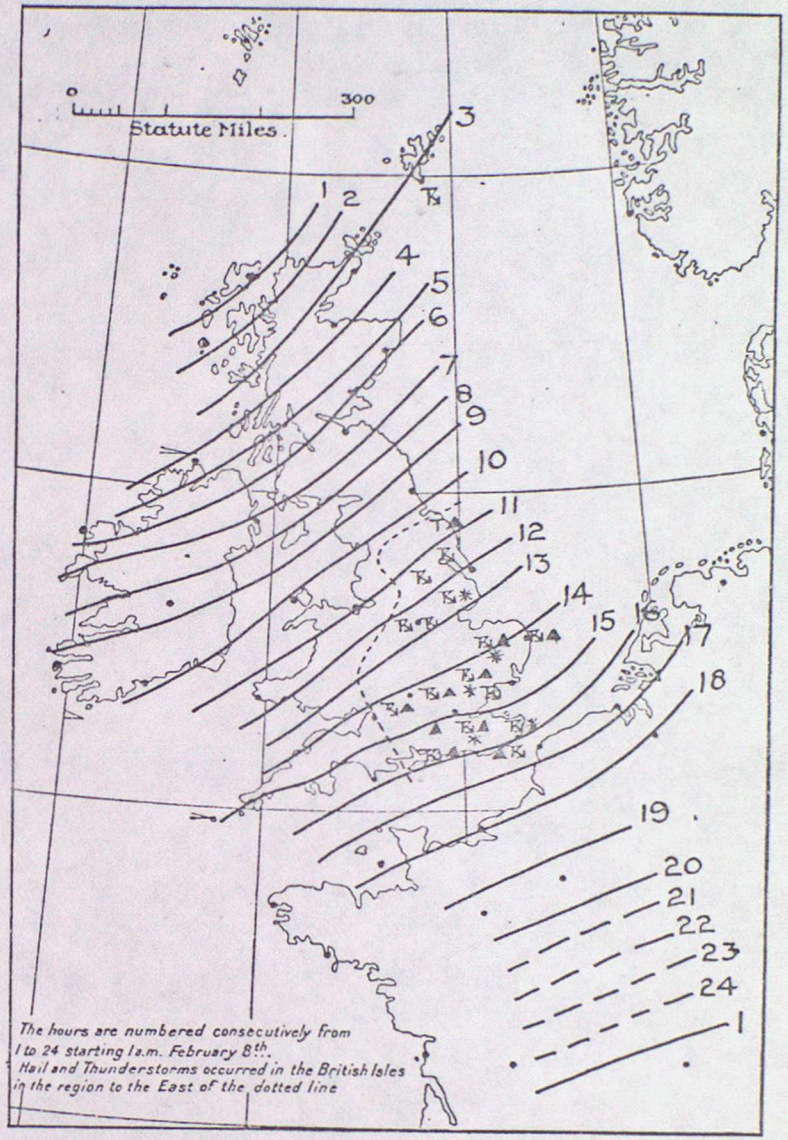

Fig. 6. Isochrones of the 'line squall' of 8 February 1906.

(after Shaw, 1911)

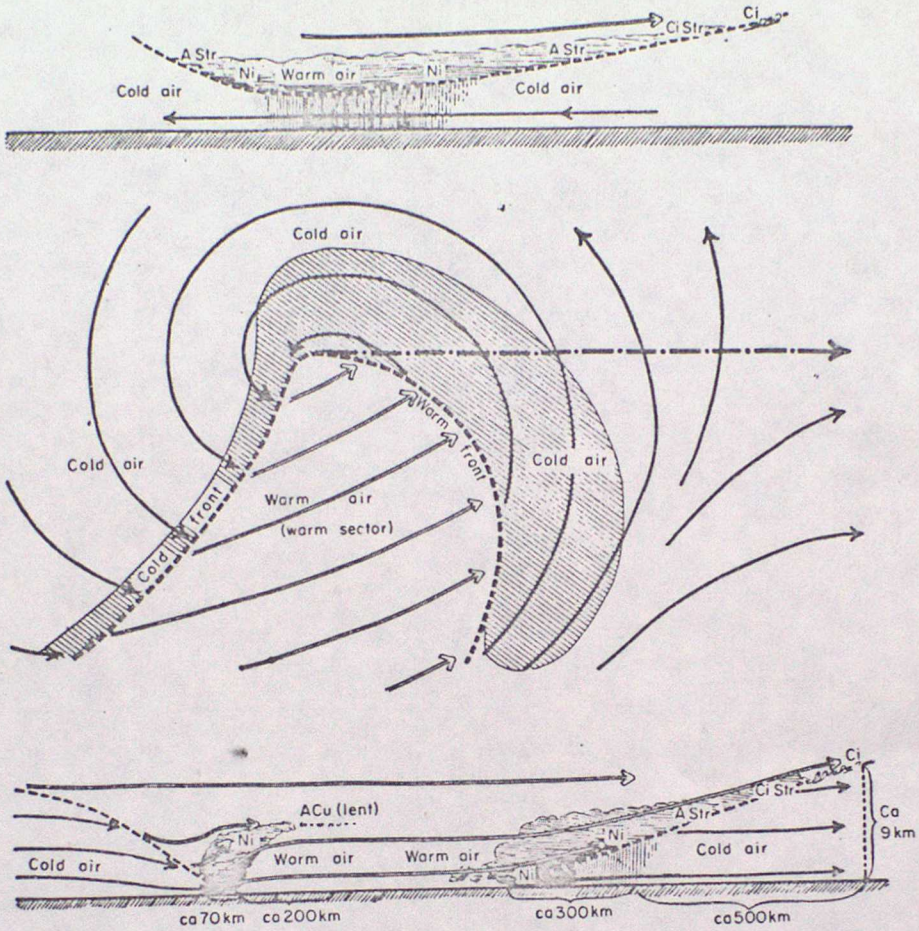

FIG. 7. Idealized cyclone, from J. Bjerknes and Solberg (1921). In middle diagram, dash-dotted arrow shows direction of motion of cyclone; other arrows are streamlines of air flow at earth's surface. Top and bottom diagrams show cloud systems and air motions in vertical sections along direction of cyclone movement north of its center and across the warm sector south of its center.

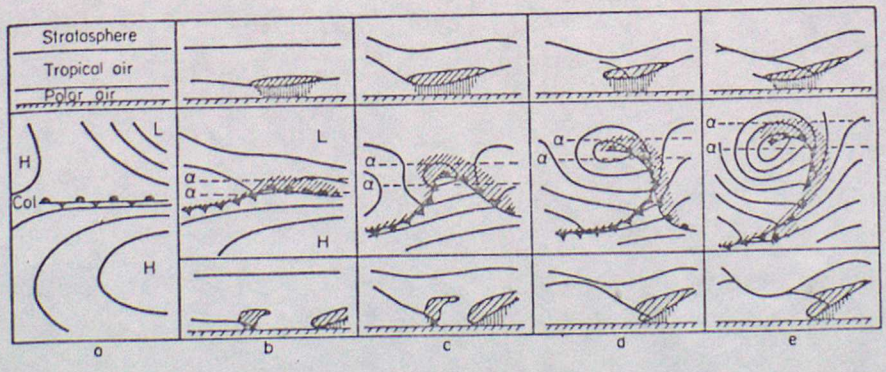

FIG. 8. Life cycle of cyclone from wave to vortex, after J. Bjerknes, from Godske *et al.* (1957). In middle figures, thin lines are sea-level isobars. Top and bottom figures shown schematic clouds, frontal surfaces, and tropopauses along lines a, a little north and south of cyclone center. The times between stages (a) and (c), and between stages (c) and (e), correspond approximately to one day in each case.

(after Palmen and Newton, 1969)

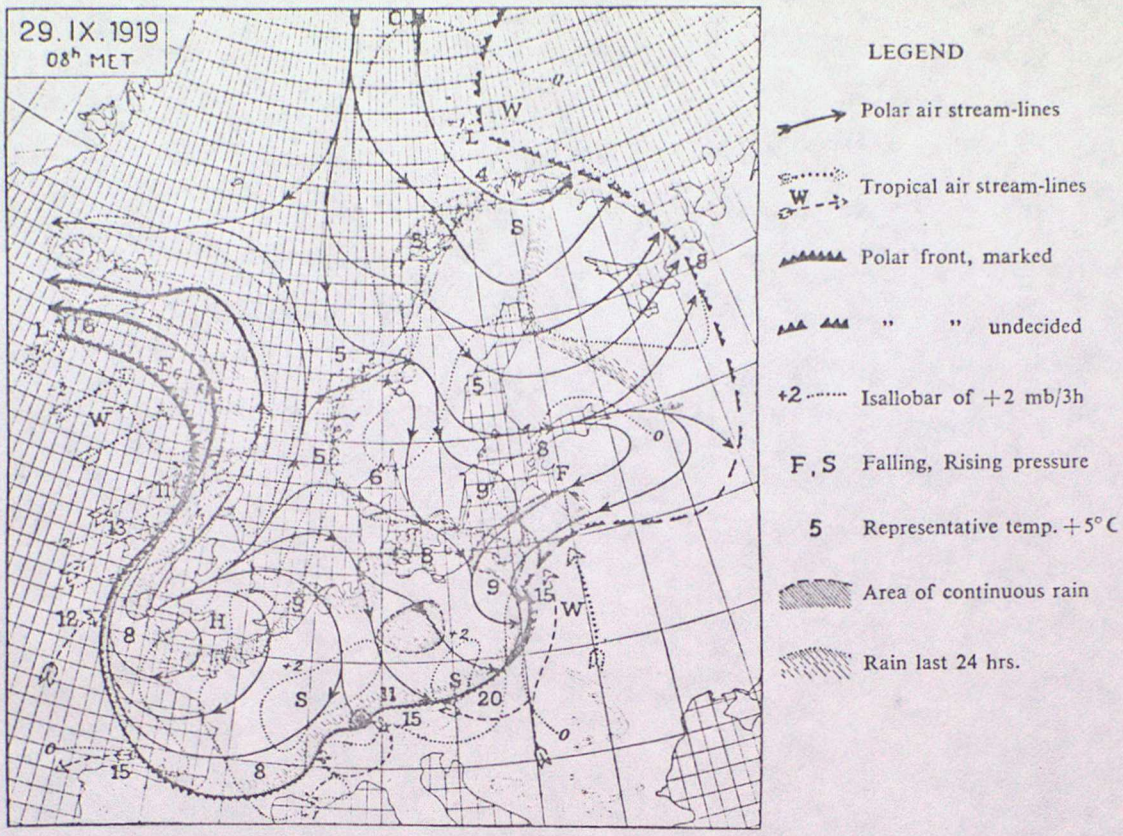

Fig. 9.—Bergen weather map of 29. IX. 1919, showing a Polar front. — Analyzed with streamlines by T. BERGERON in October 1919 (before the occlusion process was discovered).

(after Bergeron, 1959)

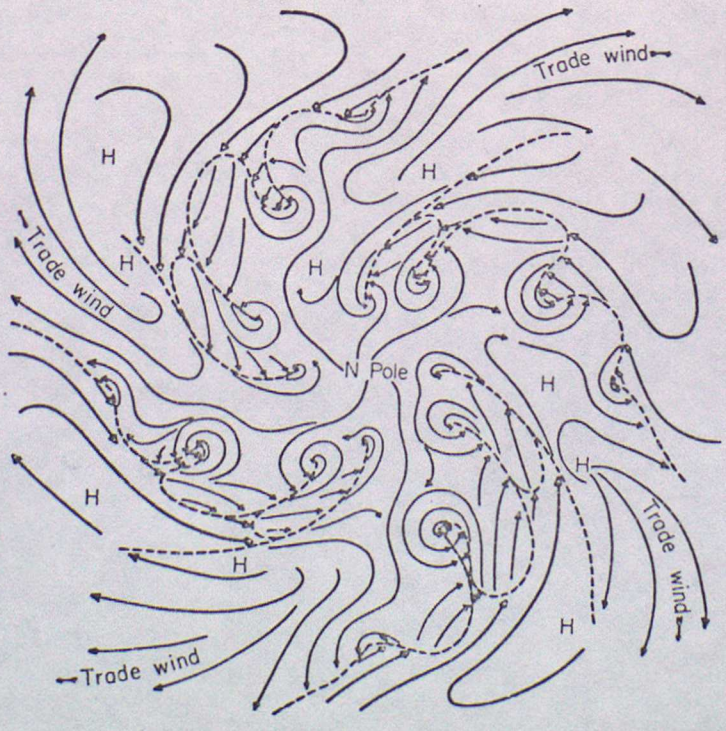

FIG. 10. General extratropical circulation of the atmosphere, from J. Bjerknes and Solberg (1922). Dashed lines show frontal systems of cyclone families; arrows are surface streamlines.

(after Palmen and Newton, 1969)

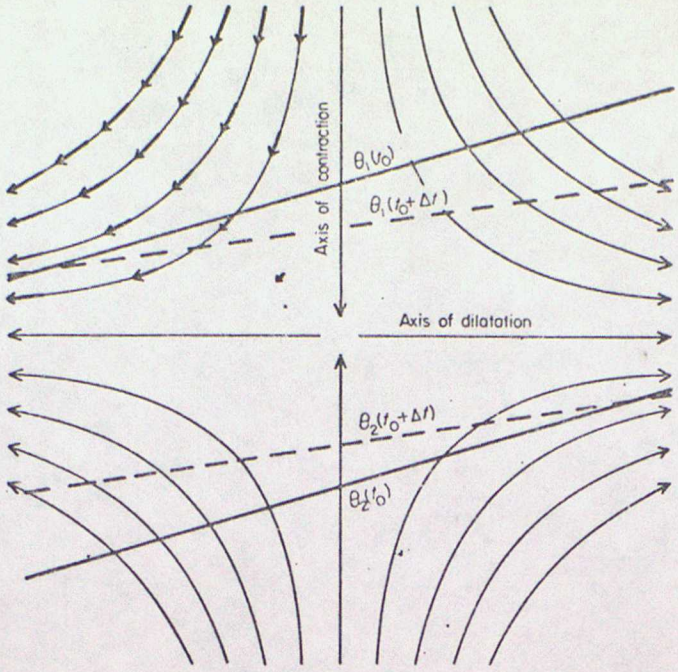

FIG. 11 Streamlines of a pure deformation field, with successive positions of two potential-temperature isopleths. (After Bergeron, 1928.)

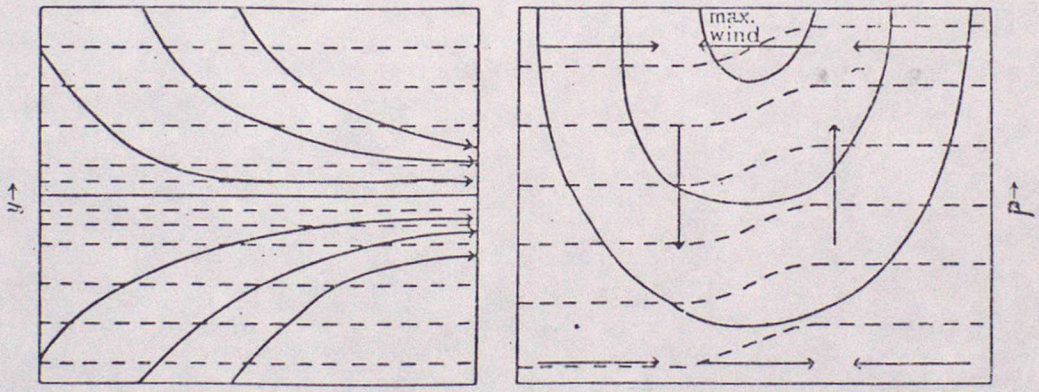

FIGURE 12(a) FIGURE 12(b)

FIGURE 12(a). Horizontal distribution of stream lines (——) and isotherms (– – – –) in a frontogenetic confluence.

FIGURE 12(b). Vertical section through frontogenetic confluence showing vertical circulation. ——, isokinetics; – – – –, isotherms.

(after Sawyer, 1956)

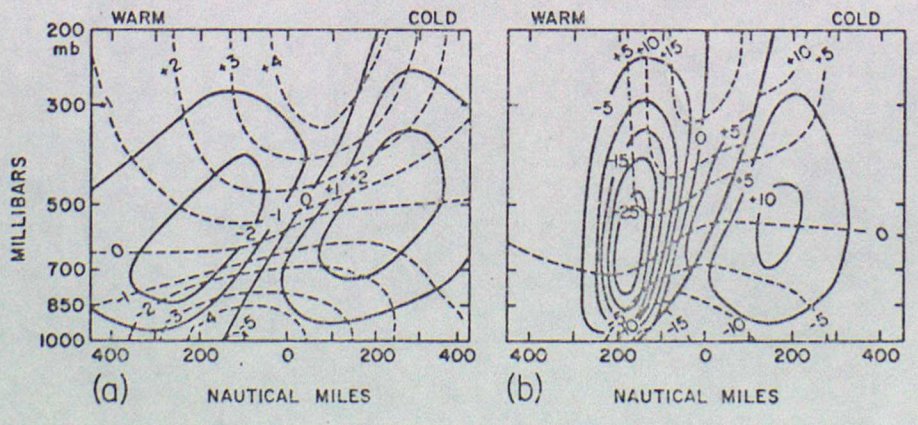

FIG. 13. Theoretical distribution of vertical motion (solid lines, mb/hr) and transverse horizontal velocity (dashed lines, kt), resulting from confluence. In (a) the air is dry; in (b) the rising air is assumed to be saturated. In both examples, the magnitude of the basic confluence was assumed to be the same; however, the stabilities and horizontal temperature gradients differed. (After Sawyer, 1956.)

AM.

FRONTS IN THE ATMOSPHERE

LECTURE TWO - Observational Characteristics of mid-latitude fronts - (Part I)

1. Introduction

Part I of this topic describes some methods used in the analysis of the 3-dimensional structure of the atmosphere in the vicinity of fronts and presents typical examples of relevant information that can be derived from conventional upper air observations. In addition the results are described of a detailed case study of the passage of a wave depression across the British Isles (Browning and Harrold (1969)), in which extensive use was made of conventional observations and radar data. In Part II further detailed case studies, involving the passage of cold fronts across the British Isles, will be covered. The intention is that discussion of such studies will serve two main purposes:

(i) provide examples of the application of the various techniques of analysis.

(ii) highlight the important air motions and associated regions of precipitation associated with frontal phenomena.

2. Analysis techniques using conventional surface and upper air observations.

(a) Vertical cross-sections

Analysis by means of vertical cross-sections can be a valuable aid in obtaining a 3-dimensional picture of the synoptic situation. It is rarely practicable to produce vertical cross-sections as routine, but the occasional drawing of one is usually helpful in gaining an insight into the vertical structure of fronts and jet streams. The vertical scale is usually logarithmic in pressure (or linear in height) while the horizontal scale is linear distance (miles or km), the vertical scale being about 100 or 200 times the horizontal scale. The horizontal line along which the section is to be drawn should be chosen to lie close to as many upper air ascents as possible, and will normally be chosen to be roughly perpendicular to the front which is the main feature of interest. Examples of cross sections are shown in Fig. 1 (temperature and potential temperature), Fig. 2 (humidity and wet-bulb potential temperature) and Fig. 3 (wind component perpendicular to the plane of the cross section); note the highlighting of the boundaries of the frontal zone and the base of stable layers, the tropopause in this case. A variant of the vertical cross-section is the time section, in which the horizontal axis refers to time instead of distance, with the sequence of events at a particular site being represented. If the system crossing the site can be assumed to be in a steady state (negligible development) and moving with a constant horizontal velocity (magnitude u) parallel to the plane of the section, then the time-height section can be transposed to a conventional distance-height cross section by equating distance interval δL to time interval δt using $\delta L = u \delta t$.

(b) Frontal contour charts

The three-dimensional structure of a frontal surface is occasionally depicted using a frontal contour chart. This consists of a chart on which are drawn a series of lines showing the position of the intersection of the frontal surface with selected pressure surfaces. The upper boundary of the frontal zone, that is the lower limit of the warm air mass, is usually taken as defining the frontal surface. An example of a frontal contour chart is shown in Fig. 4.

(c) Isentropic analysis

An isentropic chart shows the state of the atmosphere on a surface of constant potential temperature (θ) . In the absence of non-adiabatic effects such as condensation or radiation, air particles will remain on an isentropic surface. (In adiabatic processes entropy is proportional to potential temperature). Contours of the height of the isentropic surface selected are drawn up and the winds at those heights (the observed winds or the winds relative to a particular system) can also usefully be plotted (see Green, Ludlam and McIlveen (1966)). Such charts enable the 3-dimensional air motion to be evaluated, provided that the air motion can be assumed adiabatic, and, if winds relative to the system are plotted, that the system is basically steady state during the time taken for air to travel through it. In regions of cloud and precipitation the use of wet-bulb potential temperature (θ_w) surfaces rather than θ -surfaces is obviously more appropriate. An example appears in Fig. 9 (to be discussed in section 4).

The reader is referred to the Handbook of Weather Forecasting, Chapter 12 ("Further techniques of analysis") for more detailed guidance on the construction of cross sections, frontal contour charts and isentropic analysis charts.

3. Cross-sections of typical mid-latitude fronts

Examples of cross sections derived from radiosonde ascents and aircraft traverses (Freeman (1961) are reproduced in Fig.5 (warm front), Fig. 6 (ana-cold front) and Fig. 7 (kata-cold front).

4. Case study - Air motion and precipitation associated with a warm front

This section deals with a description of the main findings of an investigation by Browning and Harrold (1969) into the air motions and precipitation associated with a wave depression crossing the British Isles (16 Oct 1967) using conventional surface and upper air observations and more detailed radar-derived motion and precipitation fields.

(a) Synoptic scale analysis using conventional observations

Fig. 8 shows the synoptic situation at 1200 GMT on 16 Oct 1967; the depression travelled at about 16ms^{-1} from 245°. Isentropic analyses at θ_w = 6°C and 12°C for the same time are shown in Figure 9a and 9b (relative winds are plotted). The θ_w = 6°C surface coincides roughly with the base of the warm frontal zone (WFZ), while the θ_w = 12°C surface coincides roughly with the top of the WFZ. (see Fig. 10). Large-scale ascent in excess of 5cm s^{-1} occurred over an extensive area (stippled in Fig. 9b), roughly matching the area of frontal rain at the surface. On

the $\theta_w = 6^\circ C$ surface descent predominated ahead of the surface warm front (SWF) over Britain (near the base of the WFZ). Fig. 10 reveals the broad scale thermodynamical structure of the depression and the associated frontal zone in the vertical section along the line $P_{06} - P_{24}$ in Figs. 9a and 9b. Note the two main regions of potential instability ($\partial\theta_w/\partial z < 0$) indicated by cross-hatching, the first in the cold air ahead of the warm front where the instability was not realized due to subsidence of the air and its relative dryness, the second at low levels within the warm sector where low - θ_w mid-level air was overrunning high - θ_w air close to the surface.

The surface rainfall distribution for the 24 hours ending at 0900 on 17 Oct is shown in Fig. 11 (includes almost all the rainfall from this system); the distribution is, as usual, dominated by orographic effects. Notable features, apparantly not related to topography, are the two swaths of relatively heavy rainfall extending north-eastwards across central England. Figure 12 shows 10-min averages of rainfall over England and Wales for 1200, 1500, 1800 and 2400 on 16 Oct. Note in particular the meso-scale structure of the precipitation fields, particularly within the warm sector where some of the areas appear to be arranged in bands roughly along the direction of travel of the system; individual meso-scale precipitation areas (MPAs) travelled at about $30 ms^{-1}$ so overtaking the surface warm front (see Fig. 13). This speed corresponds to the wind strength at 3km, suggesting that the MPAs were triggered by large-scale dynamical ascent of low-level air just above the surface front. The banded structure ceased after the cold front passed through.

Fig. 14 illustrates Browning and Harrold's classification of the surface rainfall into two principal regimes:

> Type A - uniform rain, Type B - non-uniform rain, with further subdivision of type B rain into:
>
> Type B_1 - bands of rain areas aligned parallel to the warm front.
> Type B_2 - bands of rain areas aligned parallel to the winds in the warm sector.
>
> (the spatial distribution of these types for this case study is shown schematically in Fig. 14).

Orographic effects ranged from barely discernible in Type A rain areas to very pronounced within the warm sector. The swaths of relatively high rainfall extending downwind from the South Wales hills were evidently due to a succession of small mesoscale precipitation areas travelling at about $35 ms^{-1}$ from 240° along similar paths within an almost stationary Type B_2 rain band. The principal findings arising out of the analysis of the precipitation fields are summarised in Table 1.

(b) Use of radar data (Pershore)

Figs. 15a-15d show time-height distributions of u (wind component parallel to warm front), v (wind component perpendicular to warm front, relative to the motion of the front), the horizontal divergence $(\partial u/\partial x + \partial v/\partial y)$ and the stretching deformation with respect to an axis parallel to the warm front $(\partial u/\partial x - \partial v/\partial y)$. The x-axis here is parallel to the warm front and positive towards 110°, and the y-axis is perpendicular to the front, positive towards 020°.

The field of vertical air motion derived by vertically integrating the divergence field in Fig. 15c is shown in Fig. 16 (dashed isopleths). The tranverse circulation defined by the v,w field is represented by the solid streamlines here. The airflow pattern can be seen to be a circulation in the direct sense, with descent of a few cm s^{-1} in the cold air beneath the frontal zone and ascent of about 10cm s^{-1} in the warm air above it (this result is consistent with the isentropic analysis in Fig. 9.)

Fig. 17 shows a time-height distribution of precipitation echo synthesized using data from the entire period of radar observations. Broadly speaking the vertical extent of echo (thick solid contours) correlated positively with the surface rainfall rate (plotted along the abscissa). During the period of Type A rain, however, from 0930 to 1230 GMT, the correlation was inverse. According to Harrold and Nicholls (1968) this is a common occurrence in warm frontal rain. It is partly a result of evaporation beneath the frontal zone within the relatively dry subsiding air at the leading edge of the rain area; closer to the surface warm front the same low-level air has become much moister due to its previous passage through the rain area.

REFERENCES

Browning, K.A. Harrold, T.W	1969	Air motion and precipitation growth in a wave depression. Q.J.R. Met. Soc. 95, pp 288-309
Meteorological Office	1975	Handbook of Weather Forecasting, Chapter 12
Harrold, T.W. Nicholls, M.J	1968	An investigation of air motion in frontal precipitation. Met O Sci. Pap 29.
Green, J S A, Ludlam, J H, McIlveen, J F R.	1966	Isentropic relative flow analysis and the parcel theory Q.J.R. Met Soc., 92 pp 210-219
Freeman, M.H.	1961	Fronts investigated by the Meteorological Research Flight. Met. Mag., 90, pp 189-203

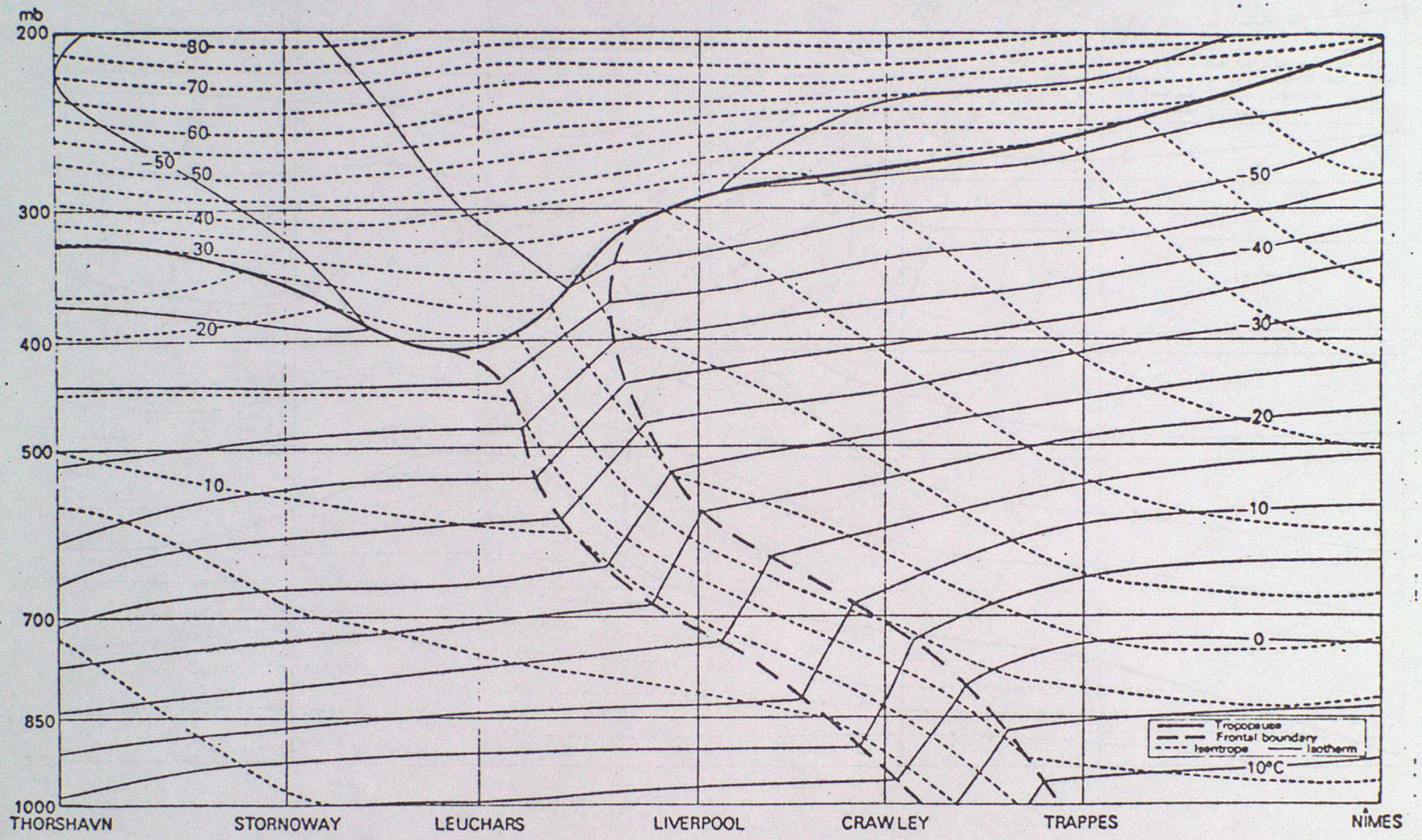

FIGURE 1. Vertical cross-section of the atmosphere from Thorshavn to Nîmes, showing temperature and potential temperature, 1400 GMT, 11 January 1955

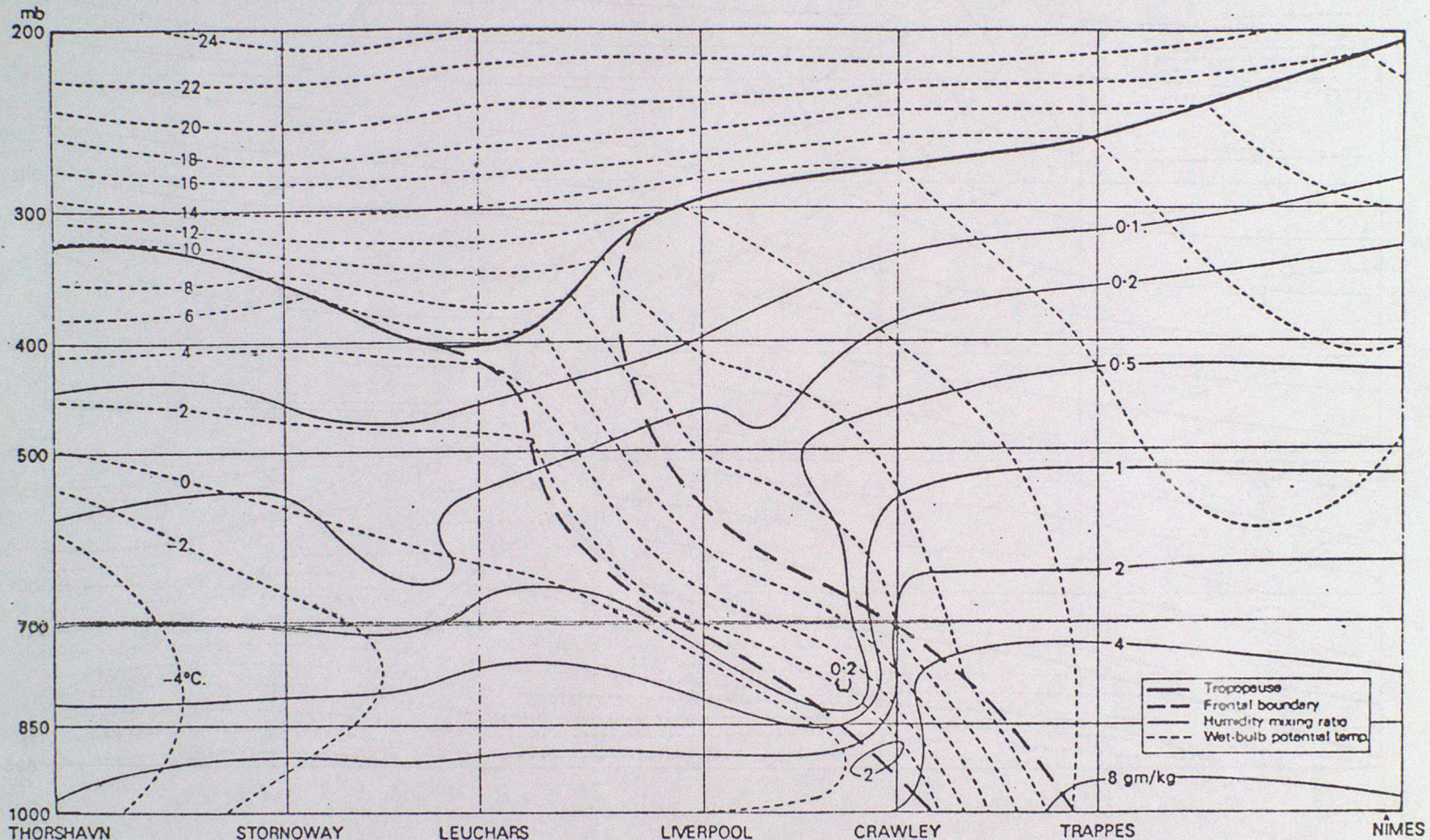

FIGURE 2. Vertical cross-section of the atmosphere from Thorshavn to Nîmes, showing wet-bulb potential temperature and humidity mixing ratio, 1400 GMT, 11 January 1955

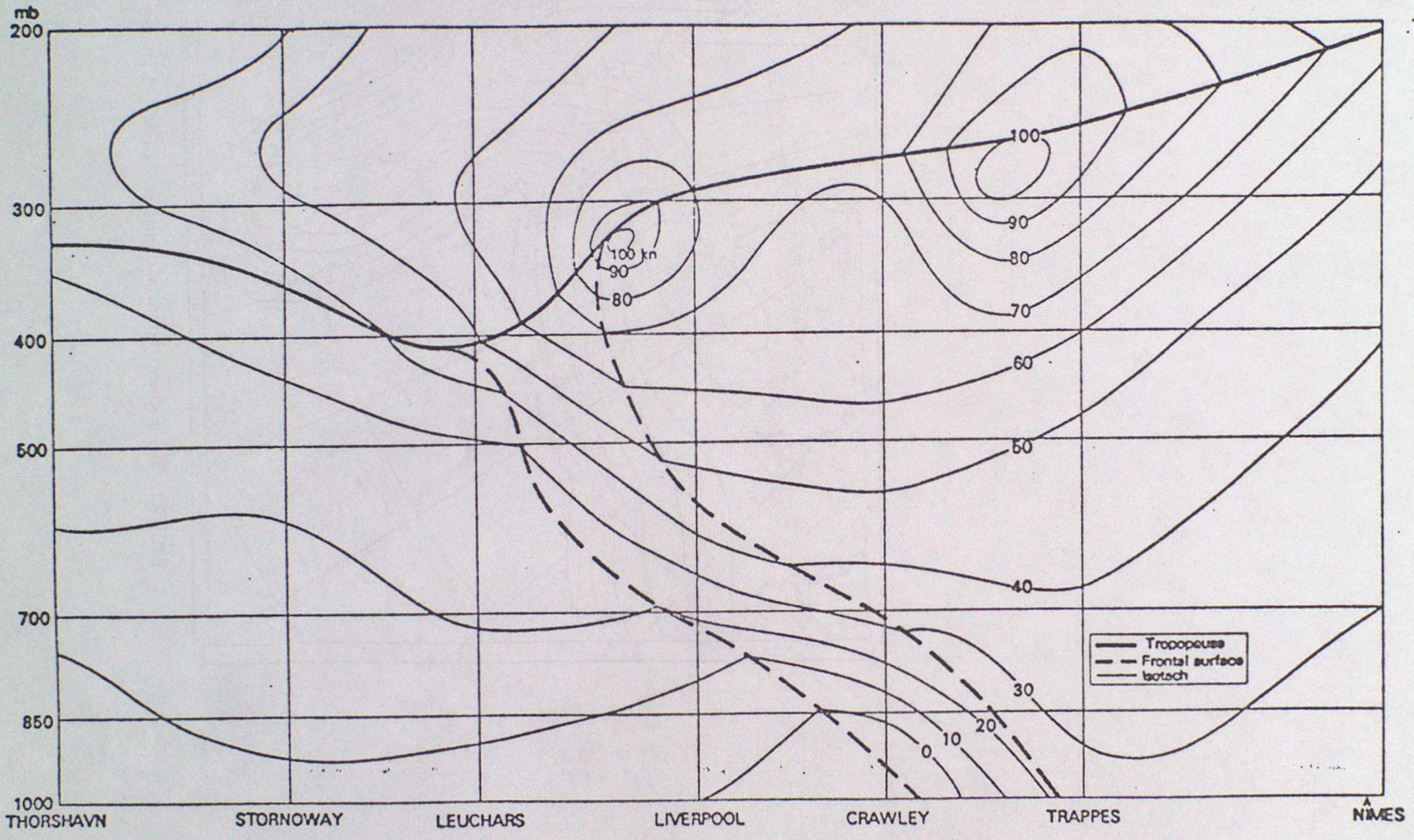

FIGURE 3. Vertical cross-section of the atmosphere from Thorshavn to Nîmes, showing isotachs of wind speed perpendicular to the plane of the section, 1400 GMT, 11 January 1955

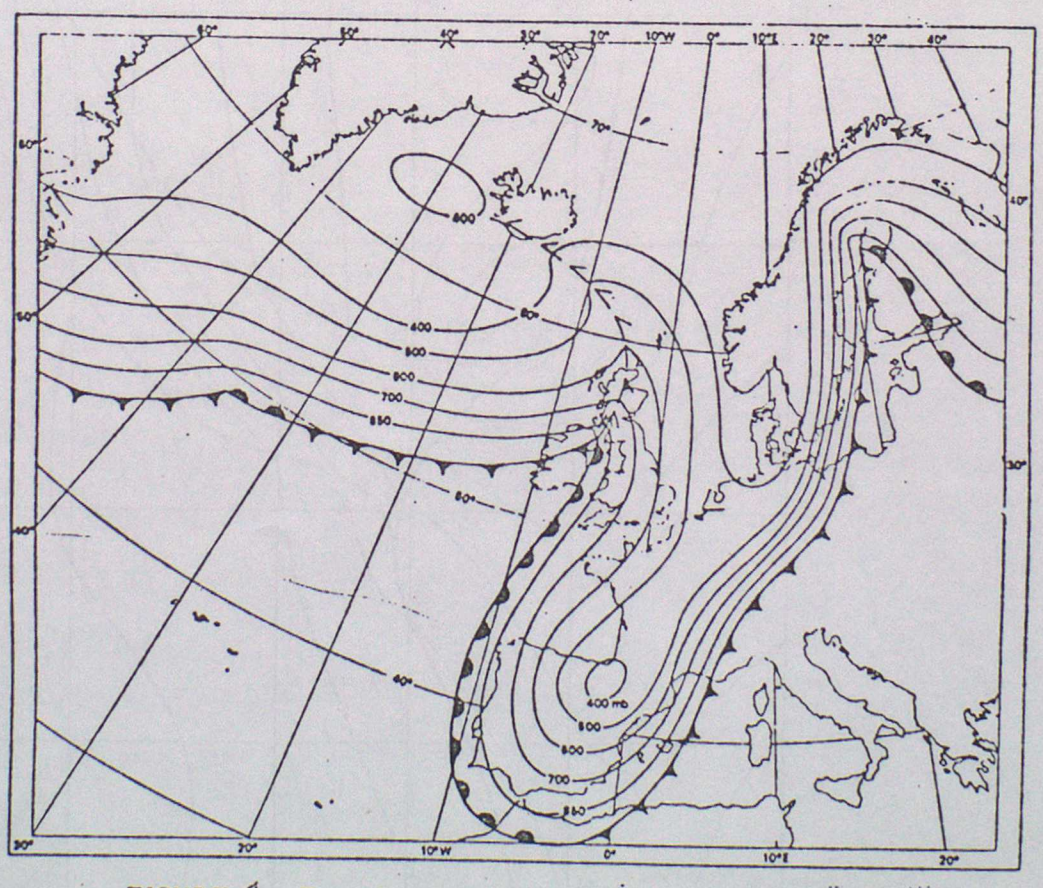

FIGURE 4 Frontal contour chart, 0001 GMT, 3 December 1960

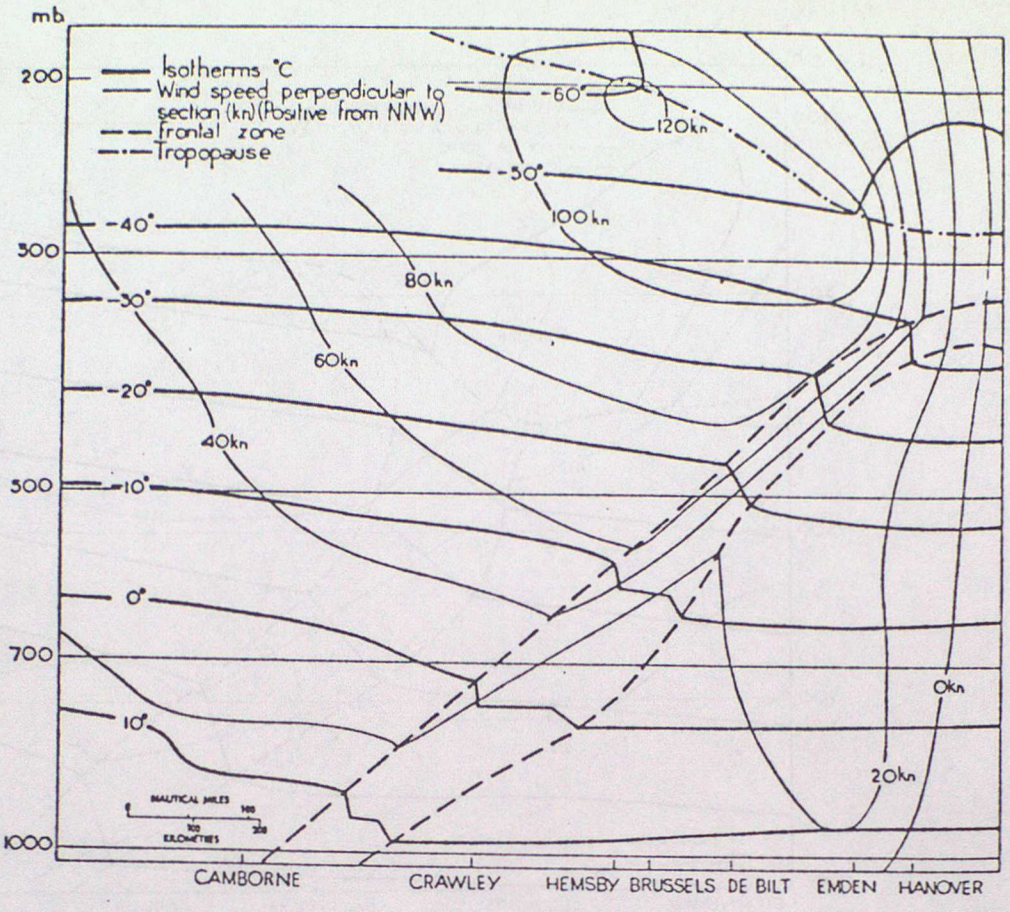

FIGURE 5(a) Vertical cross-section, Camborne to Hanover, of warm front (7/10/55) showing isotherms and isotachs

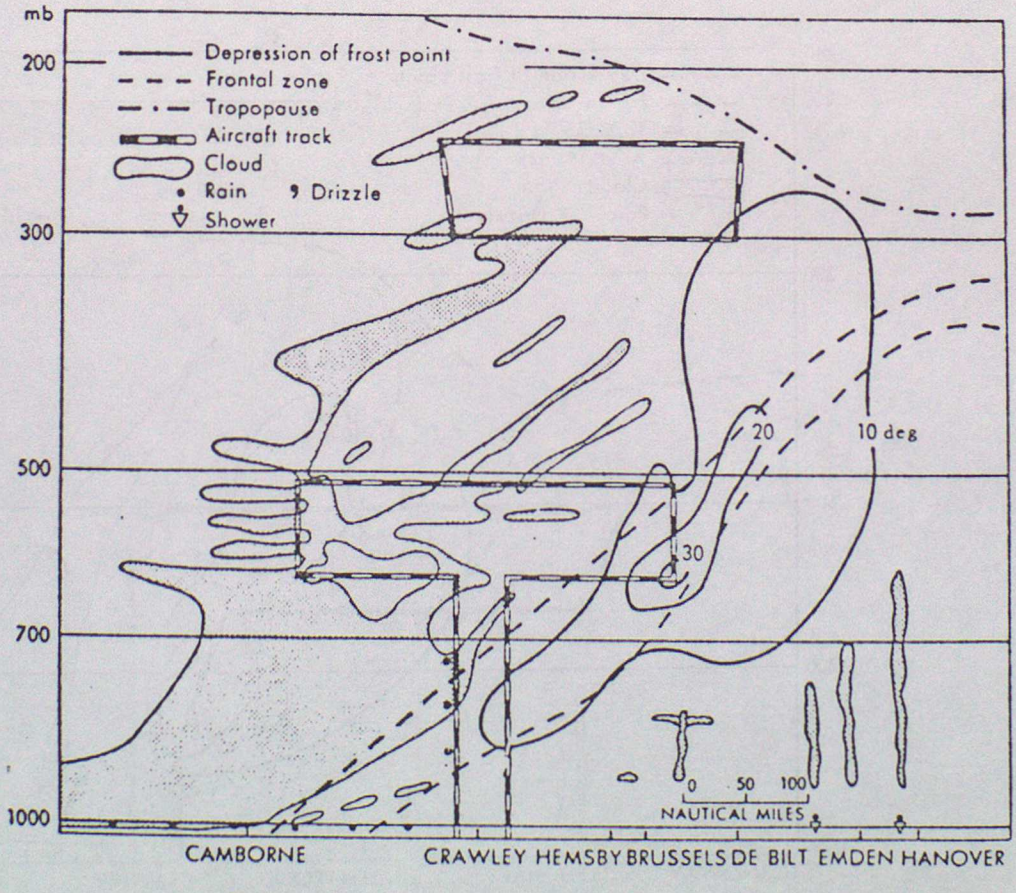

FIGURE 5(b) Vertical cross-section showing humidity and cloud

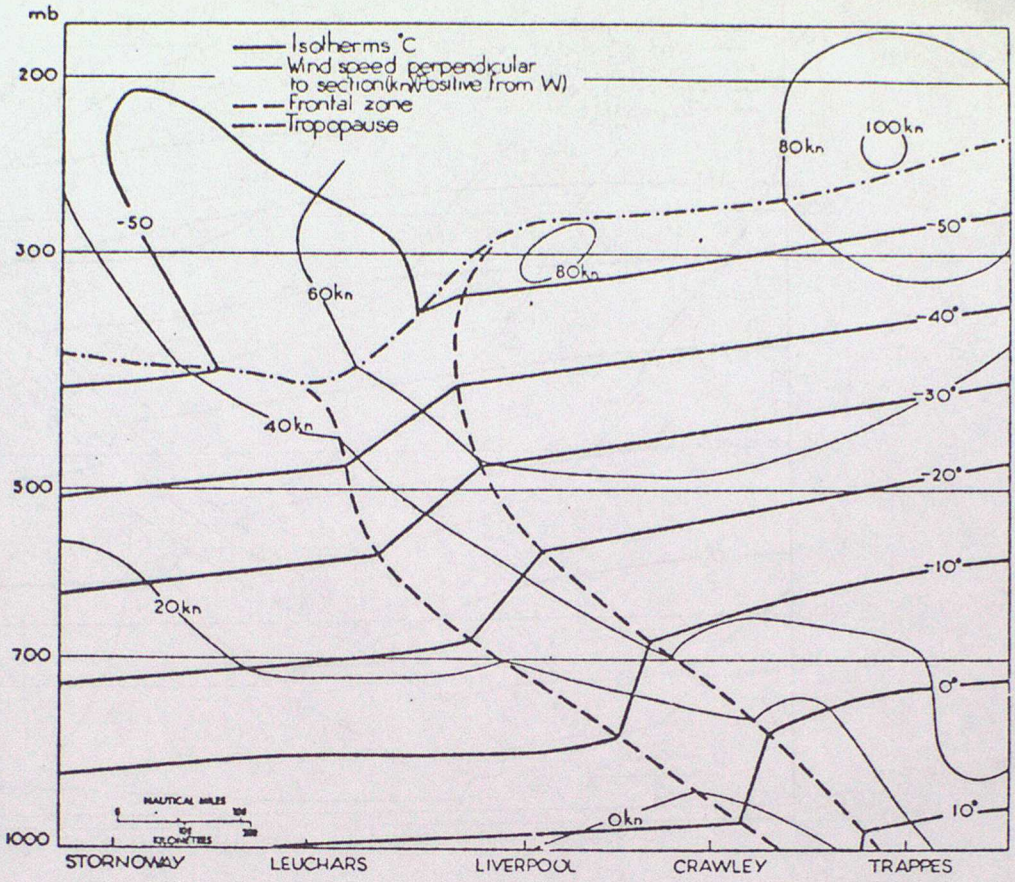

FIGURE 6(a) Vertical cross-section, Stornoway to Trappes, of cold front (11/1/55) showing isotherms and isotachs

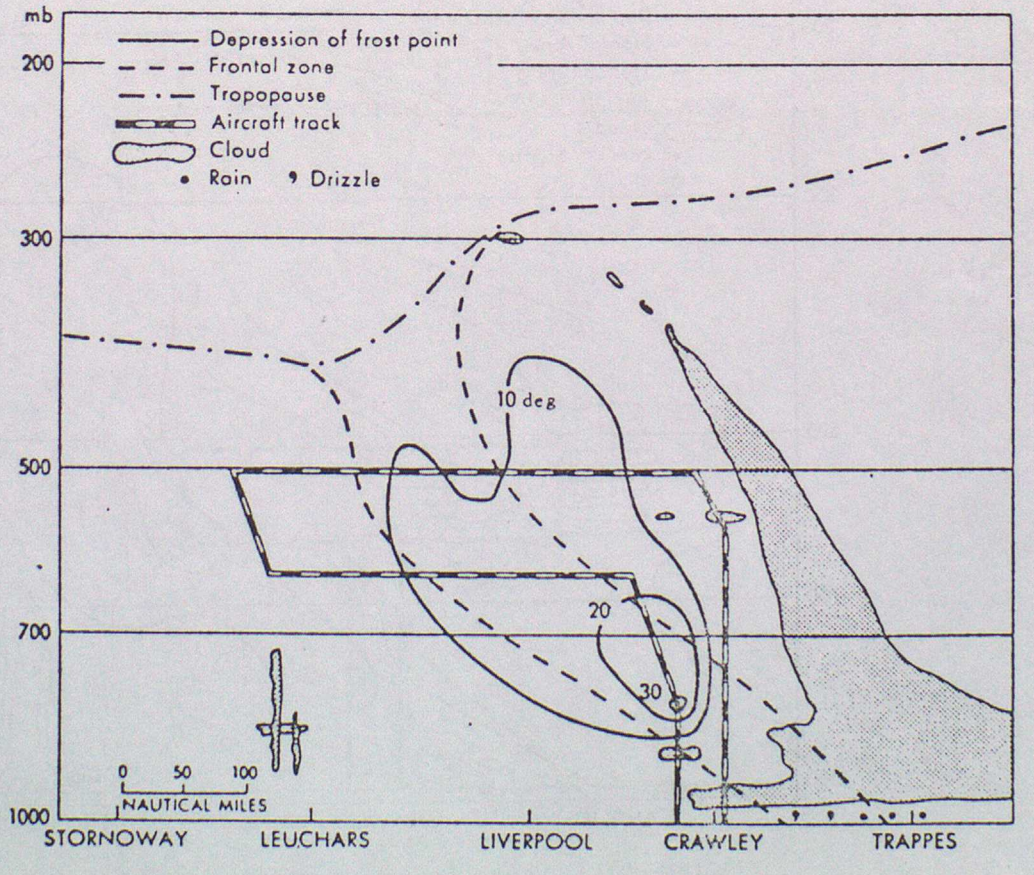

FIGURE 6(b) Vertical cross-section showing humidity and cloud

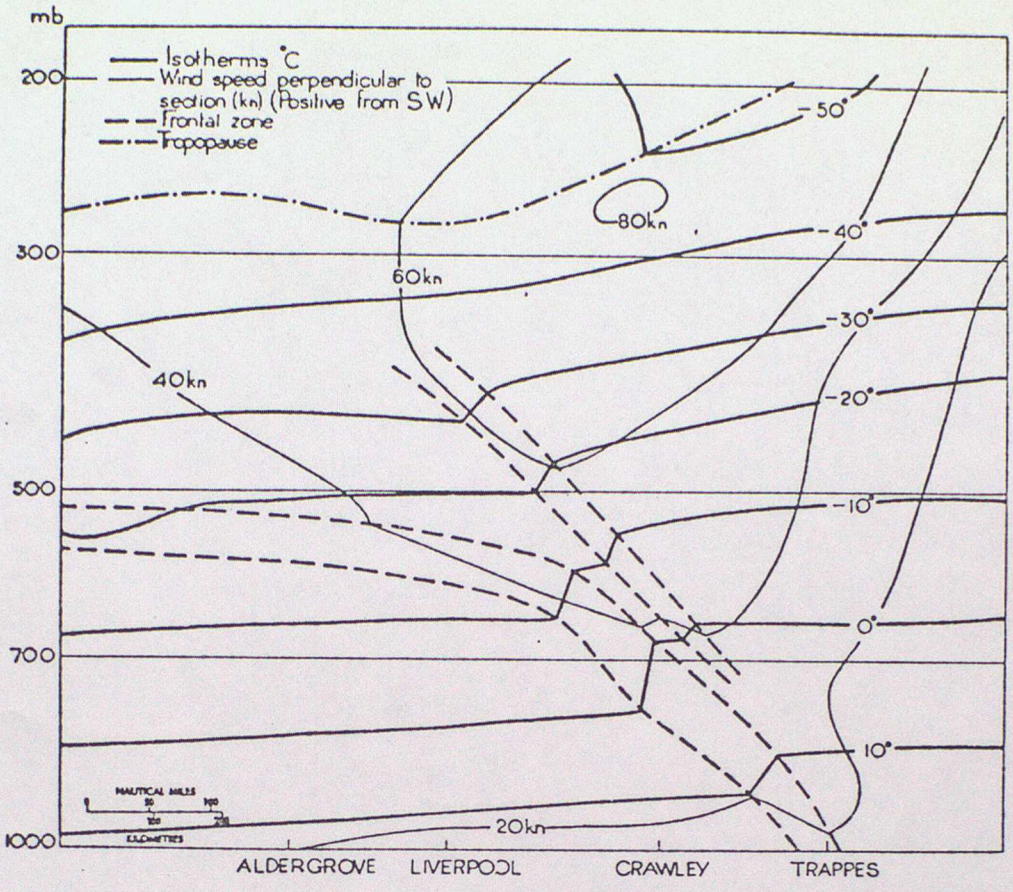

FIGURE 7(a) Vertical cross-section, Aldergrove to Trappes, of cold front (16/9/54) showing isotherms and isotachs .

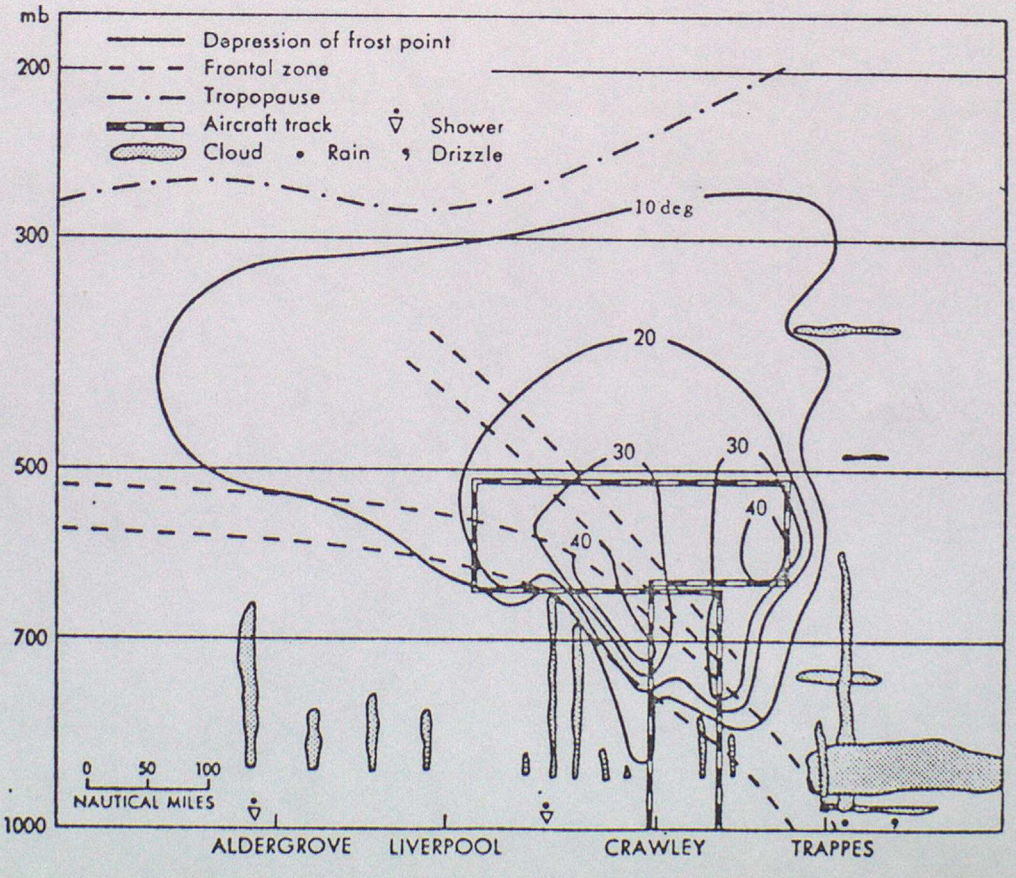

FIGURE 7(b) Vertical cross-section showing humidity and cloud

TABLE 1. RAINFALL CLASSIFICATION BASED UPON ANALYSIS OF SURFACE RAINFALL DISTRIBUTION

Type	Description	Rain intensity	Orographic effects	Velocity of small rain areas
A : Warm frontal uniform rain	Large almost uniform area of rain 150-350 km ahead of surface warm front. Only a few trackable small areas of heavier rain	Widespread moderate	Negligible orographic effects	36 ± 5 m s^{-1}, 240° (equal to wind between 4 and 5 km)
B_1 : Warm frontal rain bands	Bands consisting of small rain areas aligned parallel to surface warm front. They formed close to the front and then advanced ahead of it	Heavy within areas with horizontal dimensions of order 50 km	—	29 ± 3 m s^{-1}, 240 (equal to wind at 3 km)
B_2 : Warm sector rain bands	Bands consisting of small rain areas aligned parallel to the warm sector winds	Heavy within areas with horizontal dimensions of order 50 km	Bands persistently extended downwind from hilly areas, particularly south Wales. Very heavy orographic amounts over the higher hills themselves	36 ± 3 m s^{-1}, 230-240° (equal to wind at 3 and 6 km)

TABLE 2. CLASSIFICATION OF 16 OCTOBER RAINFALL IN TERMS OF PHYSICAL-DYNAMICAL MECHANISMS

	Rain due to large-scale ascent without vertical instability	Rain due to large-scale ascent with vertical instability
Surface rainfall régime (c.f. Table 2)	Type *A* uniform rain; moderate intensity over large area	Type *B* non-uniform rain bands; band consist of areas of heavy rain with dimensions of order 50 km. Some bands (B_1) were triggered by large-scale ascent at the surface warm front; other bands (B_2) were triggered by hills
Location within depression (c.f. Fig. 7)	150-350 km ahead of surface warm front	In warm sector, within 350 km of depression centre, and extending up to 150 km ahead of surface warm front
Distribution of vertical air motion	Absence of small-scale vertical air motions in excess of 25 cm s^{-1}. Large-scale ascent of order 10 cm s^{-1} over fairly deep layer above warm frontal zone; large scale descent of a few cm s^{-1} below warm frontal zone	Over Pershore the principal updraughts were concentrated within high-level generator cells and were of the order of 1 m s^{-1} or less; below 3 km descent predominated, except just ahead of the surface warm front. Heavy rain areas within the B_1 or B_2 bands were associated with stronger and/or deeper updraught cells
Small-scale structure of precipitation as seen on RH1 display.	Relatively uniform radar echo structure resembling Boucher's (1959) Type 3 classification	Clusters of closely spaced high level generator cells and streamers resembling Boucher's (1959) Type 2 classification. Also occasional low-level convective shower echoes resembling Boucher's Type 4 classification
Significance of orographic effects	Altogether negligible	Very important. Topography triggered B_2 bands which were responsible for rainfall rates exceeding 10 mm hr^{-1} over and downwind from hills

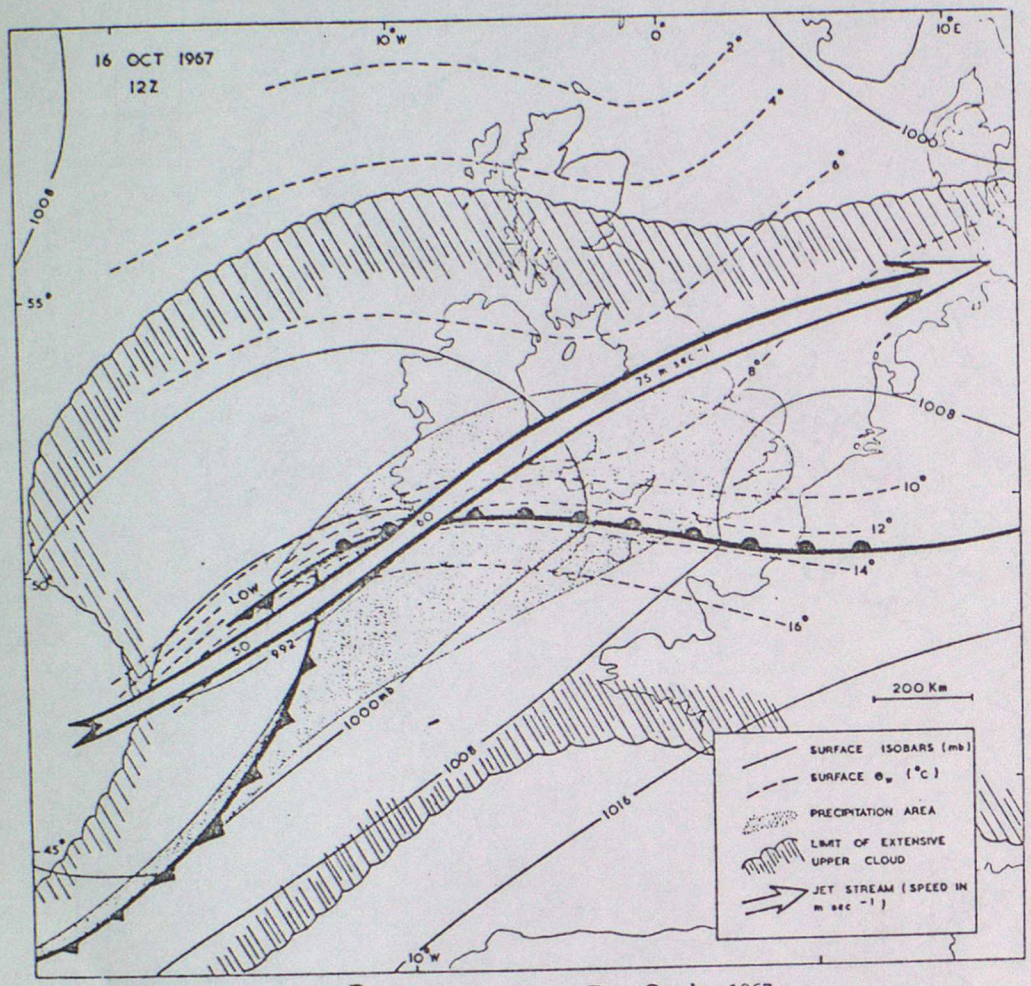

Figure 8. Synoptic situation 12 Z, 16 October 1967.

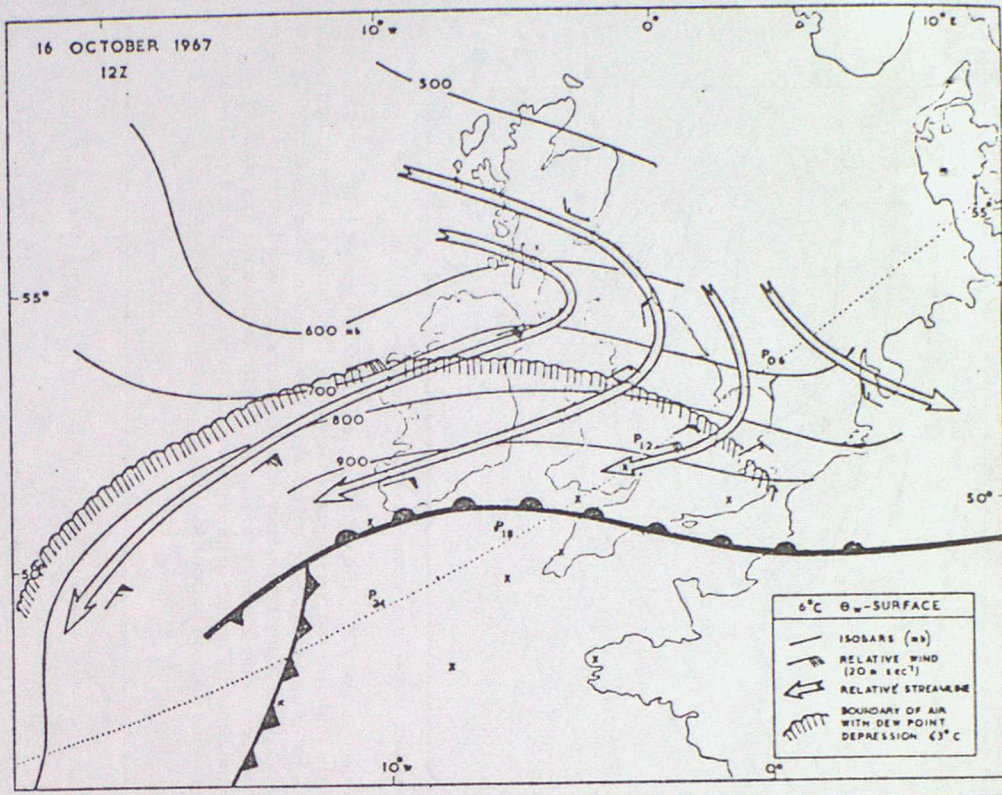

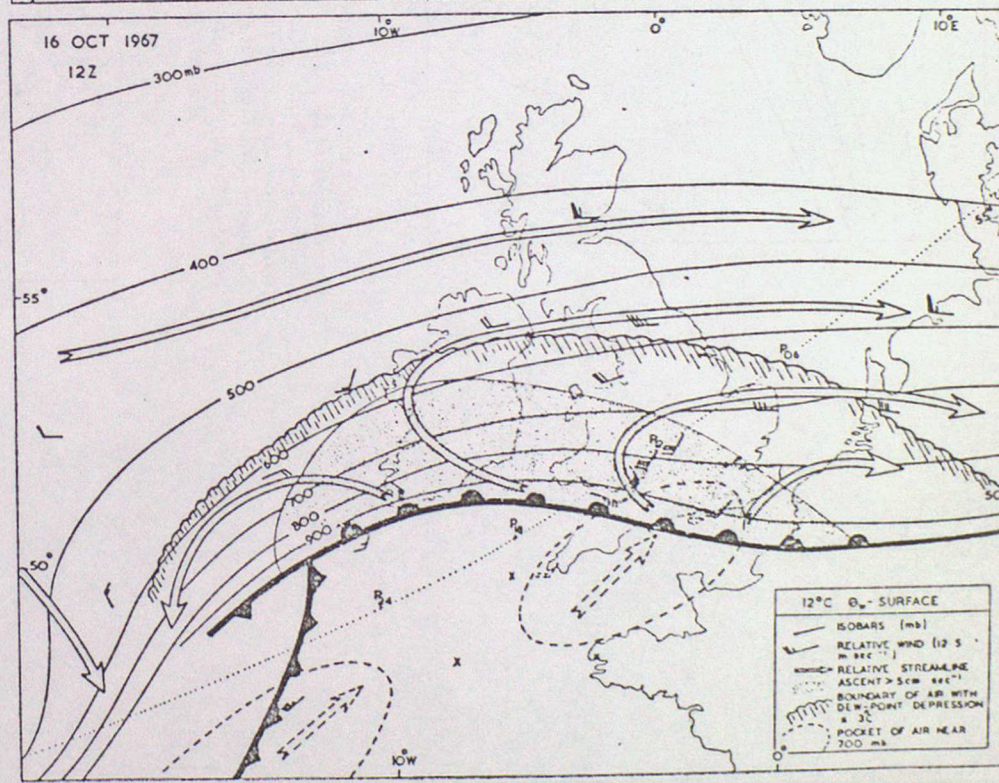

Figure 9 (a) and (b). Analyses for the 6° and 12°C θ_w-surfaces at 12 Z, 16 October 1967.

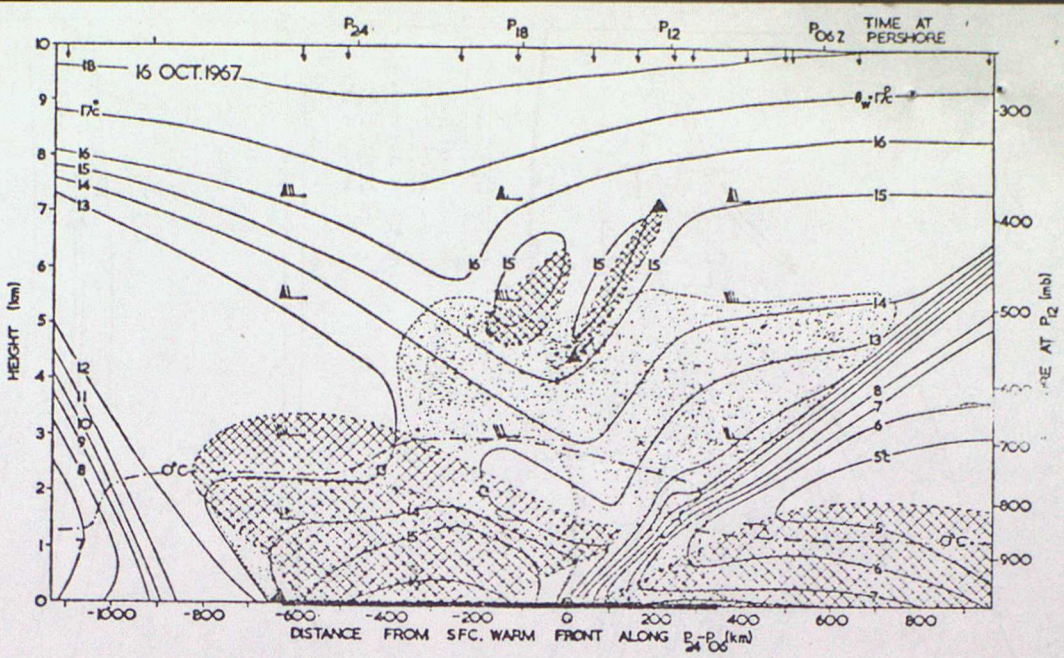

Figure 10. Analysis for vertical section along 245° through Pershore at 12 Z 16 October 1967. Solid lines are lines of constant θ_w. Wind barbs represent the component of the wind in the section relative to the system, a fullbarb being 5 m s^{-1}. Cross-hatching denotes potential instability. Stippling denotes moist air with dew point depression $\leqslant$ 3°C. The heavy line along the distance scale represents the overall extent of continuous and intermittent rain at the surface, ending at the passage of the surface cold front. The scale P_{06}-P_{24} at the top of the diagram represents time at Pershore assuming a translation velocity of 16 m s^{-1}. The arrows along the top of the diagram indicate the locations of radiosonde ascents.

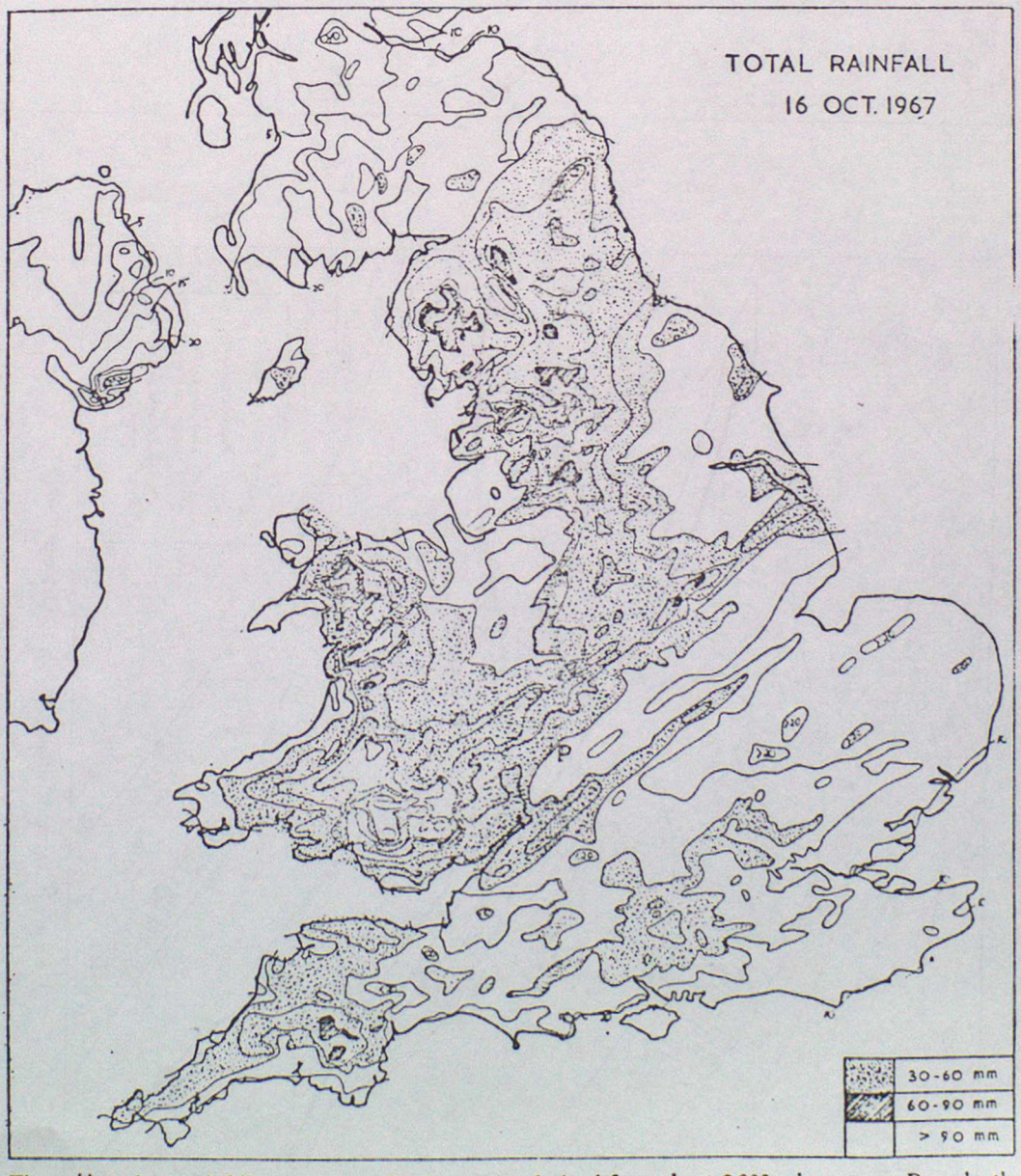

Figure 11. 24-hour rainfall amounts, 16 October 1967, obtained from about 2,000 rain-gauges : P marks the location of Pershore.

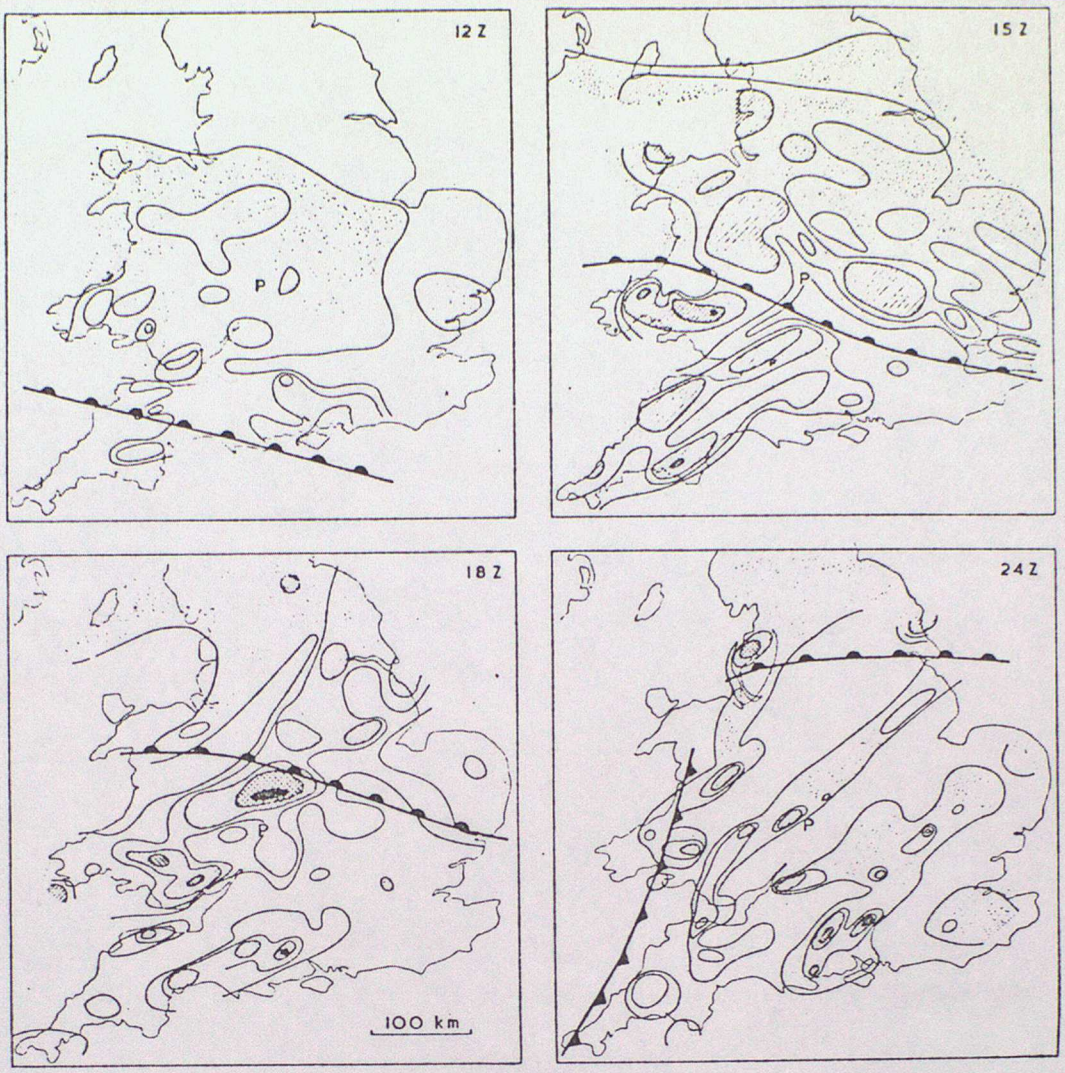

Figure 12 (a)-(d). Surface distribution of rainfall rate (averaged over 10 minutes) at 12, 15, 18 and 24 Z on 16 October 1967, obtained from the autographic rain-gauges. Isopleths are indicated for rates of 0·5, 2, 4, 8 and 12 mm hr^{-1}. Areas of moderate rain (0·5-4 mm hr^{-1}) are stippled; areas of heavy rain are hatched (4-8 mm hr^{-1}), cross-hatched (8-12 mm hr^{-1}) and black (> 12 mm hr^{-1}). *P* marks the location of Pershore.

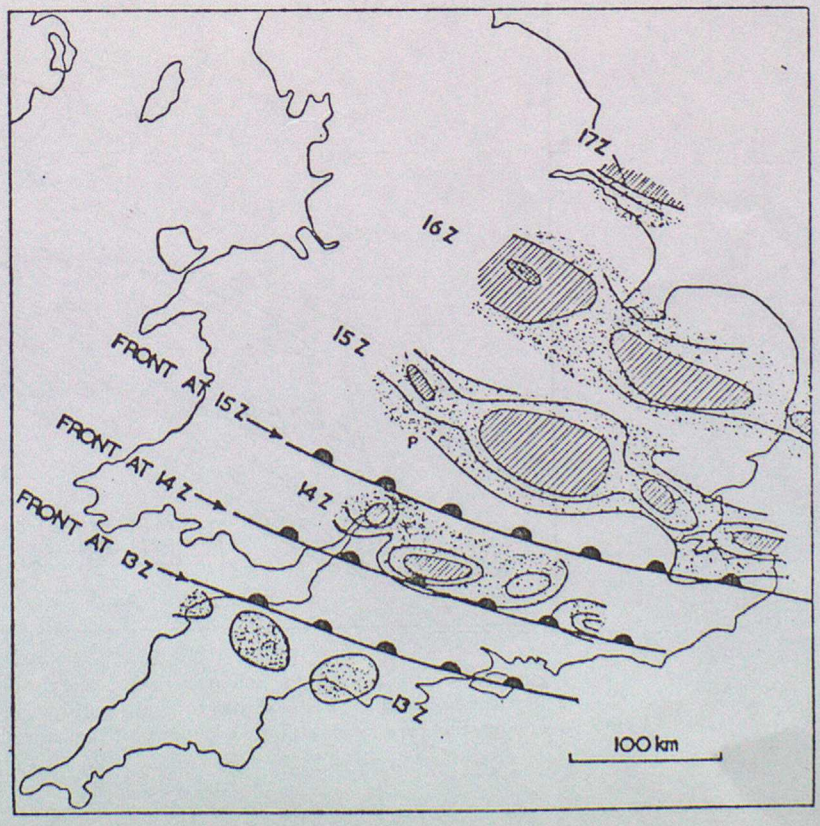

Figure 13. Successive hourly positions of a rain band (Type B_1). Isopleths are indicated for rates of 0·5, 2, 4 and 8 mm hr^{-1}. Areas of moderate rain (0·5-4 mm hr^{-1}) are stippled; areas of heavy rain are hatched (4-8 mm hr^{-1}) and cross-hatched (> 8 mm hr^{-1}).

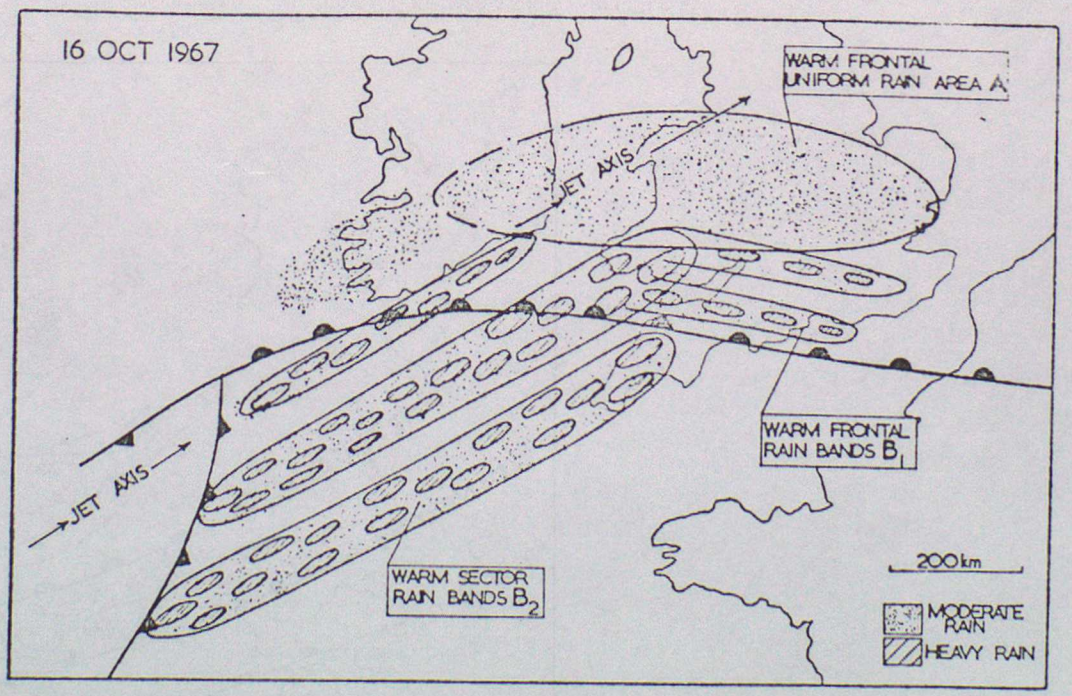

Figure 14. Composite diagram showing schematically the distribution of rainfall régimes within the depression. The outline of land at 12 Z is shown to give an indication of scale. The diagram is based upon observations over land; the Type B_2 bands were orographically enhanced and may not have been major features over the sea.

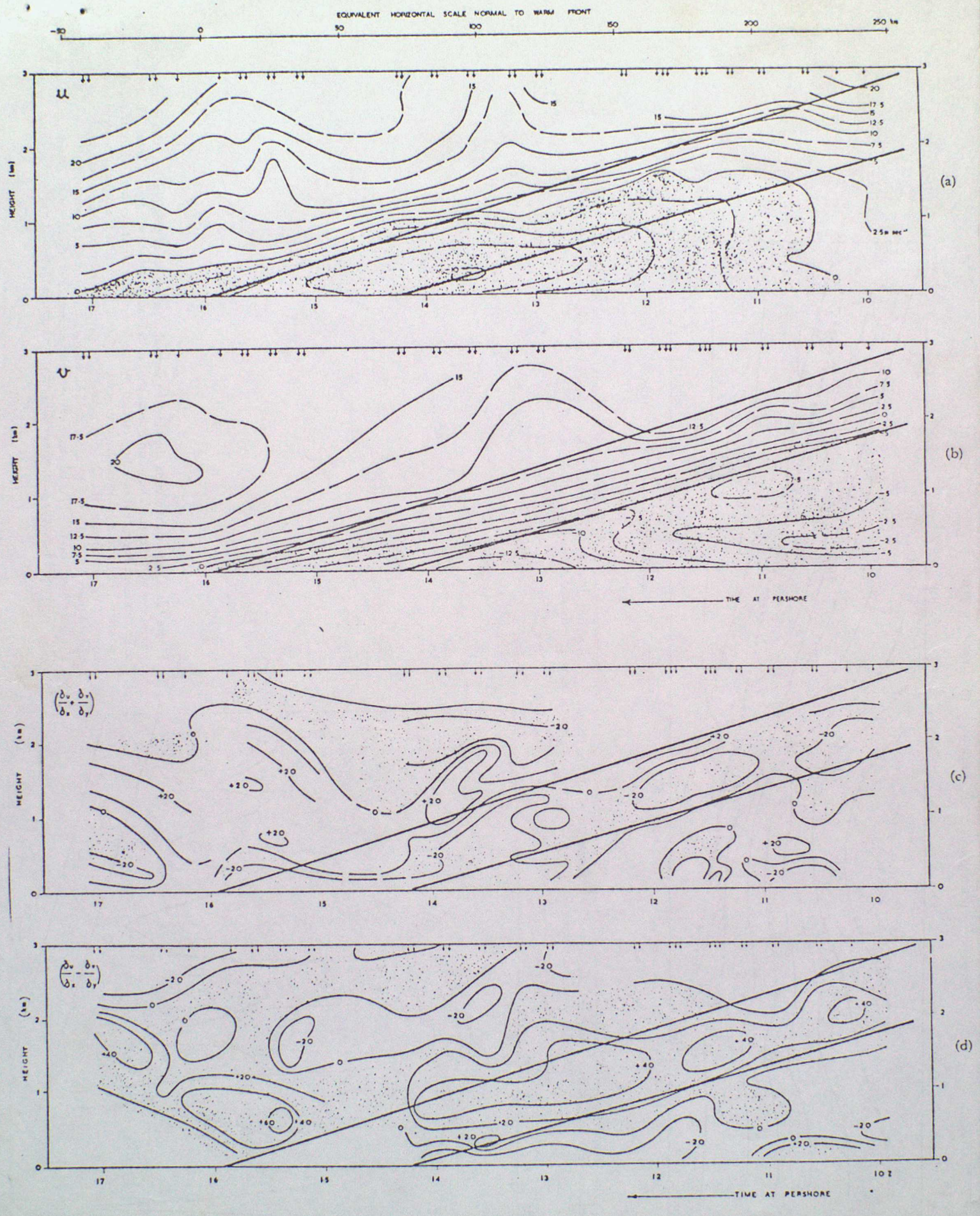

Figure 15 (a)-(d). Time-height sections showing basic wind field data in the vicinity of the warm front obtained with the Doppler radar at Pershore.

Fig 15 (a) and (b) show the u and v components of the wind, with isotachs at intervals of 2·5 m s^{-1}. (See text for definition of u and v).

Fig. 15 (c) and (d) show divergence, and stretching deformation in the parallel-front direction, with isopleths at intervals of 20×10^{-3} s^{-1}.

The warm frontal zone is indicated by the two straight lines.

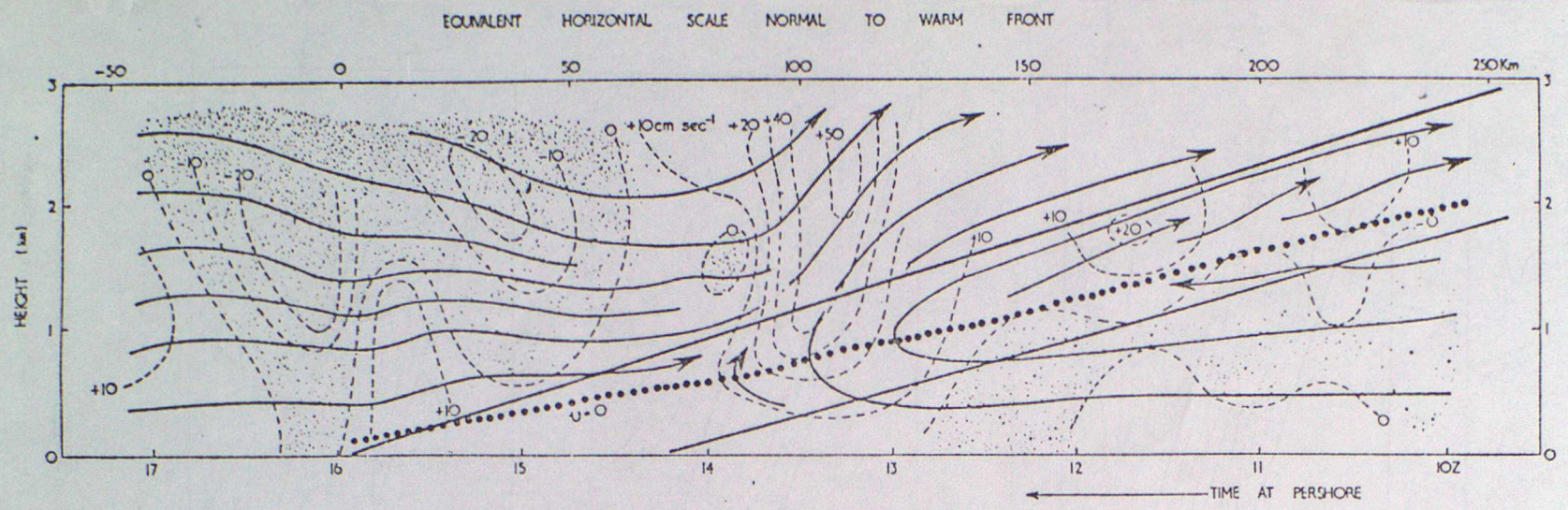

Figure 16. Time-height section showing vertical air velocity w (dashed isopleths) and the transverse circulation (solid streamlines) in the vicinity of the warm front as it passed over Pershore, derived from Fig. 15 (c) and (b). Isopleths of w are shown at intervals of 10 cm s^{-1}, regions of downward motion being stippled. The dotted line corresponds to $v = 0$. The warm frontal zone is indicated by two straight lines.

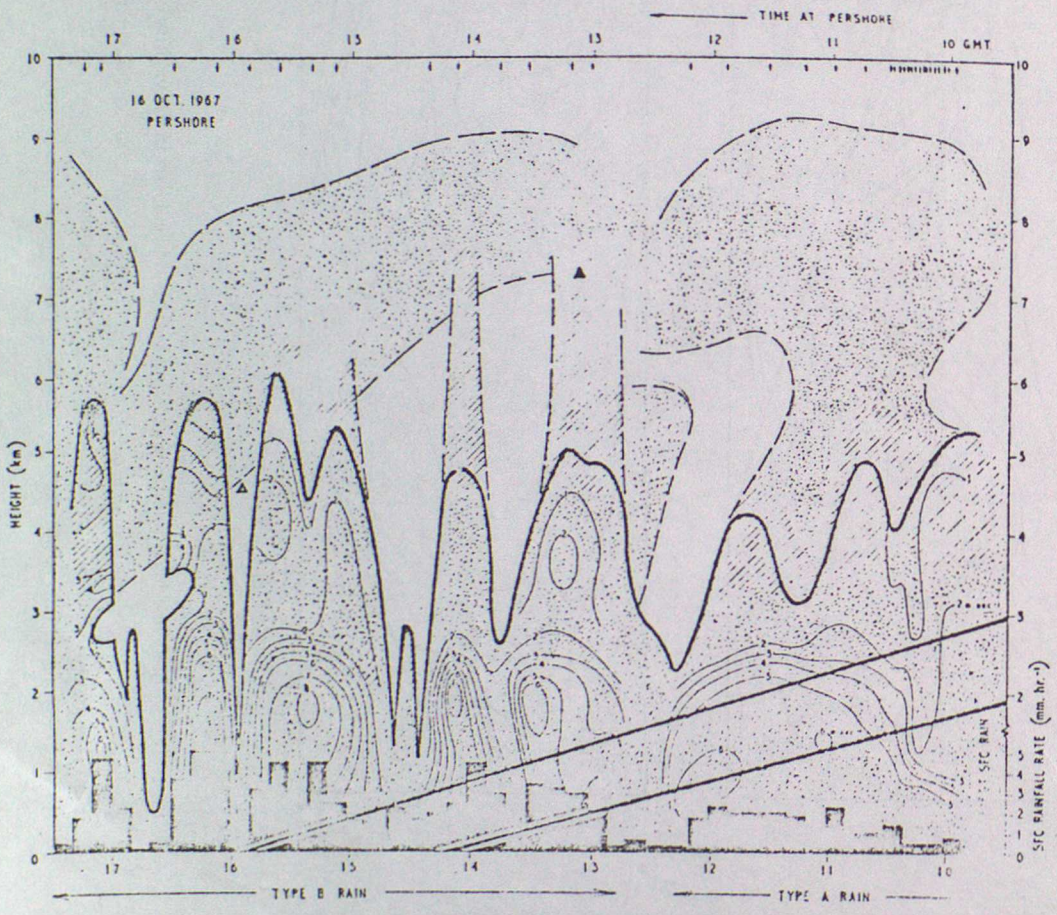

Figure 17. Time-height section showing the vertical distribution of precipitation echo in the vicinity of the warm front at Pershore. The warm frontal zone is indicated by the two straight lines. The heavy solid contours represent the extent of echo detected by the Doppler radar at Pershore when its aerial was pointing vertically. The thin solid isopleths at intervals of 1 m s^{-1} represent the reflectivity-weighted mean particle fallspeed V_f measured by the Doppler radar. The melting level is situated where V_f changes sharply in the vertical from 2 to 5 m s^{-1}. The heavy dashed contours represent the extent of relatively weak echo detected at higher levels by the TPS-10 radar. Areas where clusters of precipitation generators were observed are shown hatched. Surface rainfall rate at Pershore is plotted at the bottom of the diagram.

FRONTS IN THE ATMOSPHERE

LECTURE THREE - Observational characteristics of mid-latitude fronts - Part II

1. Introduction

In Part II of this topic further case studies of air motion and precipiation associated with fronts crossing the British Isles are presented. These studies, reported by Browning and Harrold (1970) and Browning and Pardoe (1973), deal with some characteristic features of active cold fronts.

2. Air motion and precipitation associated with active cold fronts

2.1 This section summarises the results of a case study (cold front crossing the British Isles on 6 February 1969) selected to reveal as clearly as possible the main dynamical features of an ana-cold front. The full details of this study have been described by Browning and Harrold (1970).

(a) Synoptic analysis of the cold front of 6 February 1969

Fig 1a shows the synoptic situation for 1200 GMT on 6 Feb 1969; the cold front traversed the British Isles steadily at 12 ms^{-1} from 315°. The satellite picture revealed a band of medium cloud about 160 km wide extending to the rear of the front with a much narrower line of thicker cloud (a few kilometres wide) at its leading edge associated with a line of vigorous updraught ("line convection" along the surface cold front (SCF)). Rainfall from the frontal cloud varied from 2 to 10 mm according to the orography, about half falling as heavy precipitation associated with the line convection. Note, in Fig 1a, the narrow tongue of warm air just ahead of the SCF, being advected almost parallel to the front by the strong geostrophic flow.

The isentropic ($\theta_w = 4°C$) analysis show in Fig 1b illustrates the broad scale air motions relative to the motion of the front. At levels between 1 km and 3 km the relative flow was virtually parallel to the cold front (and is represented in Fig 1b by the solid wind symbols and arrows). Below 1 km, where the winds were backed owing to the effect of surface friction, there was a significant component of relative flow towards the cold front (this is represented in Fig 1b by the dashed wind symbols and arrows, based on the 300 m winds). The overall flow pattern within the pre-frontal warm tongue was one in which the flux towards the front in the lowest kilometre was fed by subsiding air which had been advected parallel to the front. Data presented in (b) below indicates that air from the lowest kilometre of the warm tongue ascended almost vertically in the line convection at the SCF. Behind the SCF the air with $\theta_w = 4°C$ occupied a layer between 0.5 km and 1 km deep as it continued to ascend at a small angle to the horizontal.

Fig 1c shows a vertical cross-section normal to the SCF; the main cold front zone (CFZ) extends downwards from 5 km with an average slope of 1 in 50, finally reaching the ground as a near-upright wall about 1 km high. Ahead of the front the warm moist air (within what has come to be termed the "conveyor belt") lay beneath a subsidence inversion associated with an anticyclone over Europe.

(b) Fine-scale air motion and precipitation (radar data)

Fig 2 shows an outline of the precipitation echo as the SCF moved across the radar site (Pershore) at about 1117 GMT. It can be seen that, to a first approximation the flow near the SCF may be treated as 2-dimensional (with $\partial w/\partial x \ll \partial v/\partial y$). Several Doppler radar scans normal to the front were made, as indicated by the arrows in Fig 2. Fig 3a shows the distribution of v (relative horizontal motion perpendicular to front) close to the front, derived from a Doppler radar scan at 1124-1125; note the implied large values of $\partial v/\partial y$ ($\approx 10^{-2}$ s^{-1}) very close to the SCF.* An approximate field of vertical motion (w) derived from the continuity equation ($\partial v/\partial y \approx -\partial w/\partial z$) is shown in Fig 3b, together with a schematic impression of the tranverse (v, w) circulation associated with the front at 1125. Fig 3c shows a similar diagram for 1127. Eight of these diagrams (one for each Doppler radar scan) were constructed, effectively covering a 24 km length of the front, and Fig 3c represented the largest observed deviation from the simple flow pattern in Fig 3b.

The average structure at the leading edge of the cold front was as follows. In the warm air the flowwas nearly parallel to the front above the friction layer, with a component of only 1 or 2 ms^{-1} away from the front compared with one of 24 ms^{-1} parallel to it. Below 1.1 km the warm air approached the front at an average rate of 110 kg s^{-1} (per cm parallel to the front). Half of this flux occurred within the lowest 400 m and would have been very susceptible to the influence of topography. The warm air began ascending abruptly just ahead of the SCF and convergence values averaged over 500 m horizontally and vertically were as large as 10^{-2} s^{-1}. The updraught flow ascended at 60° to the horizontal, reaching a maximum rising speed of 8 ms^{-1} at 1.2 km. The top of the updraught was at about 3 km; beneath the summit divergence values averaged over 500 m horizontally and vertically were as large as 9×10^{-3} s^{-1}. Although a small proportion of the air left ahead of the front, most of it subsided briefly and left the summit area towards the rear at heights between 1.2 and approximately 2.7 km.

Browning and Harrold comment that, although the cold front of 6 February 1969 was sharper than most in the British Isles, the form of the air flow at the SCF was not thought to be exceptional, and in order to support that view, they presented another example of the tranverse air motion at another sharp cold front (3 October 1967) - see Fig 4. The configuration of the streamlines here is remarkably similar to that of 6 Feb 1969 (Fig 3b).

To examine more closely the nature of the shallow slope convection above the CFZ, time-height sections of u, v, divergence, deformation and w (integrated divergence) are shown in Fig 5(a-e); Fig 6 depicts the implied tranverse (v, w) circulation and shows that, after the initial abrupt ascent at the SCF, the warm air from the friction layer ascended rearwards relative to the system through

---

* The orientation of the x-y axes relative to the front is similar to that adopted in the warm front study in Part I.

a rather shallow gap between the advancing wedge of cold air and the stable layer at 3 km. Overall there was a well-marked direct circulation, with ascent of typically 20 cm s^{-1} in the warm air and generally rather weaker descent in the cold air.

Fig 7 shows the radar-derived precipitation structure associated with the front, together with approximate precipitation trajectories which were derived by combining the mean particle full-speeds measured by the Doppler radar with the wind data in Fig 5b. Calculations of the efficiency of precipitation production indicated that a large proportion (about 60 per cent) of the water vapour influx reached the ground as precipitation. Of the remainder about 20 per cent evaporated during the descent of precipitation through the cold air.

2.2 In this section the main findings of six case studies of pre-cold frontal low-level jets (Browning and Pardoe (1973)) are summarised. Figures 8a-8f shows the 1000-500 mb thickness fields and surface frontal analyses for the six cases, one of which has already been discussed from other points of view in section 2.1 above. The lines AB (and ab in Fig 8c) indicate the plane of the cross sections presented later. These studies were based on routine upper air data, supplemented by special sequential radiosonde and/or Doppler radar wind data from a single site. Most of the data are presented in the form of vertical sections perpendicular to the relevant cold front, derived from data acquired within ± 6 hr of map time and displaced according to the velocity of travel of the frontal system. Five of the cases used supplementary detailed data obtained as the fronts crossed the RRE field sites at Pershore or Defford (Worcestershire). The other case (11 November 1970) uses data obtained on the Isles of Scilly (IOS); this data has the advantage of being free from the complicating effects of topography.

Radar observations revealed that all of the fronts where characterized by a well-defined band of heavy rain which was essentially two-dimensional, containing hardly any cellular structure. This rain band was typically only 2 km wide and extended to a height of 3 km at most. It occurred at the forward edge of the main cold outflow (the SCF), and is what would be identified by the ordinary weather analyst as the cold front. The band of heavy rain was produced by an equally narrow band of vigorous line convection; this feature coincided in every case with the very sharp, cyclonically sheared, boundary of the pre-frontal low-level jet (LLJ). The heavy rain due to the line convection occurred in conjunction with a more extensive region of lighter rain due to slantwise convection, this being associated with the further ascent of the same air which earlier had ascended in the line convection. In cases (b), (c), (e) and (f) the light surface rainfall extended between 70 and 150 km behind the SCF; in case (d) the light rain extended about 100 km behind and 50 km ahead of the front; in case (a) the extent of rain was small, the front only just having become active at the time of observation.

The low-level jets of 11 Nov 1970

Fig 9 shows the distribution of wind speed at 900 mb, with the hatched area indicating the main LLJs. Figs 10a (isotachs of wind component parallel to front), 10b (potential temperature) and 10c (wet bulb potential temperature) indicate the broad-scale features in the vertical section along the line AB in Fig 8c. Three apparently discrete LLJs are located ahead of the SCF with wind maxima between 900 and 850 mb. At low levels the strongest winds (> 25 ms^{-1}) are

within the part of the LLJ system bounding the SCF; the jet is usually sharply bounded at the SCF with cyclonic shear $\approx 10^{-2}$ s^{-1}. These jets are often thousands of kilometres long and appear to be in approximate geostrophic balance. Fig 10b highlights the reversed temperature gradient ahead of the SCF which is responsible for the decrease in wind above the LLJ. In the absence of friction the jet maximum would be stronger and would probably occur at the surface. The anomolous warmth of the moist air associated with the jet just ahead of the SCF is attributable partly to the trajectories there originating farther south than other trajectories. Fig 10c highlights in particular the cold frontal zone (CFZ), the top of the convective boundary layer (CBL) ahead of the SCF, and the humidity structure. Note that at higher levels the air is relatively dry except where air from the CBL is "extruded" upwards above the CFZ. Axes of maximum veered and backed wind are indicated in this Figure by wavy lines. The backed flows correspond to air which has been turned frictionally towards the SCF and to the slantwise ascent of this same air above the CFZ where it has a distinct rearward component of motion relative to the advancing frontal system. The veered flows correspond to regions of descent and they occur within layers of locally lower relative humidity where the flow is forward, relative to the system.

Other examples of pre-cold frontal low-level jets

Cross sections similar to those in Fig 10a are shown in Figs 11a-15a, with the horizontal distribution of θ_w across the jets shown in Figs 11b-15b. These five cases all display many of the features noted in the 11 Nov 1970 case. Note, for example, the similarities in the heights and intensities of the LLJs, and their locations with respect to the SCF, the cold frontal zones and the associated upper level jets. In all cases there was an extrusion of moist air from the CBL into a region of relatively dry air in the middle troposphere, the initial extrusion having occurred in the form of shallow line convection at the SCF.

Mesoscale structure of the low-level jet of 11 Nov 1970

A sequence of special ascents, plus Doppler radar wind measurements, was made over an 11-hr period during the passage of this cold front over the Isles of Scilly (IOS). These have been synthesized to provide a detailed picture of the LLJ and the associated cold frontal convection in an area free from the complicating effects of topography. Time-height sections (corresponding to the line a-b in Fig 8c) are shown in Fig 16a and 16b, depicting the air motion and thermal structure respectively. In Fig 16a the flow pattern is relative to the moving cold front which was travelling from left to right with a component normal to the front of 6 ms^{-1}. After ascending at the SCF, air flows both forwards and rearwards; the forward flow descends a little and the rearward flow ascends. The ascent occurs in a slantwise manner with a maximum rearward velocity of typically 10 ms^{-1} and a vertical velocity of typically 10 cms^{-1}. It is associated with backed winds, and is concentrated over a depth of about 100 mb (1 km). The descending return flow is associated with locally veered winds and has a maximum relative forward velocity of 3 ms^{-1}. The forward return flow descends at a mean velocity of 1 or 2 cms^{-1} while advancing 100 km ahead of the SCF, during which time it will have travelled as much as 1000 km in a direction parallel to the front.

Tephigrams from three radiosonde ascents at IOS are shown in Fig 17. They correspond to positions 50 km behind the SCF (Fig 17a), 35 km ahead of the SCF (Fig 17b) and 150 km ahead of the SCF (Fig 17c). Fig 17b shows moist air up to about 750 mb within the CBL just ahead of the SCF where the weak return flow has not descended sufficiently to become noticeably drier or warmer. Fig 17c

shows the subsidence inversion within the descending return flow. The top of the return flow in the CBL is marked in Fig 17c by a pronounced decrease in relative humidity above 700 mb.

The analyses described here, combined with those of Browning and Harrold (1970) suggest a model of an ana-cold front with line convection and a low-level jet, as schematically depicted in Fig 18.

The majority of cold fronts can be placed in the two main categories of ana-cold and kata-cold fronts. As we have already seen, an ana-cold front is a cold front at which the warm air is ascending because it is moving forward less rapidly than the frontal surface beneath. A kata-cold front on the other hand is one in which the warm air is moving forward more rapidly than the front and therefore descending (although there may be a region of ascending warm air some distance ahead of the front). In view of the different vertical motions it would be reasonable to expect the kata-cold front to display quite different characteristics to those of the ana-cold front. Typically the kata-cold front contains very little frontal cloud and there is usually a rapid clearance of the cloud at the passage of the SCF; the temperature drop across the SCF is often small and precipitation generally slight (if any at all), and there may be only minimal veering of the surface wind following the passage of the front.

References and further reading:

BROWNING, K.A. HARROLD, T.W.	1970	Air motion and precipitation growth at a cold front. Q.J.R. Met.Soc.,96, pp 369-389.
BROWNING, K.A. PARDOE, C.W.	1973	Structure of low-level jet streams ahead of mid-latitude cold fronts. Q.J.R. Met Soc.,99, pp 619-638.
KREITZBERG, C.W. BROWN, H.A.	1970	Mesoscale weather systems within an occlusion J.Appl.Met., 9, p 417
BOSART, L.F.	1970	Mid-tropospheric frontogenesis Q.J.R. Met Soc., 96, p 442.
BROWNING, K.A. HARDMAN, M.E. HARROLD, T.W. PARDOE, C.W.	1973	The structure of rainbands within a mid-latitude depression Q.J.R. Met Soc., 99, p 215.
HARROLD, T.W.	1973	Mechanisms influencing the distribution of precipitation within barodinic disturbances Q.J.R. Met Soc., 99, p 232.
BROWNING, K.A. PARDOE, C.W. HILL, F.F.	1975	The nature of orographic rain at winter time cold fronts. Q.J.R. Met Soc., 101, p 333
ROACH, W.T. HARDMAN, M.E.	1975	Mesoscale air motions derived from windfinding dropsonde data: the warm front and rainbands of 18 January 1971. Q.J.R. Met Soc., 101, p 437.
BOSART, L.F.	1975	New England coastal frontogenesis Q.J.R. Met Soc., 101, p 957

Figure 1 (c) Analysis for the vertical section through Pershore (*P*) at 12 Z, 6 February 1969, along APB in Fig. 1 (a). Thick solid lines represent lapse rate discontinuities. Thin solid lines are isopleths of θ_{te} at 1°C intervals. Dashed lines are isotherms. The dotted line denotes the extent of ascent exceeding 10 cm s^{-1}. Areas of cloud or dew-point depression less than 4°C are stippled. The extent of precipitation echo is hatched. Jet axes are labelled *J*. Vertical lines indicate radiosonde ascents close to the section.

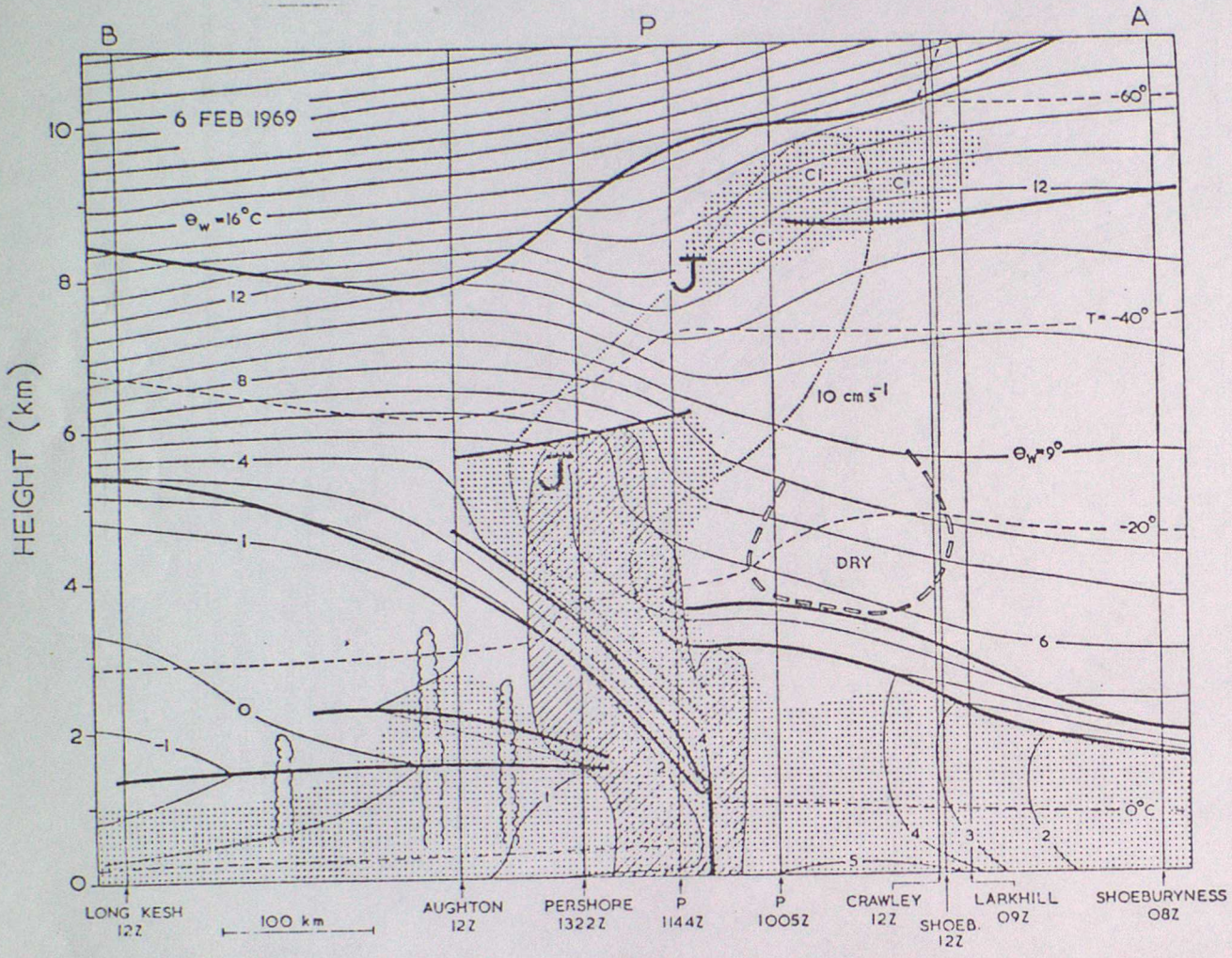

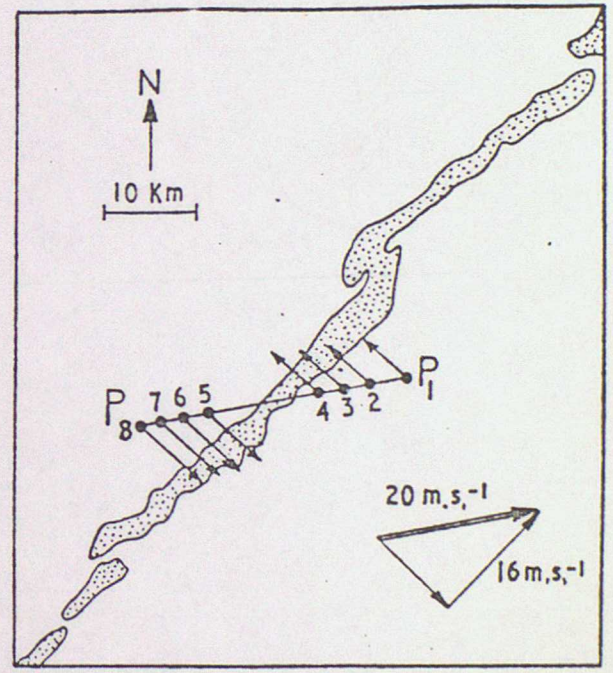

Figure 2. Outline of intense PPI radar echo corresponding to the period of heavy precipitation at the SCF as it crossed Pershore at 1117 Z on 6 February 1969. Recognizable elements within the line of echo travelled with a velocity of 20 m s^{-1} from 260° relative to the ground. P_1, ... P_8 represents the relative positions of Pershore at times 1102, 1106, 1110, 1113, 1120, 1123, 1125 and ... Arrows from these positions indicate the orientation of the vertical sections scanned by the Doppler radar.

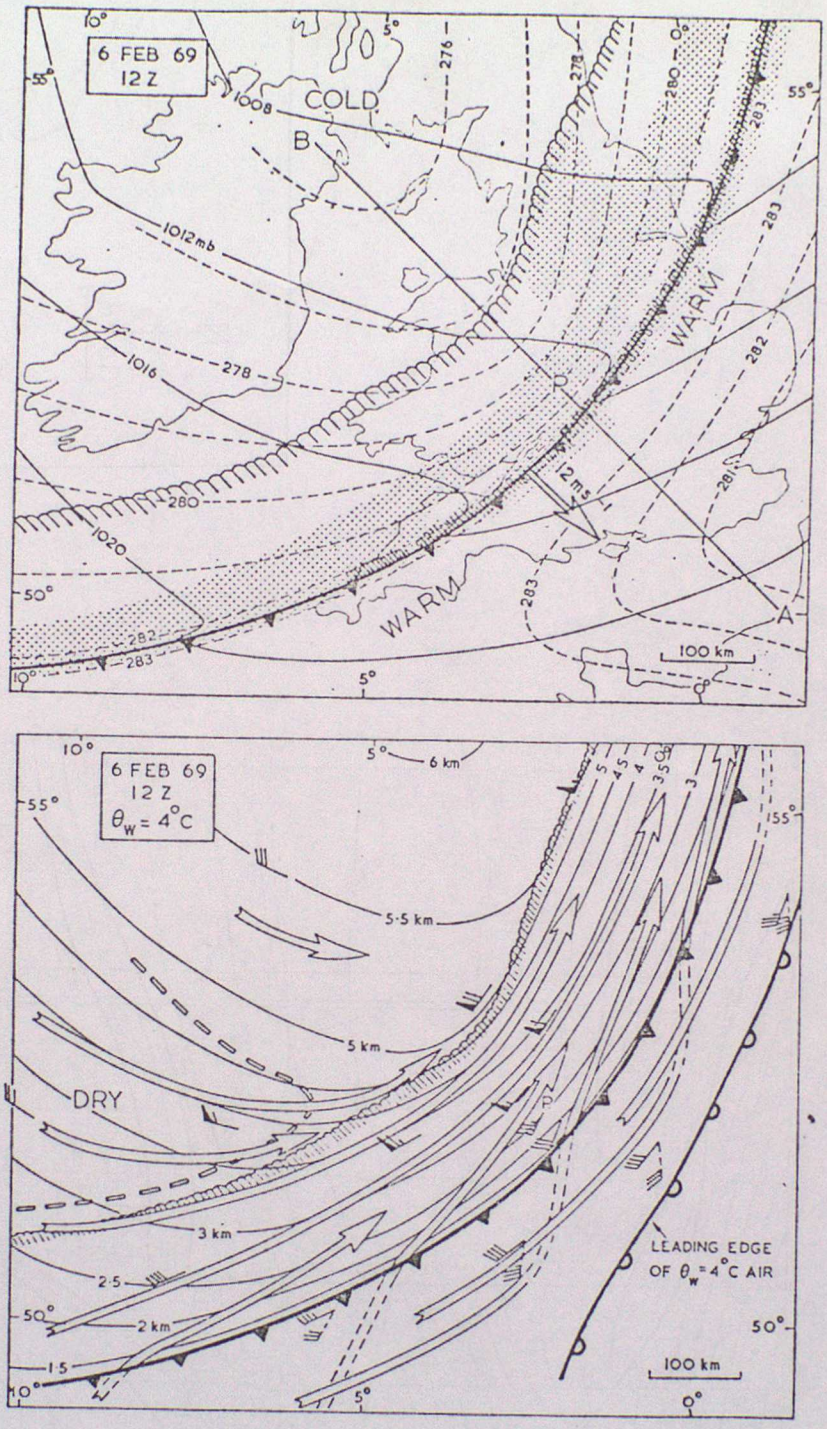

(a)

(b)

Figure 1 (a) Synoptic situation for 12 Z, 6 February 1969. Sea-level isobars are drawn at 4 mb intervals (solid lines), and 1,000-700 mb thickness contours at 10 m intervals (dashed lines). The leading edge of unbroken frontal cloud was close to the SCF, and the position of the trailing edge of the cloud belt is indicated by hatching. Surface precipitation is shown stippled, heavy precipitation along the SCF being closely hatched. APB marks the orientation of Fig. 1 (c), where *P* is the radar site at Pershore;

(b) Analysis in the layer with $\theta_w = 4°C$ at 12 Z, 6 February 1969. Height contours are at intervals of 0·5 km. Winds and streamlines show flow relative to the system, a full barb corresponding to 5 m s^{-1}. The number of wind observations corresponds to the number of radiosonde ascents used in this study. The outlined-dash contour represents the extent of air with a dew-point depression exceeding 8°C.

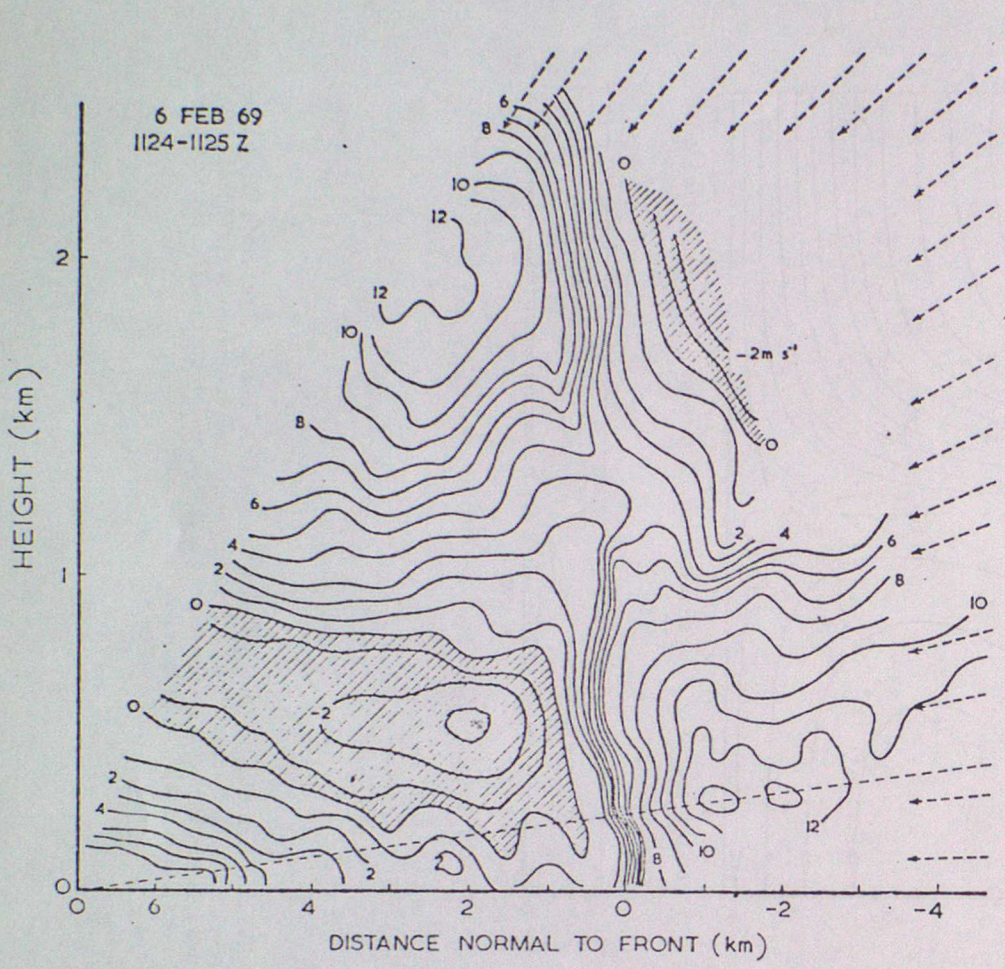

Figure 3 (a) Distribution of v in a vertical section normal to the SCF on 6 February 1969

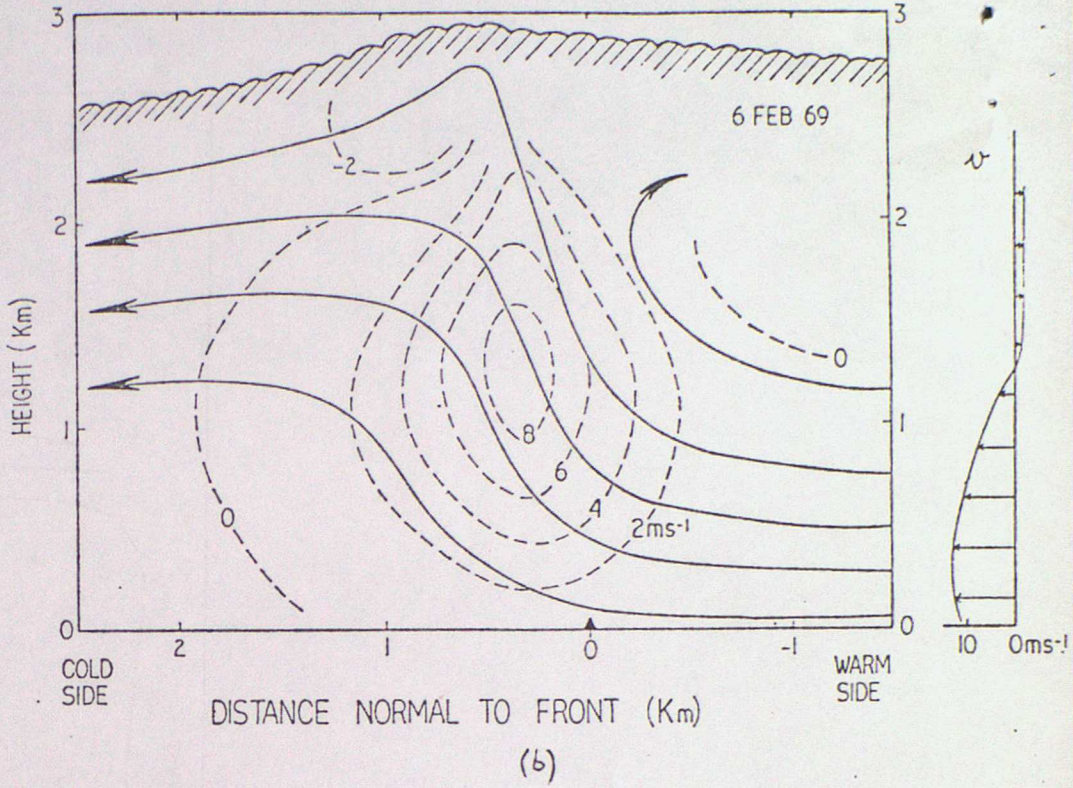

(b)

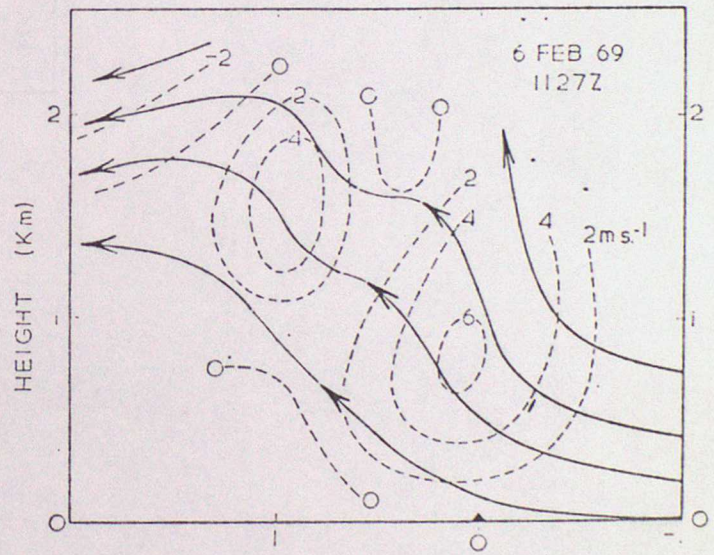

(c)

Figure 3 (b) Transverse circulation at the SCF at 1124-1125 Z on 6 February 1969, derived from Fig. 3(a) and from other similar data. The dashed lines represent vertical velocity at 2 m s^{-1} intervals; continuous solid lines are streamlines relative to the front, with a constant flux of 25 kg s^{-1} cm^{-1} between streamlines. The relative flow was weak and variable within the cold air behind the SCF. The profile on the right side of Fig. 3(b) represents the relative inflow (v) 2 km ahead of the SCF. Hatched shading denotes the top of the precipitation echo ; (c) Transverse circulation at the SCF at 1126-1127 Z on 6 February 1969, derived as for Fig. 3(b)

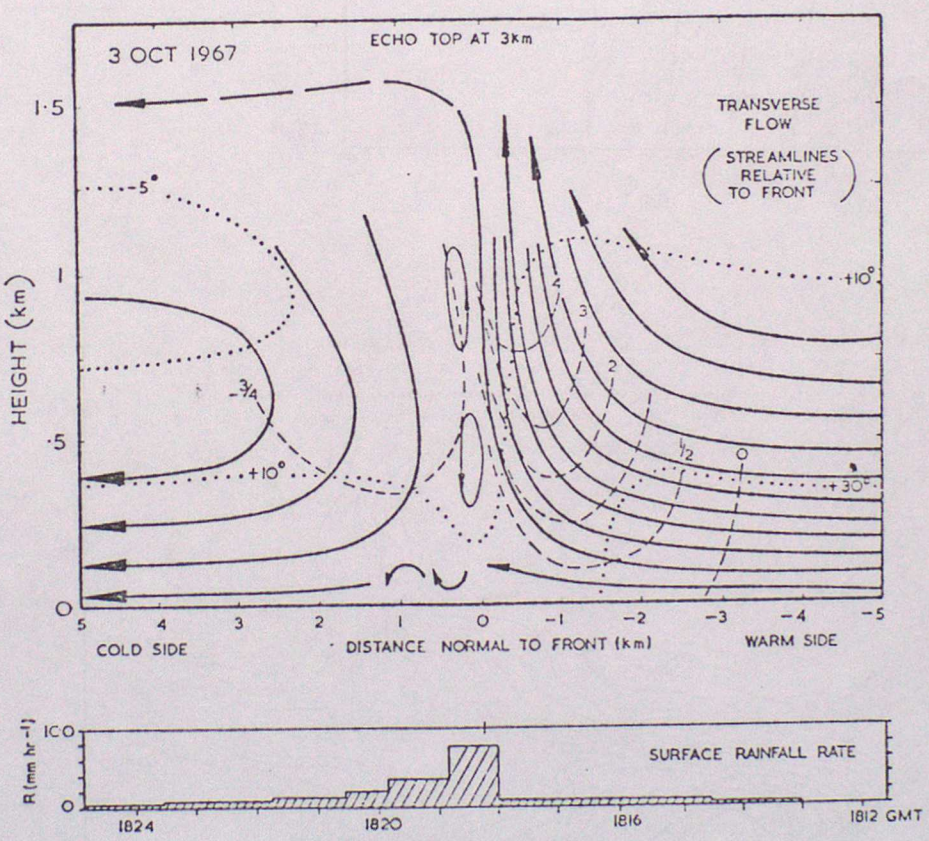

Figure 4. Transverse circulation at the SCF on 3 October 1967. Format is similar to Fig. 3 (c) and (d) except that streamlines relative to the front have arbitrarily been drawn at intervals of 11 (instead of 25) kg s^{-1} cm^{-1}, and dotted isopleths are shown giving the angle of flow relative to the front (i.e. $\tan^{-1} v/u$). Rainfall rate at the radar site is plotted below on an equivalent distance scale

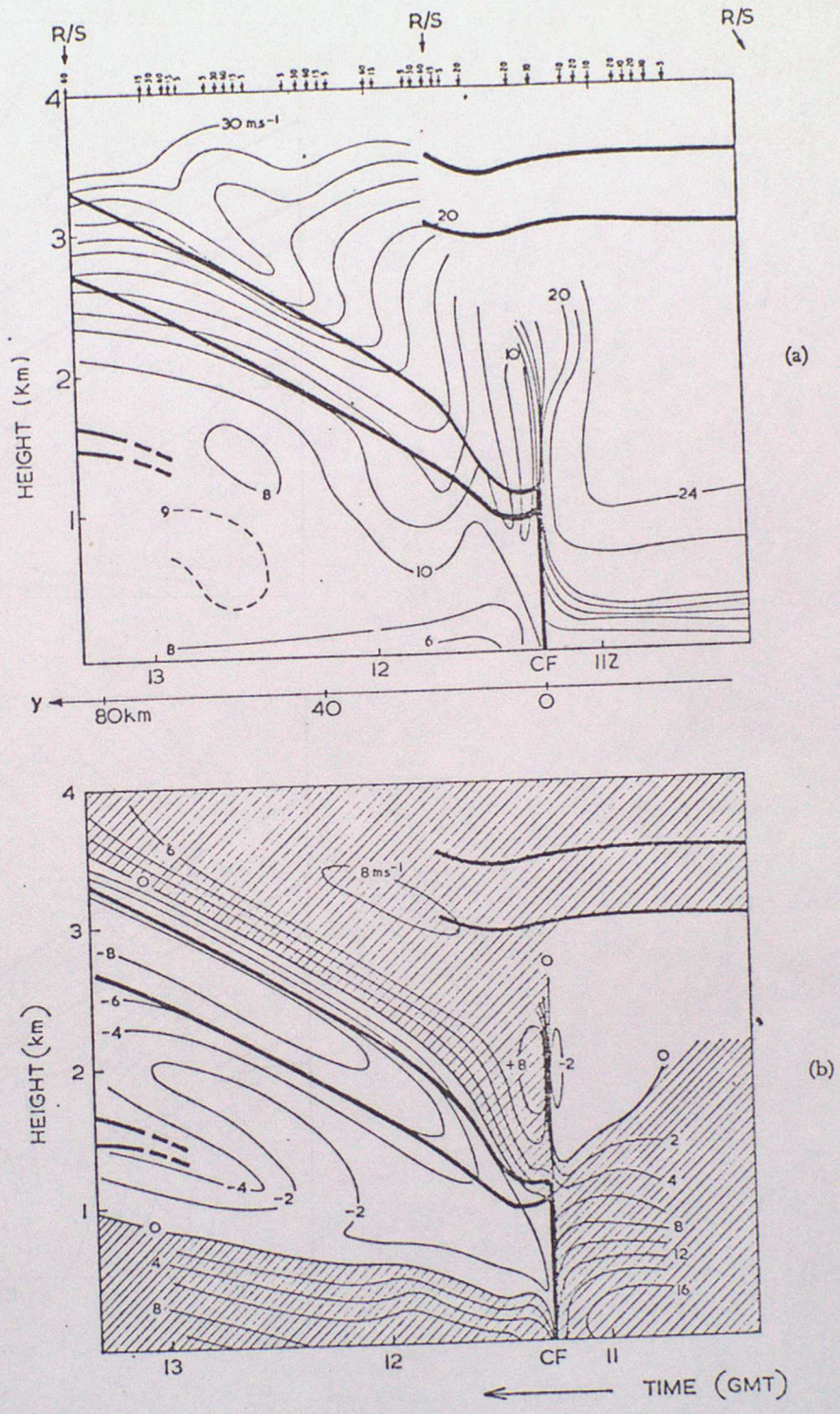

Figure 5 (a) Time-height distribution of u in the vicinity of the cold front of 6 February 1969 derived using conical scanning data from the Doppler radar at Pershore. Thin lines are isotachs of u at intervals of 2 m s^{-1}. Thick lines denote the boundaries of the frontal zone and other stable layers. Further details in text; (b) Time-height distribution of v in the vicinity of the cold front of 6 February 1969. Format is similar to Fig. 5 (a). Regions where v is directed rearwards relative to the front are hatched.

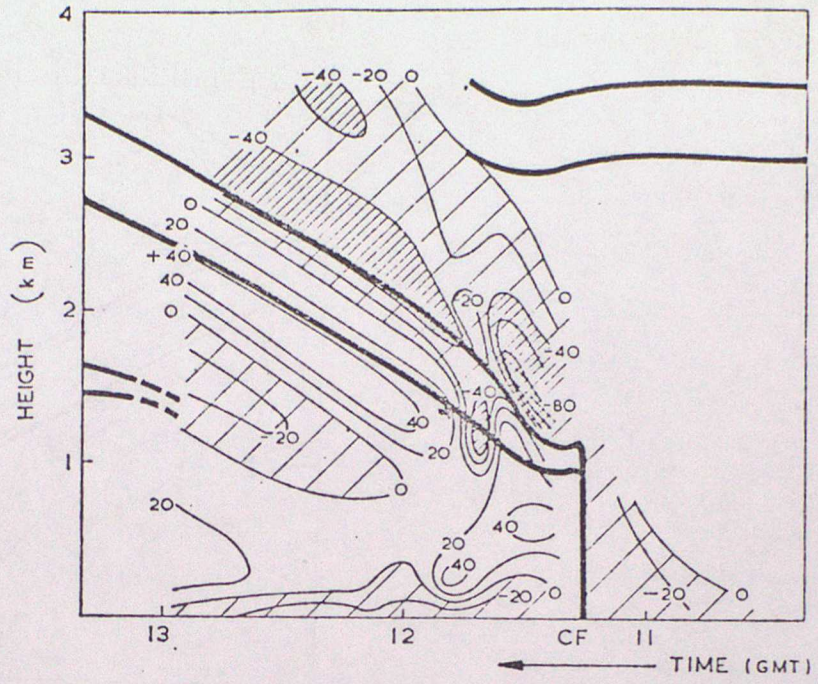

(c)

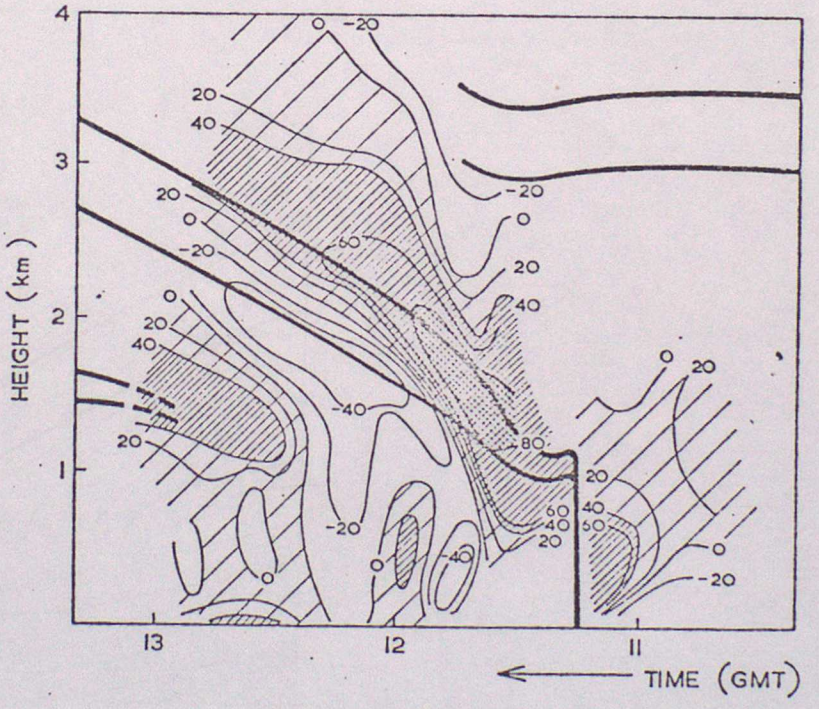

(d)

Figure 5 (c) Time-height distribution of divergence (div $V = (\partial u/\partial x) + (\partial v/\partial y)$) in the vicinity of the cold front of 6 February 1969. Format is similar to Fig. 5 (a). Thin lines are isopleths of div V at intervals of 20×10^{-5} s^{-1}. Regions with div V negative are hatched; the hatching is widely spaced where div V is between 0 and -40×10^{-5} s^{-1} and closely spaced where div V is less than -40×10^{-5} s^{-1}; (d) Time-height distribution of stretching deformation along the x-axis (def $V = (\partial u/\partial x) - (\partial v/\partial y)$) in the vicinity of the cold front of 6 February 1969. Format is similar to Fig. 5 (a). Thin lines are isopleths of def V at intervals of 20×10^{-5} s^{-1}. Regions with def V positive are hatched; the hatching is widely spaced where def V is between 0 and 40×10^{-5} s^{-1}, closely spaced where def V is between 40 and 80×10^{-5} s^{-1} and is cross-hatched where def V exceeds 80×10^{-5} s^{-1}.

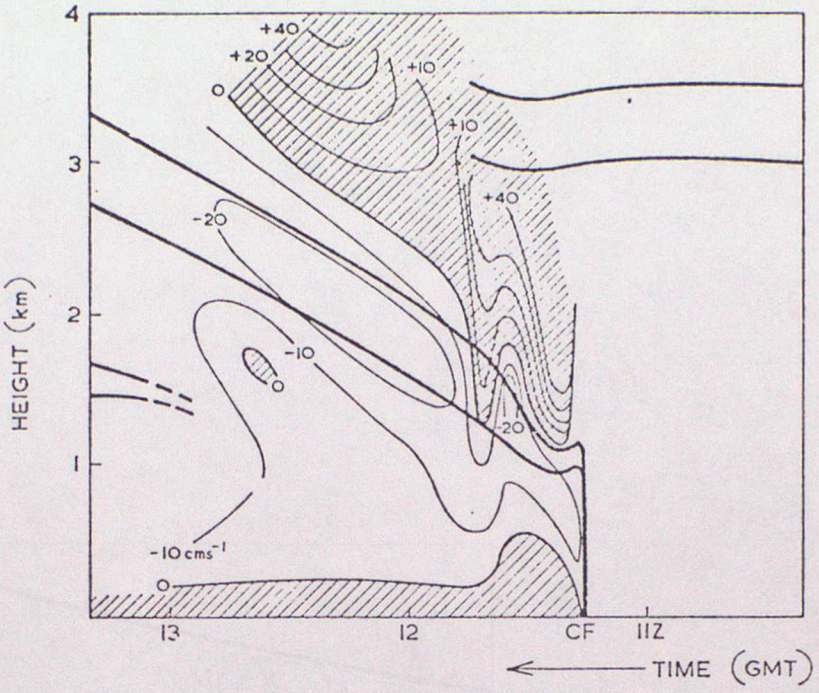

(e)

Figure 5 (e) Time-height distribution of w in the vicinity of the cold front of 6 February 1969, computed from Fig. 5 (c). Thin lines are isotachs at intervals of 10 cm s^{-1}. Regions of ascent are hatched.

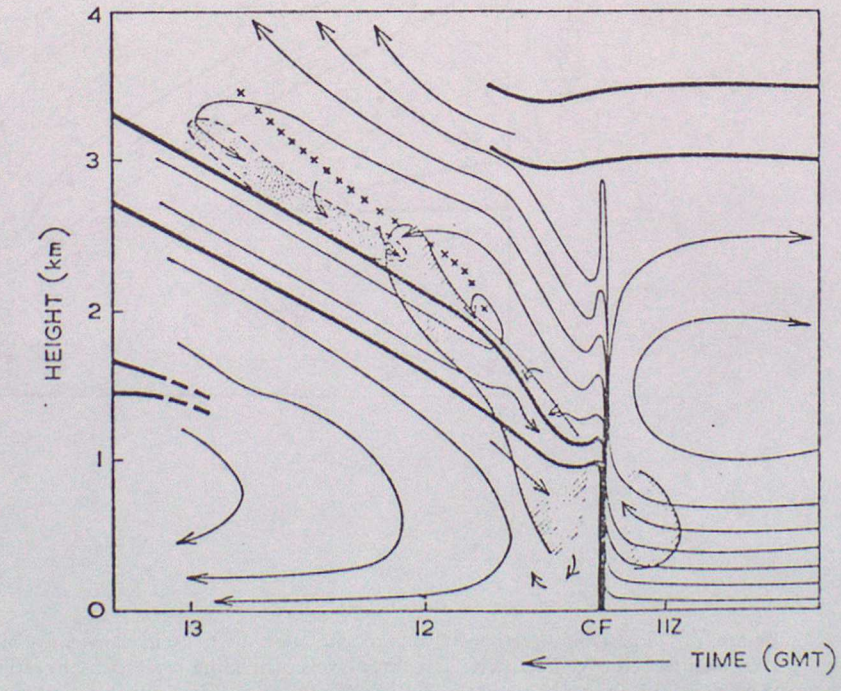

Figure 6 Time-height section showing the transverse circulation in the vicinity of the cold front of 6 February 1969 as it passed over Pershore, derived from Fig. 5. Thin solid lines are streamlines of flow relative to the system. Thick lines denote the boundaries of the frontal zone and other stable layers. Crosses denote the base of the main frontal cloud deck as inferred from the $w = 0$ isotach in Fig. 6 (e). Hatched shading indicates $(\partial u/\partial x) > 20 \times 10^{-5}\ s^{-1}$; stippled shading indicates $|\partial V/\partial z| > 3 \times 10^{-2}\ s^{-1}$.

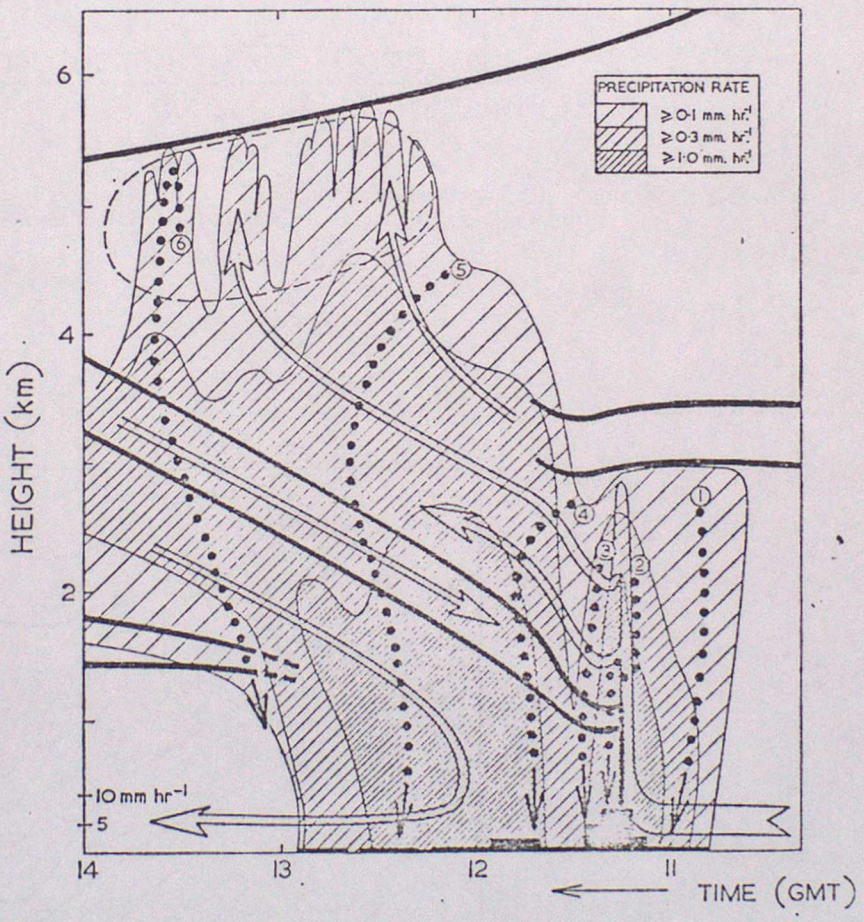

Figure 7. Time-height section showing precipitation intensity in the vicinity of the cold front of 6 February 1969 as it passed over Pershore. The three levels of shading correspond to estimated precipitation rates aloft in excess of 0·1, 0·3 and 1 mm hr^{-1}. Surface rainfall rate at Pershore is indicated along the abscissa. (The most intense precipitation occurred at the SCF ; however, because of the presence of hail in this region it is not possible to interpret quantitatively the radar reflectivity in terms of precipitation rate aloft). Solid arrows are streamlines, dotted lines are precipitation trajectories, thick lines denote the boundaries of the frontal zone and other stable layers, and the dashed line delineates the extent of small-scale convection at high levels.

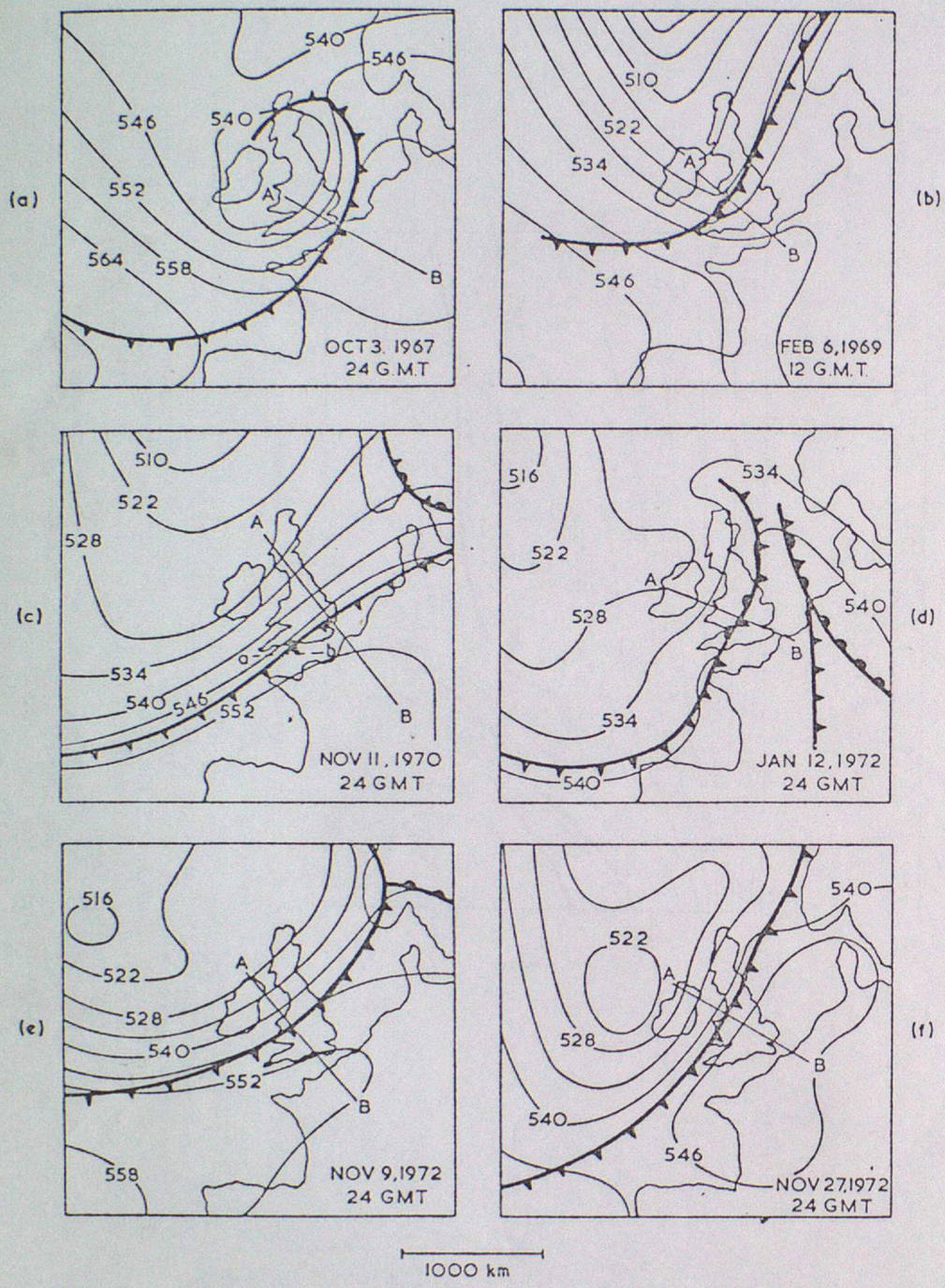

Figure 8 (a)-(f). 1,000-500 mb thickness patterns with isopleths labelled in decametres and surface frontal analyses for the 6 case studies. Taken mainly from the Daily Aerological Records.

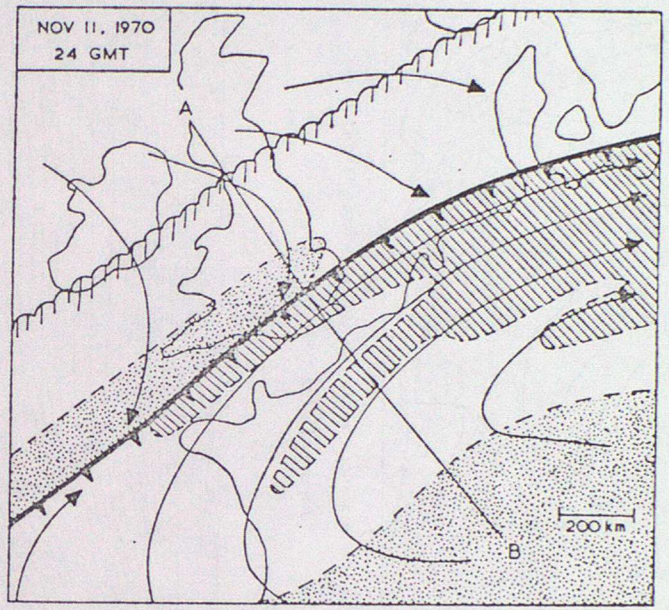

Figure 9. 900 mb analysis for 24 GMT on 11 November 1970 showing low-level jets with total windspeed in excess of 20 m s^{-1} as hatched shading and regions with winds less than 10 m s^{-1} as stippled shading. Streamlines represent flow at 900 mb relative to the cold frontal system. The rear edge of the cold front cloud deck aloft is drawn partly hatched.

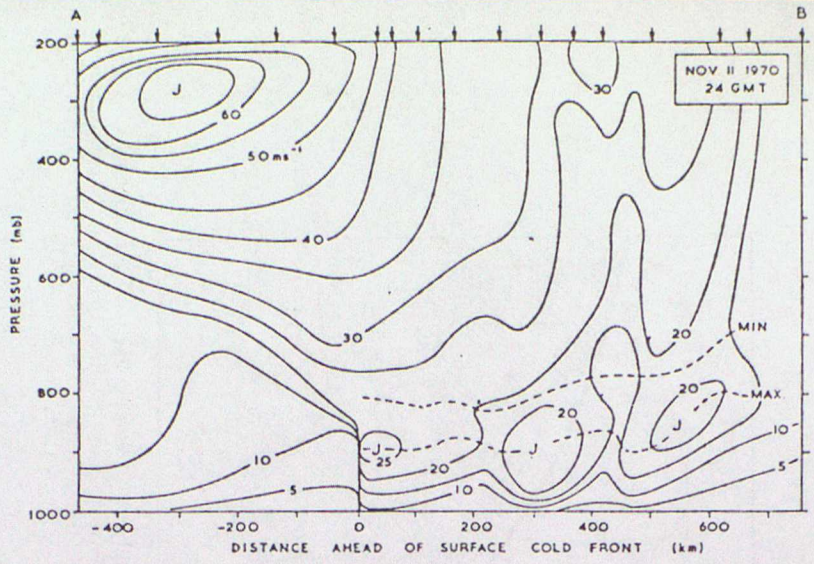

Figure 10(a)

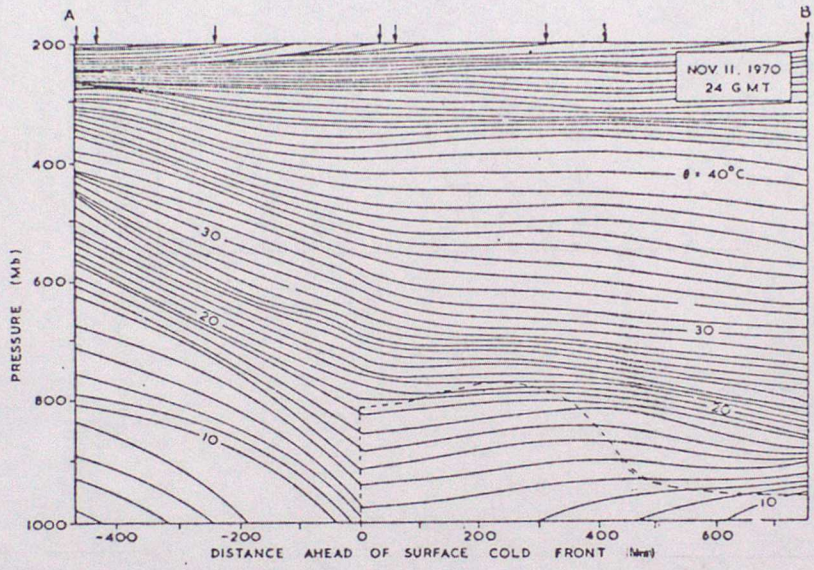

Figure 10(b)

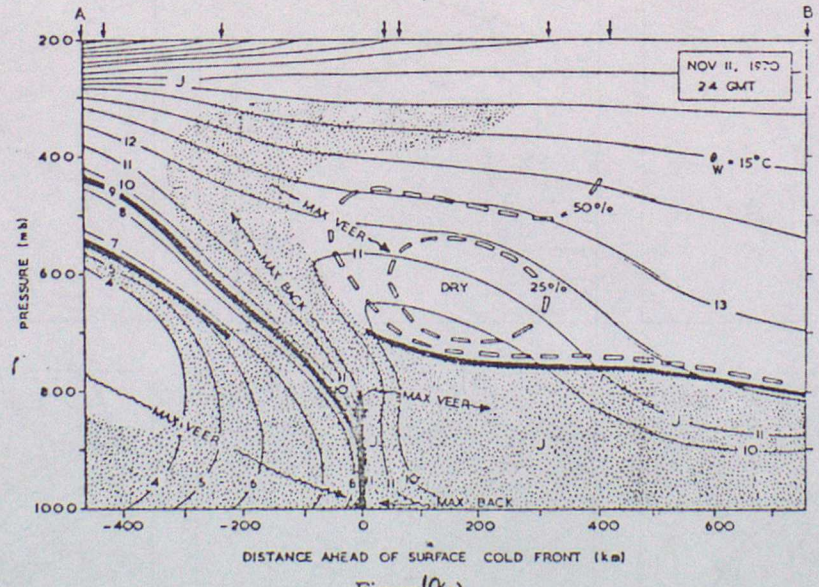

Figure 10(c).

Figure 10(a)-(c). Vertical cross sections along AB in Figs. 8(c) and 9 showing structure perpendicular to the SCF at 24 GMT on 11 November 1970. Arrows at top of diagrams show the locations of soundings close to the section. Fig. 10(a) shows the component of the wind parallel to the SCF (235°), with isotachs at intervals of 5 m s^{-1}. Fig. 10(b) shows the dry bulb potential temperature, θ, with isentropes at intervals of 1°C. The dashed line encloses a region where temperature increases towards the left (NW). The abruptness in the change of slope of isentropes above the position of the SCF has been inferred from additional data obtained on the Isles of Scilly. Fig. 10(c) shows the wet bulb potential temperature, θ_w, with isopleths at intervals of 1°C. The thick lines represent schematically the positions of the main cold frontal zone, a secondary cold frontal zone, and the top of the convective boundary layer ahead of the SCF. Contours are shown for relative humidities of 25 and 50 per cent, and areas exceeding 75 per cent are stippled. Wavy lines denote the axes of veered and backed airflows.

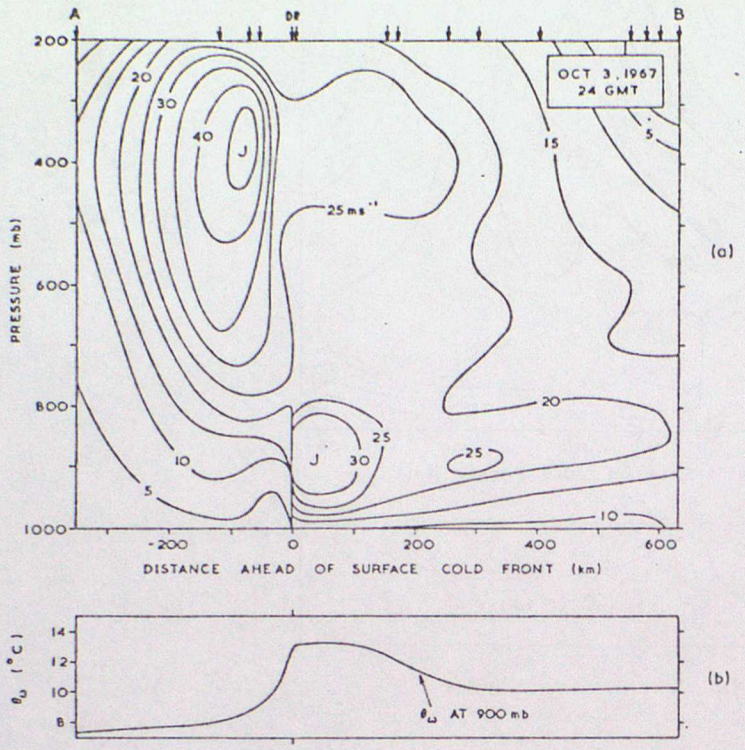

Figure 11.

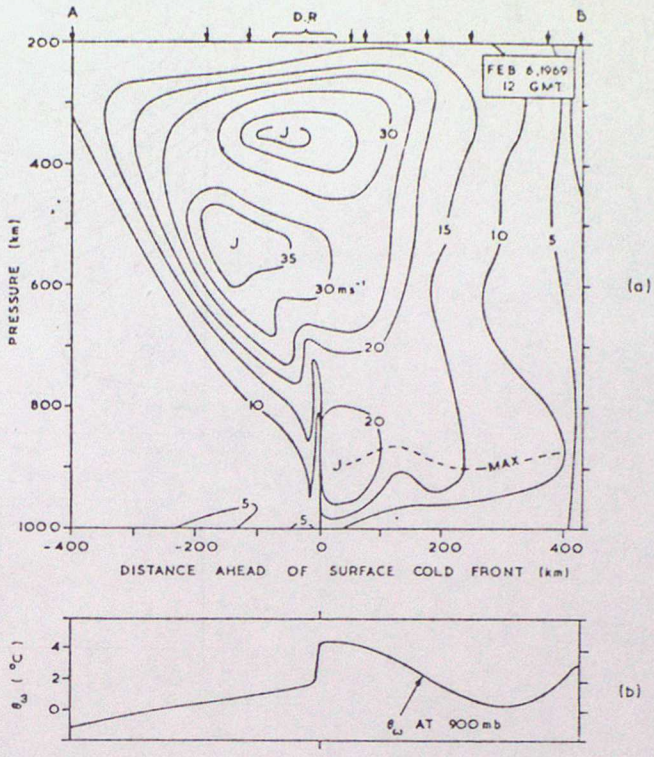

Figure 12

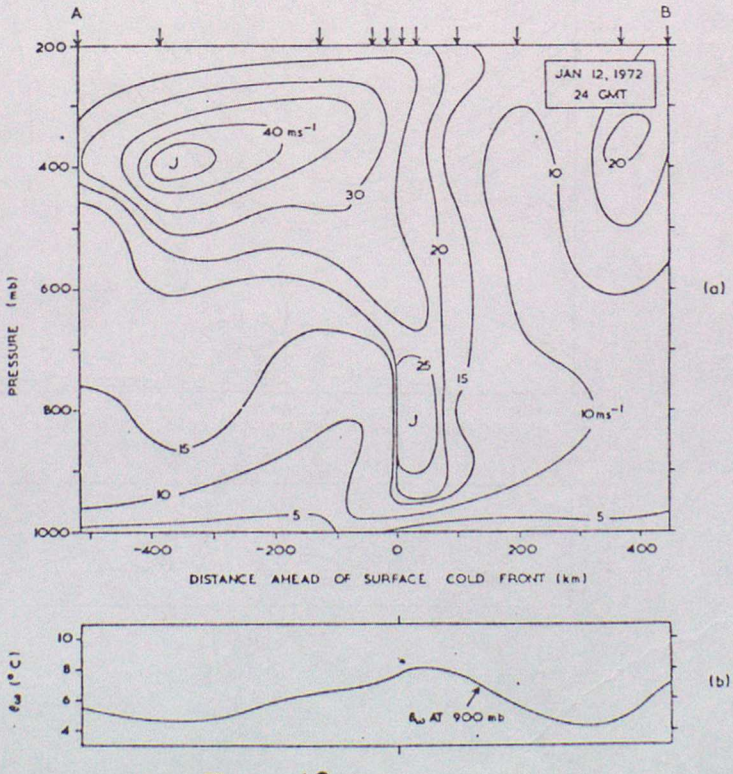

Figure 13

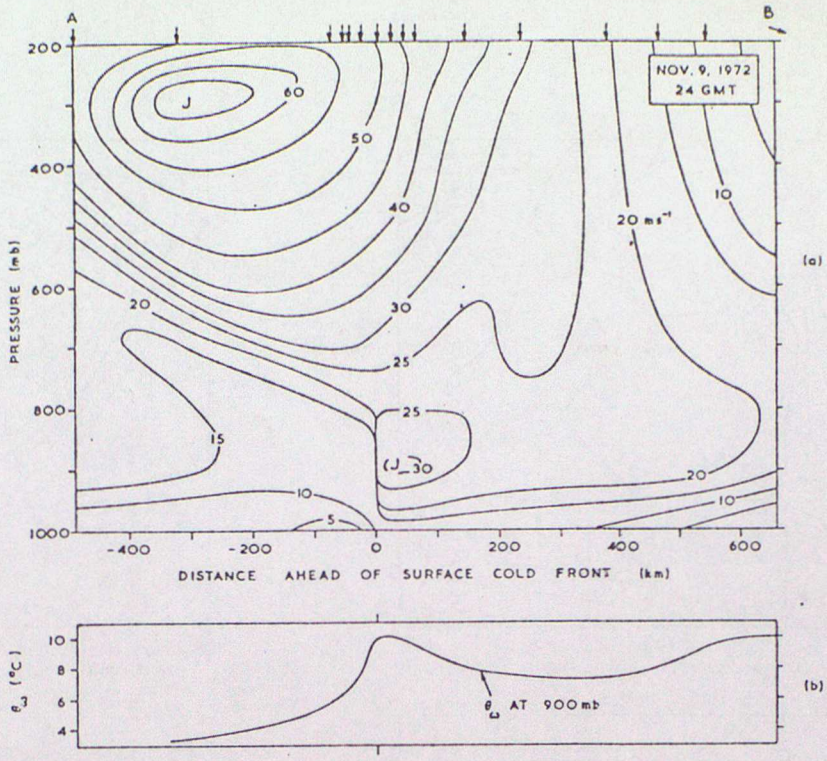

Figure 14

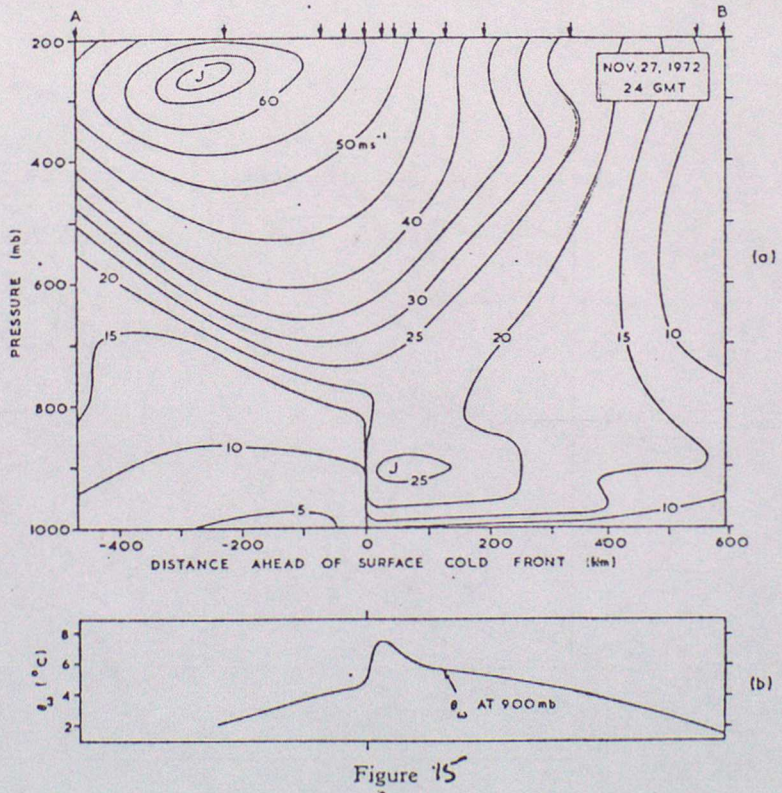

Figure 15

Figures 11-15. Vertical cross-sections along AB in Fig. 8(a), (b), (d), (e) and (f), showing the component of the wind parallel to the SCF on 3 October 1967, 6 February 1969; 12 January 1972; 9 November 1972 and 27 November 1972, respectively. Format in Figs 11(a)-15(a) is similar to Fig. 10(a), except that data from Doppler radar are also used in the vicinity of the SCF on two occasions (see DR at top of Figures). Figs 11(b)-15(b), at the foot of these diagrams, show the wet bulb potential temperature, θ_w, along AB at the 900 mb level. Note the θ_w-maximum in the main low-level jets.

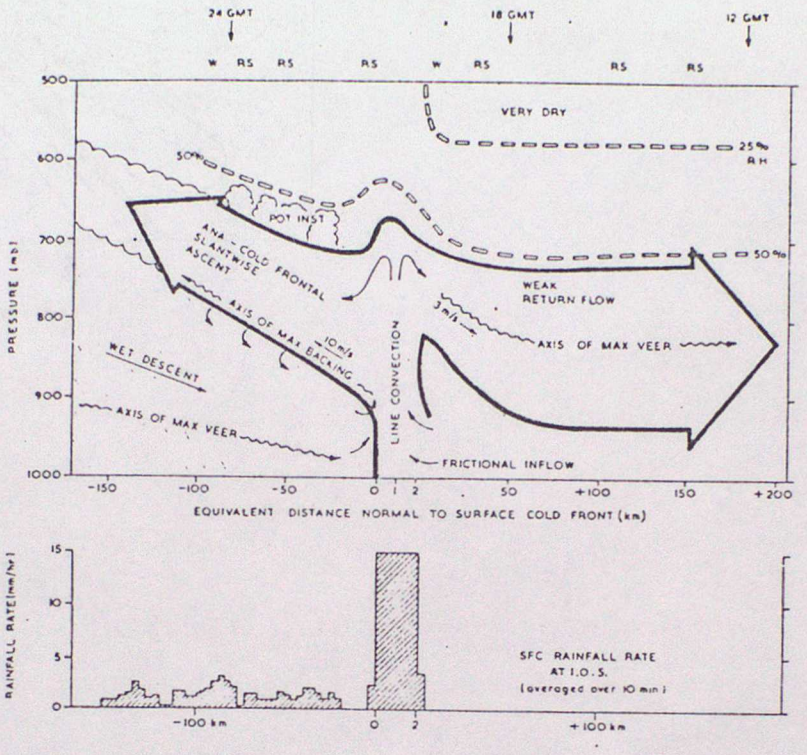

(a)

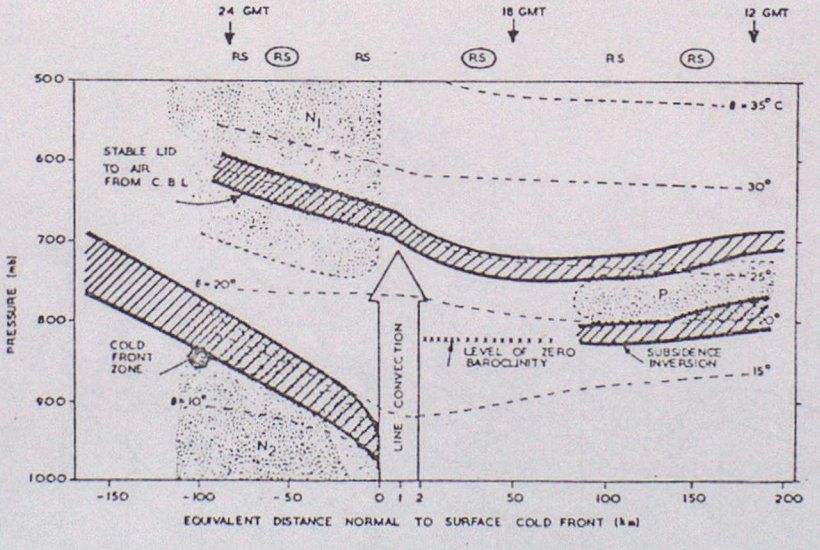

(b)

Figure 16(a)-(b). Vertical section (along 'ab' in Fig. 8(c)) showing (a) the transverse circulation and (b) the thermal structure of the cold front and associated low-level jet on 11 November 1970, derived from data from the Isles of Scilly. A time scale and times of data are indicated at the top of the Figures. An equivalent distance scale is plotted at the bottom of the Figures showing distance normal to the surface cold front (positive ahead of the front). The horizontal scale has been expanded at distances between 0 and 2 km ahead of the SCF in order to make the narrow region of line convection stand out more clearly.

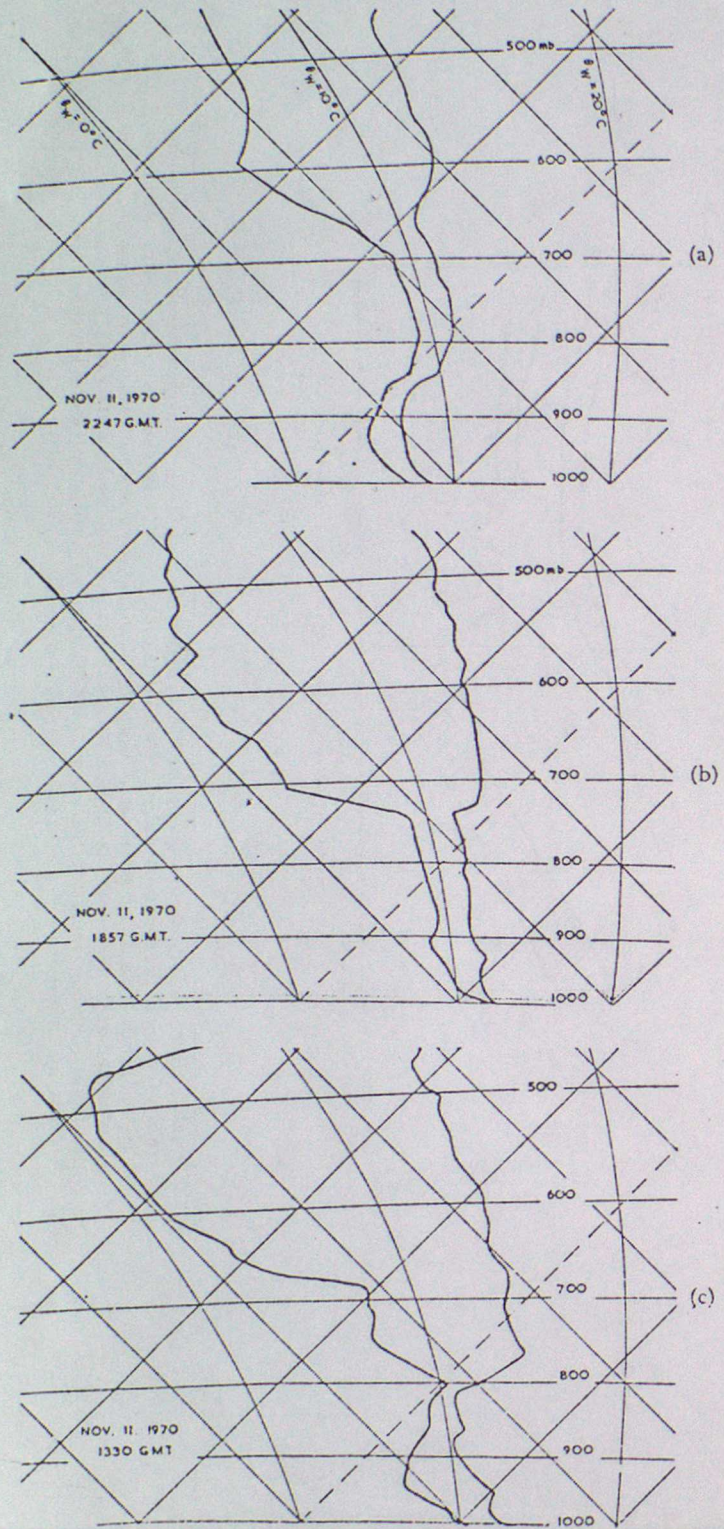

Figure 17. Tephigrams corresponding to 3 of the 6 radiosonde ascents from the Isles of Scilly on 11 November 1970, showing temperature and dew point in the lower atmosphere (a) 50 km behind the SCF, (b) 35 km ahead of the SCF and (c) 150 km ahead of the SCF.

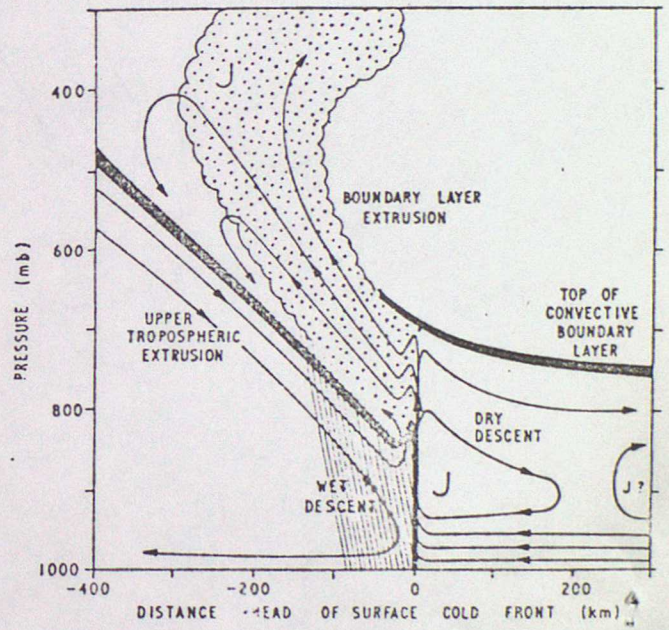

Figure 18. Schematic model of the airflow associated wit[h] ana-cold front. Thin lines are stream lines, relative to the moving system. Thick lines represent the [on]tal zone and the top of the convective boundary layer. Regions of satu[ration] are stippled.

FRONTS IN THE ATMOSPHERE

LECTURE 4 - DYNAMICS AND SIMULATION OF SQUALL LINES

The dynamics of organised convection is an important aspect of atmospheric research. Squall-lines represent one of the most energetic and organised examples of convection, and their persistent or steady character makes them amenable to a considerable degree of theoretical analysis. The transports of heat, momentum and kinetic energy effected by squall-lines are large, and thus their contribution to the atmospheric energy budget, especially on limited areas, may be out of proportion to their number.

As a theoretical simplification it is useful to consider the flow within squall-lines to be steady relative to a set of cartesian axes moving with the travel speed of the system. Moreover, since the macroscale circulation is important and dominates the sub-cloud-scale turbulence (a definition of organisation), it is useful to assume that the motion is inviscid.

These constraints can be relaxed when the squall lines are simulated numerically, since this approach is much more flexible. It is instructive to compare analytic and numerical models of the squall-lines, as will be demonstrated later. The dynamics will be represented analytically and simulations used to generalise and demonstrate the principles.

4.1 - Basic Equations

The equation set used in the analytic work is the quasi-Boussinesq set, in which perturbations of thermodynamic state from a static mean are represented. The set is as follows:

Momentum: $$\frac{D\underset{\sim}{v}}{Dt} + \nabla\left(\frac{\delta p}{\rho_0}\right) - g\delta\phi\,\underset{\sim}{k} = 0 \qquad (1)$$

Mass: $$\mathrm{div}(\rho_0 \underset{\sim}{v}) = 0 \qquad (2)$$

Thermodynamics: $$\frac{D\phi}{Dt} = Q \qquad (3)$$

where $p = p_0(z) + \delta p$; $\frac{dp_0}{dz} = -\rho_0 g$

$\phi = \phi_0(z) + \delta\phi$; $p_0 = R\rho_0 T_0$

$\phi = \ln\theta$

Q = non-adiabatic heat source.

The effect of the earth's rotation is neglected since the time taken by particles to flow through the system is much smaller than $1/f$. The main contribution to Q is latent heating and evaporative cooling.

4.2 - Conservation Properties in Steady Flow

If the flow is steady then certain properties of the flow can be shown to be conserved, a considerable mathematical convenience. Forming an energy equation by operating $\underset{\sim}{v}\cdot$ on Eq.(1)

$$\frac{D}{Dt}\left(\frac{1}{2}\underset{\sim}{v}^2\right) + \underset{\sim}{v}\cdot\nabla\left(\frac{\delta p}{\rho_0}\right) - g\delta\phi w = 0$$

Now any function of the form wF can be written in steady flow as

$$-wF = \frac{D}{Dt}\int_{z_0}^{z} F\,dz$$

where F is evaluated along streamlines. (This is a form which follows from the fundamental theorem of calculus); $z-z_0$ is a displacement from a reference level z_0 , the inflow level on a streamline.

Consequently, it follows that

$$\frac{D}{Dt}\left(\frac{1}{2}\underset{\sim}{v}^2 - \int_{z_0}^{z} g\delta\phi_{\not p}\,dz\right) + \underset{\sim}{v}\cdot\nabla\frac{\delta p}{\rho_0} = 0$$

where the subscript $\not p$ in the integrand shows that $\delta\phi$ is evaluated along streamlines. Since the flow is steady, clearly

$$\underset{\sim}{v}_0 \cdot \nabla \left(\tfrac{1}{2} \underset{\sim}{v}^2 + \frac{\delta p}{\rho_0} - \int_{z_0}^{z} g \delta\phi_p \, dz \right) = 0$$

and so

$$\tfrac{1}{2} \underset{\sim}{v}^2 + \frac{\delta p}{\rho_0} - \int_{z_0}^{z} g \delta\phi_p \, dz = C_1(\psi) \qquad (4)$$

is conserved along streamlines.

Now if the heat source Q is written as $w\Gamma$, a form approximately representing latent heat release, then it follows that if B is the undisturbed static stability $d\phi_0/dz$, that

$$\delta\phi_p - \int_{z_0}^{z} (\Gamma - B) dz = C_2(\psi) \qquad (5)$$

is the thermodynamic equation written in conserved form. Note that on inflow $\delta\phi = \delta p = 0$ so $C_2(\psi) = 0$ and $C_1(\psi) = \frac{1}{2} \underset{\sim}{v}_0^2$, the inflow kinetic energy per unit mass.

Mass continuity can be expressed in flux form as

$$\rho_0 \underset{\sim}{v} \cdot d\underset{\sim}{S} = 0$$

where $\underset{\sim}{S}$ is a streamtube cross section.

4.3 - Displacement Equation

It is convenient for analytic practicability to make some simplifications. First, if Γ is taken to be constant $\Gamma = \gamma$ and B is also considered constant, then

$$\delta\phi_p = (\gamma - B)(z - z_0)$$

and it follows that on substitution into Eq.(3) that

$$\frac{1}{2}\underset{\sim}{v}^2 + \frac{\delta p}{\rho_0} - \frac{1}{2}g(\gamma - B)(z - z_0)^2 = \frac{1}{2}\underset{\sim}{v}_0^2 \qquad (6)$$

Note that Γ is effectively a lapse rate of ϕ following a particle and

$$\int_{z_0}^{z} g\,\delta\phi_p\,dz = CAPE(z, z_0)$$

is the convective energy release during the displacement $z - z_0$ The integral thereby represents the positive area on a tephigram.

Now, following a particle from inflow where the flow is horizontal, through the system and to outflow where the flow is again approximately horizontal, the flow must be hydrostatic there, so

$$\frac{\partial}{\partial z}\left(\frac{\delta p}{\rho_0}\right) = g\,\delta\phi$$

[This approximation will not apply in the flow interior.]

Let subscript "1" denote outflow and "0" inflow, then if z_x represents a reference level

$$\left(\frac{\delta p}{\rho_0}\right)_1 = \left(\frac{\delta p}{\rho_0}\right)_x + \int_{z_x}^{z_0} g\,\delta\phi_1\,dz_1 \qquad (7)$$

Referring Eq.(6) to outflow,

$$\frac{1}{2}\underset{\sim}{v}^2 = \frac{1}{2}\underset{\sim}{v}_0^2 - \left(\frac{\delta p}{\rho_0}\right)_x + \frac{1}{2}g(\gamma - B)(z_1 - z_0)^2 - \int_{z_x}^{z} g\,\delta\phi_1\,dz_1$$

but $\delta\phi_1 = (\gamma - B)(z_1 - z_0)$ so

$$\tfrac{1}{2}\underset{\sim}{V}_1^2 = \tfrac{1}{2}\underset{\sim}{V}_0^2 - \left(\frac{\delta p}{\rho_0}\right)_* - g(\gamma-B)\left[\frac{(z_1-z_0)^2}{2} - \int_{z_x}^{z_1}(z_1-z_0)\,dz_1\right]$$

Now if $\underset{\sim}{V}_0 \neq 0$ it follows that

$$\frac{\underset{\sim}{V}_1^2}{\underset{\sim}{V}_0^2} = 1 - \frac{\delta p_*}{\tfrac{1}{2}\rho_0 \underset{\sim}{V}_0^2} + g(\gamma-B)\left[\frac{(z_1-z_0)^2}{2} - \int_{z_x}^{z_1}(z_1-z_0)\,dz_1\right]$$

But since $\rho\, \underset{\sim}{V}\cdot d\underset{\sim}{S} = 0$ it follows that

$\rho_0 \underset{\sim}{V}_0 . d\underset{\sim}{S}_0 = -\rho_1 \underset{\sim}{V}_1 . d\underset{\sim}{S}_1$ and so

$$\left(\frac{\rho_0\, dy_0\, dz_0}{\rho_1\, dy_1\, dz_1}\right)^2 = 1 - \frac{\delta p}{\tfrac{1}{2}\rho_0 \underset{\sim}{V}_0^2} + \frac{g(\gamma-B)}{\tfrac{1}{2}\underset{\sim}{V}_0^2}\left[\frac{(z_1-z_0)^2}{2} - \int_{z_x}^{z}(z_1-z_0)\,dz_1\right]$$

where $dS_0 = dy_0\, dz_0$; $dS_1 = dy_1\, dz_1$

If the flow is two dimensional in the sense that $dy_0 = dy_1$ (streamtubes same width on inflow and outflow) then

$$\left(\frac{dz_0}{dz_1}\right)^2 = \left\{1 - \frac{\delta p_*}{\tfrac{1}{2}\rho_0 \underset{\sim}{V}_0^2} - \frac{g(\gamma-B)}{\tfrac{1}{2}\underset{\sim}{V}_0^2}\left[\frac{(z_1-z_0)^2}{2} - \int_{z_x}^{z_1}(z_1-z_0)\,dz_1\right]\right\} e^{\frac{2(z_0-z_1)}{H_0}}$$

where density has been written in the scaled form

$\rho = \rho_s e^{-z/H_0}$ where H_0 is the density scale height.

Making the incompressibility assumption, the displacement equation simplifies to

$$\boxed{\left(\frac{dz_0}{dz_1}\right)^2 = 1 - \frac{\delta p_*}{\tfrac{1}{2}\rho_s \underset{\sim}{V}_0^2} + \frac{g(\gamma-B)}{\tfrac{1}{2}\underset{\sim}{V}_0^2}\left[\frac{(z_1-z_0)^2}{2} - \int_{z_x}^{z_1}(z_1-z_0)\,dz_1\right]} \quad (8)$$

Equation (8) is a nonlinear equation for the displacement of Particles from an inflow level z_0 and is generally useful for the later models.

4.4 - Analytic Squall Line Models

The displacement equation defined in Eq.(8) can be used to give useful model results which assist the interpretation of the more complicated numerical simulation presented later. The most basic distinction between the different models lies in the form of the relative flow. In the following models the most idealised versions will be presented as archetypes, and the more realistic flows will be demonstrated in the numerical simulation; the important point is that the archetypes and numerical simulations both reproduce the same regime of organisation if appropriate mean flow parameters are comparable.

4.4.1 - Propagating (Tropical) Squall Line Model

Suppose solutions to the displacement equation are sought which represents a relative flow structure as shown in Fig.(1).

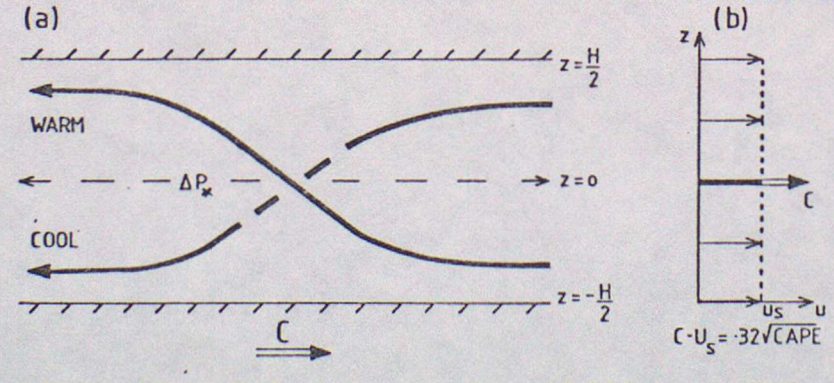

Figure 1. (a) Schema of the relative flow in the propagating model. ΔP_* is the normalized pressure change at the mid-level, $z = 0$. (b) The relationship between the propagation speed (c) and the undisturbed flow relative to the ground (U_s).

The system moves to the right at a speed C, and if the atmospheric wind speed relative to the ground is assumed to be zero, then the relative inflow is $\underset{\sim}{v}_0(z_0) = -C\,\underset{\sim}{i}$

Assume that the updraught air which originates at $z_0 = 0$ exits

at $z_1 = H$, and downdraught air which originates at $z_0 = H$ exits at $z_1 = 0$. The flow in the interior must then be three dimensional. However, since the displacement equation only represents displacements between inflow and outflow, the interior of the flow cannot be determined from this equation. If the lapse rates in the downdraught and updraught are assumed to be the same, then the flow is symmetric around $z = H/2$, the mid-level and the streamline originating at $H/2$ is undisplaced in the vertical.

Using Eq.(8) with $z_x = H/2$, it is readily seen that constant inflow introduces considerable simplification, since this equation can be differentiated with respect to z_1 to give

$$\frac{dz_0}{dz_1}\left[\frac{d^2z_0}{dz_1^2} + \frac{g(\gamma-B)}{c^2}(z_1-z_0)\right] = 0$$

Except where $dz_0/dz_1 = 0$, that is at outflow stagnation points, clearly

$$\frac{d^2\zeta_0}{d\zeta_1^2} = \frac{1}{F^2}(\zeta_0 - \zeta_1) \qquad (9)$$

where $\zeta = z/H$; $F^2 = c^2/g(\gamma-B)H^2 = c^2/2\,CAPE(0,H)$

Solutions to Eq.(9) are of the form

$$\zeta_0 = \zeta_1 + a e^{\frac{z_1}{FH}} + b e^{\frac{-z_1}{FH}}$$

where a and b are constants. The boundary conditions in the problem defined by Eq.(9) are

$$\zeta_0 = 1 \quad \text{when} \quad \zeta_1 = 0$$

$$\zeta_0 = 1/2 \quad \text{when} \quad \zeta_1 = 1/2$$

$$\frac{d\zeta_0}{d\zeta_1} = -\sqrt{1-E} \quad \text{when} \quad \zeta_1 = 1/2$$

where $E = \delta p^* / \frac{1}{2} \rho_s c^2$ The gradient condition is obtained by substituting $\zeta_0(1/2) = 1/2$ into Eq.(8) with $z_* = H/2$

Substituting the boundary conditions, it can be shown that

$$\zeta_1 = \zeta_0 + F(1+\sqrt{1-E}) \sinh\left(\frac{z_1 - H/2}{FH}\right)$$

if F satisfies

$$(1+\sqrt{1-E})F \sinh(1/2F) = 1 \quad .$$ Clearly $E \leq 1$ and this limiting value represents the inflow at $z_0 = H/2$, stagnating on outflow $z_1 = H/2$. The function $F(E)$ is plotted in Fig.2.

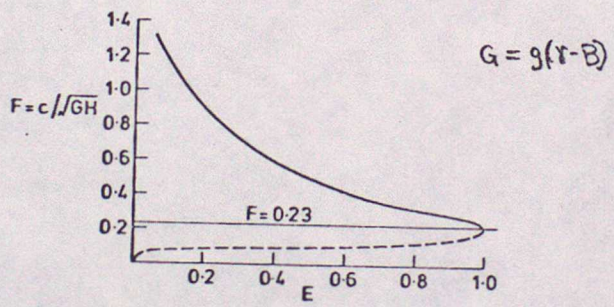

Fig 2

The case of $E = 1$ is useful as an example and $F(1) = 0.23$. Thus the propagation speed of the squall line can be written

$$C = 0.23\sqrt{g(\gamma-\beta)H} = 0.32\sqrt{CAPE}$$

So given the value of CAPE (the positive area on a T-ϕ) the propagation speed of a squall-line can be estimated. For example, with CAPE = 1000 J kg^{-1}, this gives $C \simeq 10$ m s^{-1}.

The change in the environment wind and thermodynamic vertical structure can be found from the displacement solutions. The relative outflow is given by

$$u_1(z_1) = -c\frac{dz_0}{dz_1} = F\sqrt{CAPE}\left(1 - \cosh\frac{z_1}{FH}\right)$$

$$\frac{\delta\theta_1}{\theta_2} = \frac{F \times CAPE}{gH}\sinh\frac{z_1}{FH}$$

These changes are shown in Fig.(3).

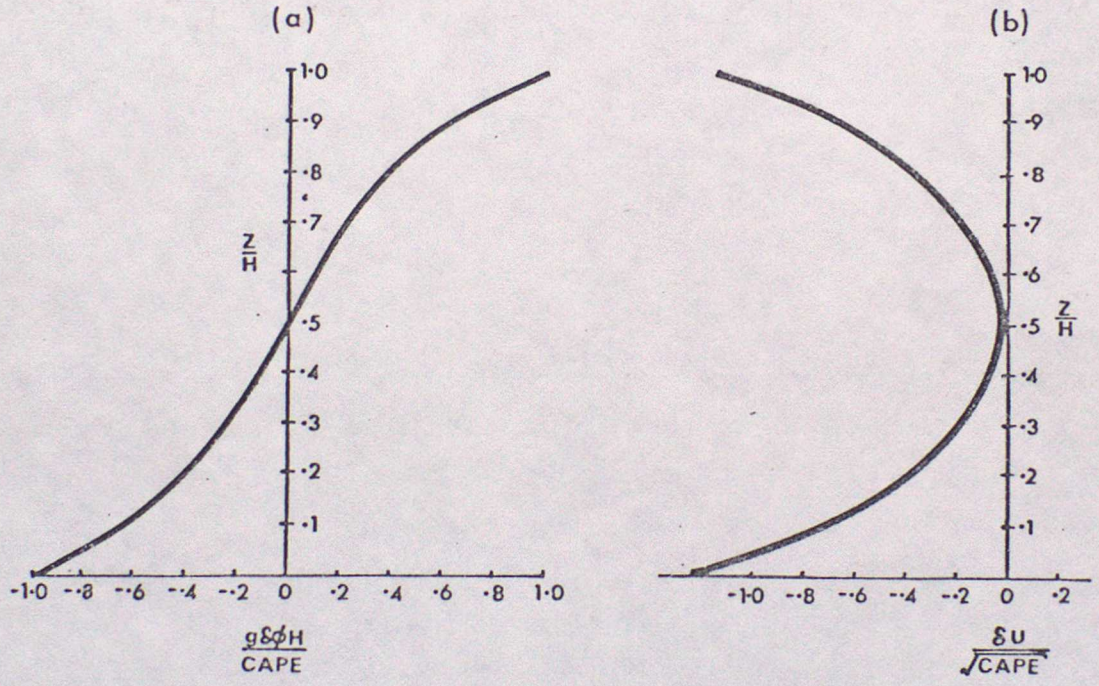

Figure 3. The modification effected by the propagating model: (a) thermodynamics (log-potential temperature); (b) momentum.

The transport of momentum is interesting because a jet-like profile has been established. The fact that the transport properties can be determined directly from the solutions is useful in the context of parameterisation of deep convection in large-scale numerical models. More details can be found

in Moncrieff and Miller (1976) (MM) and Moncrieff (1981).

This type of squall-line in which the system propagates relative to the tropospheric flow at all levels with outflow towards the rear, appears to be prevalent in tropical regions, the main reason being that the initiation of the convection is associated with a reverse shear and the presence of a low-level jet such as is frequently found in the tropics (see MM). The displacement equation can be solved in the case of a jet-like profile and the effect of the squall-line is to intensify this jet by superposing a profile similar to that in Fig.(3). The main region where this squall-line type has been identified is in Venezuela during VIMHEX II (Betts, Grover and Moncrieff (1976)) in the tropical Atlantic (Zipser (1969)), and in GATE (Mansfield (1979)). The squall-lines occurring in West Africa during April and May are very important examples of this type of system. It is likely that this squall-line also occurs during the southeast Asia monsoon.

4.4.2 - Steering-Level (Mid-Latitude) Squall-Line Model

The presence of the propagating squall lines in the tropics is closely related to the reverse shear and jet profiles often found in that region. In mid-latitudes the shear is predominantly westerly and in this case another type of relative flow appears to be prevalent. This two-dimensional type is schematically shown in Fig.(4).

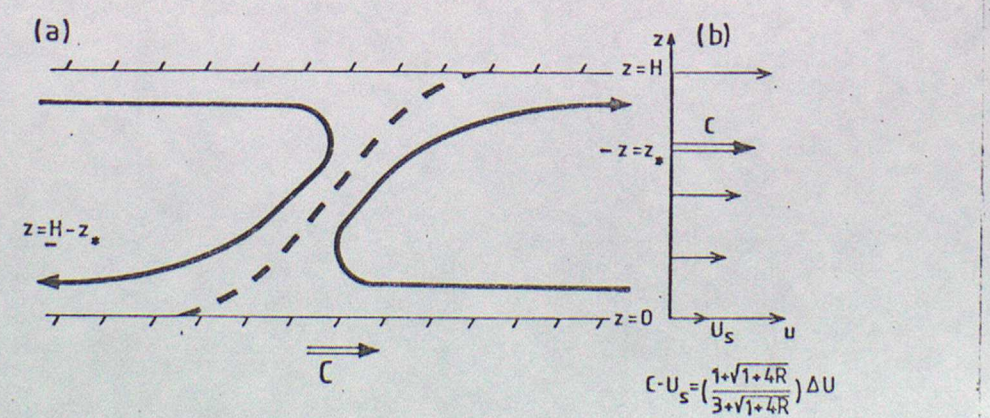

Figure 4. (a) Schema of the relative flow in the steering-level model. The level $z = z_*$ is the height at which the travel speed equals the environment windspeed. (b) The relationship between the travel speed (c) and the undisturbed flow relative to the ground.

In this case the system moves to the right at a speed (C) which is equal to the tropospheric winds at the level $z = z_*$; this level is referred to as a steering level and hence the name of the regime. This level has to be determined as part of the solution of the relevant equations.

Assume that in a coordinate system which moves with speed C , the updraught air which originates at $z_0 = 0$ exits at $z_1 = H$ but, contrasting with the propagating model, in the opposite sense. At the level $z_0 = z_*$, the relative flow velocity is zero (stagnation point). Likewise, for the present analysis, assume that the downdraught originates at $z_0 = H$ and exits at $z_1 = 0$. Let the inflow air have constant shear $du_0/dz_0 = A$ Thus $u_0(z_0) = A(z_0 - z_*)$ and substitution into Eq.(8) shows that the solution will depend on the prescription of the non dimensional parameter $R = g(\gamma - \beta)/A^2 = CAPE/\frac{1}{2}(\Delta u)^2$ form of bulk Richardson number.

With boundary conditions defined as $z_0 = z_*$ when $z_1 = z_*$; $z_0 = 0$ when $z_1 = H$ and $dz_0/dz_1 = \beta$, an analytic solution to Eqn.(8) is

$$z_0 = z_* - \beta(z_1 - z_*)$$

with $R = \beta(\beta - 1)$ and $z_*/H = \beta/(1+\beta)$. It follows that $z_*/H = (1 + \sqrt{1+4R})/(3 + \sqrt{1+4R})$ and so $C = \bar{U}_0 + \left(\frac{z_*}{H} - \frac{1}{2}\right)\Delta u$

where U_0 is the low level wind speed, and $\Delta u = U_0(H) - U_0(0)$ This is the solution found in Moncrieff and Green (1972) and is further discussed there.

The form of the flow within the squall line, being two dimensional in this case, can also be found. As an example, taking a symmetric system with R identical in updraught and downdraught branches, it can be shown (Moncrieff (1978)) that the flow is orientated with a downshear slope. The conclusion is that a steady system with a deep downdraught in constant

shear is not physically acceptable on the grounds that the downdraught has no physical mechanism to maintain itself; with a forward sloping interface, precipitation particles will be discharged into the updraught and not into the downdraught branch.

Recent work has shown that two dimensional, steady line convection can exist if non-constant shear and a shallower downdraught is allowed. An important aspect of the flow is that a third region exists in which the low-level updraught air exits at the rear of the squall-line, rather like the propagating model except that air particles do not overturn. The form of this model is shown schematically in Fig.(5) An important factor in determing this flow pattern is the presence of strong low-level shear and weak upper-level shear (Thorpe and Miller (1981), Thorpe and Moncrieff (1981)).

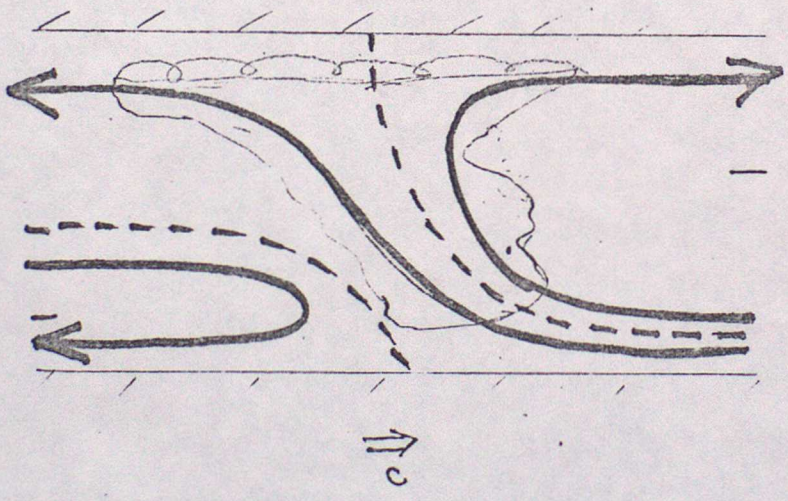

Fig 5.

4.5 - Numerical Simulation of Squall-lines

While very important for understanding the idealised basic dynamics of squall-lines, the analytic steady models cannot hope to reproduce real storms, nor to investigate the growth of the initial-value problem to the steady state solution. The inherent nonlinearity with large particle displacements is the rule rather than the exception, and makes numerical simulation the only realistic method of studying the squall-line formation.

A number of numerical models have been used for the explicit purpose of examining the macroscale dynamics of deep convection. Many of these models are concerned with the three-dimensional or cellular aspects of convection and for this reason only a subset which is concerned with the maintenance and generation of line convection will be considered.

From the viewpoint of longevity and efficient regeneration of new cells, one major aspect is of note; that is the role of the downdraught-generated density current (Miller (1978), Thorpe and Miller (1978). The enhanced convergence at the upstream propagating density current head is an extremely important mechanism for regenerating storm cells, and new cells usually develop where this is a maximum, Thorpe, Miller and Moncrieff (1980). It is beyond the scope of this lecture to review the dynamics of density currents but some main points are worth note. The upstream propagation speed of density current heads is well known to be represented by an equation of the form

$$c_d = \bar{u}^d + F\sqrt{g\frac{\Delta\theta_d}{\theta}D} \qquad (10)$$

where $\bar{u}^d$ is the mean wind speed in the density current layer of depth D, $\Delta\theta_d$ is the potential temperature deficit in the density current and F is a nondimensional (Froude) number of order unity. The size of F is influenced by the density-current dynamics, $\Delta\theta_d$ is determined by evaporative cooling and D is influenced by the environment stability and the strength of the cooling.

In the last section it was shown that squall-line updraughts propagate according to a formula of the form

$$c = \bar{u} + f(\Delta u, CAPE, H) \qquad (11)$$

where the function f is given by the analytic models, in each case.

Considering the updraught and downdraught as two dependent subsystems whose travel speeds are given by the above two formulae, then the essence of the steadiness (or persistence) problem is demonstrated. Taking first the example of two-dimensional sys tems, then steadiness is only possible if $C \simeq c_d$ in which case

$$\bar{u}^d + F\sqrt{g\frac{\Delta\theta_d}{\bar{\theta}}D} = \bar{u} + f(\Delta u, CAPE, H) \quad (12)$$

Consequently there must be a subtle inter-relationship between mean flow parameters and squall-line flow parameters.

4.5.1 - Three-dimensional squall-line Structure

The above equation demonstrates formal relationship between density currents and squall-line parameters in two-dimensional (unidirectional) flow. If a vector shear exists, then the situation is more complicated. The surface convergence at the density current head is usually a maximum in the direction of the relative surface wind, while squall-line cells tend to travel in a direction which is the mean wind in the convection layer. In mid-latitude (northern hemisphere), the boundary layer mean wind is usually to the right of the mean tropospheric wind, consequently cells will preferentially redevelop on the right of squall-line cells. This tendency is demonstrated in the following figure from Thorpe and Miller (1978) and shows that although cells are moving with the mean wind, the line of cells is regenerating, and propagating to the right of the cell velocity.

Rainfall totals up to 80 min for A, contoured every 5 mm. The position of cells is superimposed with times marked in minutes. Unit grid side is 1 km.

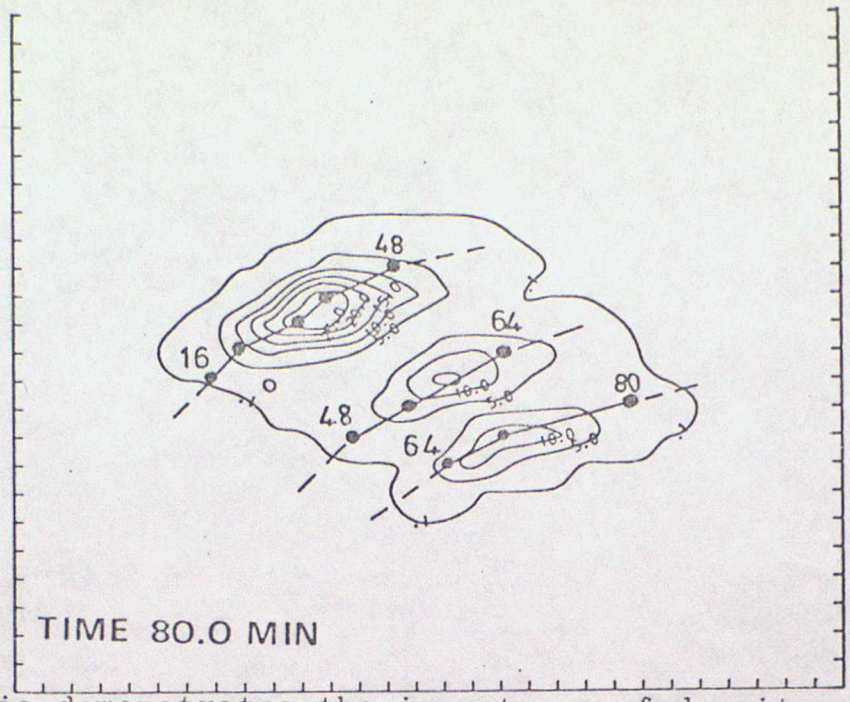

This demonstrates the importance of density currents in the squall-line dynamics, particularly in choosing the regions of preferential development, a well known observational result to be to the right of the parent cells. This is further demonstrated in the time-lapse movie of deep convection.

5 - Summary and Conclusions

It has been shown that the dynamics of squall lines are governed by mean-flow parameters such as the wind shear and convective available potential energy, and the steady analytic results are reproduced in more complicated numerical simulation. The growth of squall line cells is shown to be greatly influenced by the propagation of density currents. The squall-line can thus be viewed as a combination of the dynamics of density currents and the dynamics of updraught circulations.

References:

Moncrieff, M.W. and Green, J.S.A. 1972 The propagation and transfer properties of steady convective overturning in shear. Quart.J. Roy.Met.Soc., 98, p.336

Moncrieff, M.W. and Miller, M.J. 1976 The dynamics and simulation of tropical cumulonimbus and squall lines. *Ibid.* 102, p.373

Moncrieff, M.W. 1978 The dynamical structure of two dimensional steady convection in constant vertical shear. *Ibid.* 104, p.543

Moncrieff, M.W. 1981 A theory of organised steady convection and its transport properties. *Ibid.* 107, (Jan.)

Thorpe, A.J. and Miller, M.J. 1978 Numerical simulations showing the role of the downdraught in cumulonimbus motion and splitting. *Ibid.* 104, p.876.

Thorpe, A.J. and Miller, M.J. 1981

Thorpe, A.J and Moncrieff, M.W 1981

- unpublished mss -

Zipser, E. 1979 The role of organized unsaturated convective downdrafts in the structure and decay of an equatorial disturbance. J.App. Met., 8, p.299

Miller, M.J. and Betts, A. 1977 Traveling convective storms over Venezuela. Mon.Wea.Rev., 105, p.834

Miller, M.J. 1978 The Hampstead Storm. A numerical simulation of a quasi-stationary cumulonimbus system. Quart.J.R. Met.Soc., 104, p.413

Betts, A.K., Grover, R.W. and Moncrieff, M.W. 1976 Structure and motion of tropical squall lines over Venezuela. Quart.J.R.Met.Soc., 102, p.395

Mansfield, D.A. 1977 Squall lines observed in GATE. *Ibid.* 103, p.569.

FRONTS IN THE ATMOSPHERE

LECTURE SEVEN - Sea-breeze fronts

Summary

1. Diurnal differences between land- and sea-surface temperatures set up a land- or sea-breeze (vertical) circulation. This circulation is modified by the synoptic weather conditions.

The onset of the sea-breeze can be forecast in terms of the land-sea temperature difference and the strength of the offshore wind. The frequency of occurrence of the sea-breeze front inland and depth of inland penetration has been recorded in some districts.

2. Detection and investigation of sea-breeze fronts. A line of typical cloud may form in association with the upward branch of the vertical circulation, sometimes with cloud-base at two different heights, and the front may be marked with haze. Surface records of wind strength and direction and of humidity are useful. Fronts have been traced by radar and by vertically-pointing acoustic sounders. Pilot balloons are a classic method. Detailed cross-sections have been made by aeroplanes carrying a variety of instruments. Methods are illustrated by a research project on 14 June 1973.

3. The dynamics of a sea-breeze front A deeply penetrating sea-breeze front has the characteristics of a gravity current head, where a dense fluid moves along the ground displacing a lighter one above it. Laboratory work using saline flows in water tanks has led to a practical model describing the behaviour of such fluid flows.

4. Applications The details of the sea-breeze front have important applications in the fields of air pollution, insect pest control and aircraft safety.

5. Present research Details are beginning to emerge of the behaviour of sea-breeze fronts after sunset, when the front combines in some way with a solitary wave in the low-level nocturnal inversion. Atmospheric observations, laboratory tank experiments and mathematical wave-theory all suggest that a solitary wave (or "cut-off vortex") with closed streamlines can form at the head of a sea-breeze front.

Bibliography

McCaffery, W.D.S. 1966 On sea-breeze forecasting techniques.
Met.Office. Forecasting Techniques Memo. No.12.

Simpson, J.E. Mansfield, D.A., Milford, J.R. 1977 Inland penetration of sea-breeze fronts.
Quart.J.R.Met.Soc., 103, 47-76.

Simpson, J.E. and Britter, R.E. 1980 A laboratory model of an atmospheric mesofront.
Quart. J.R. Met.Soc., 106, 485-500

VS

FRONTS IN THE ATMOSPHERE

LECTURE EIGHT - Practical forecasting of frontal phenomena
Part I - Short to medium range forecasts

1. Introduction

This note deals briefly with some general concepts in the preparation of analyses and forecasts, with particular reference to frontal phenomena.

The forecast periods covered here (in Part I) fall into two categories: 12- to 36-hr (short-range) forecasts and 2- to 7-day (medium-range)forecasts. Frequent reference will be made to the use of output from operational numerical models in the preparation of these forecasts.

Part II of this topic will cover some aspects of very short range (up to 12-hr) forecasts.

2. Analysis

When considering the analysis of charts with a view to the preparation of a forecast for at least 12 hours ahead, it is important that contemplation (a time-consuming process) should be concentrated on the important features; the importance to be attached to any particular feature tends to be a function of the intended forecast period. Initially, the broad view should be taken, and this will involve consideration of the major synoptic systems, which form a vital part of the long wave pattern over the chart area. Within the broad flow pattern of these major features there will usually be found a number of smaller features, of sufficient size to be important on the synoptic scale for example, a few hundred kilometres in extent and with a lifetime in excess of a few hours. In the short term, behaviour of these smaller synoptic scale systems is often closely controlled by the larger systems. At the lower end of the length scale, individual meso-scale features with dimensions of less than about 100km, such as squall lines, thunderstorms and sea-breeze fronts, have lifetimes significantly shorter than the 12-hour minimum forecast period considered in this note. Forecasting techniques relevant to such features are the subject of Part II of this topic.

To achieve a better understanding of the charts being analysed, forecasters often find it helpful to estimate, from the preceding series of charts, the expected positions of the important features (depressions, anticyclones, fronts) on the current charts (i.e. the use of continuity). It is also important to be able to identify and concentrate on certain key areas of the chart where the development is uncertain or is somewhat different from that previously expected. The ability to identify the important areas on any particular chart is achieved through a combination of theoretical knowledge, practical experience and good judgement.

An objective approach on the part of the analyst, although difficult to achieve with any consistency, is another important attribute. In particular, when a substantial number of observations are at variance with the previously expected developments, substantial errors may arise if the forecaster persists with his previous line of thought.

When considering analyses it is important to take into account the likely effect of any differences between the computer analyses or initialized fields, on which the model's prognoses are based, and the latest manual analysis, which may include

later information or which may have treated differently the observations from data-sparse regions.

In the analysis of major frontal phenomena, heavy reliance is placed on conventional surface and upper air observations, but satellite photographs can often be an extremely useful additional source of information, particularly valuable in data-sparse regions. In addition the type and extent of cloud evident from examination of visible and infra-red photographs can be useful in assessing the activity of a front.

3. Short-range forecasts (12-36 hours)

3.1 General remarks on the preparation of forecasts

Objective (numerical model) surface forecasts generally give a good idea of the movement and development of synoptic scale features and should be regarded as the main guidance tool in the preparation of forecasts, but there are occasions when the numerical model tends to underestimate development rates and/or phase speeds, particularly for the shorter wavelength, more mobile, features and the forecaster should try to allow for any known tendencies of this kind on the part of the model. In particular he can study the performance of the earlier computer forecasts in the region of interest to try to assess how the model has dealt with the situation. If, for example, the feature being considered has developed more quickly that forecast, the same type of error may persist for a while (but this assumption must not be made blindly).

As a first step in the preparation of a forecast it is usual to mark lightly in pencil, with reference to the numerical model prognosis, the probable positions of any large-scale synoptic features (which may be relatively slow-moving) and estimate their central pressures, checking against continuity and general dynamic ideas on development. On occasions when confidence in these quasi-stationary dominant systems is high, a few tentative isobars can be lightly sketched in. The next stage is to consider the more mobile systems; these may tend to move around a major system (thermally steered) and, again using the objective forecast as a guide, a fair estimate of their track can be made by considering their present position and structure, and also the present and future position and thermal characteristics of the steering system. On some occasions the mobile system may move and develop in such a way as to interact with and modify the larger system. If new systems seem likely to form, either on pre-existing fronts or within air masses, tentative estimates should be made of their future positions and central pressures, and these should be entered lightly on the chart. Consideration must now be given to the probable location of major frontal systems, taking account of possible frontogenesis or frontolysis wherever possible. Again continuity and the computer products provide a good deal of assistance here; the predicted thermal gradients and precipitation fields from the fine-mesh (Rectangle) model frequently provide valuable guidance in estimating frontal positions and development for 12-36 hour forecasts, although the rainfall amounts predicted can often be somewhat misleading (usually underestimated), particularly in regions where there is orographic enhancement of the precipitation (see, for instance, Riddaway (1979)). Examples of fine-mesh model forecasts of surface pressure and precipitation rate are shown in Figures 1a and 2a; they illustrate the models ability to indicate clearly the existence of major mid-latitude frontal systems. (selected verifying analyses are at Figs 1b and 2b).

Throughout the preparation of the surface prognosis, the forecaster should have a good appreciation of current and model-predicted developments in the upper air, in order to ensure the necessary consistency in the vertical of the finished product. In particular the predicted development and movement of the major jet streams should correspond in a coherent manner with the predicted evolution of the associated major frontal systems at the surface. The upper-air forecasts produced by the numerical model, together with a knowledge of the relationship between upper air and surface features, are invaluable in the preparation of a surface prognosis.

The forecaster should now be in a position to complete the frontal patterns and draw in some tentative isobars, although it is almost inevitable that the first sketch will not inspire much confidence; gradients may not match expected frontal movements, or a major synoptic feature may have been extended to swamp large areas of the chart. Frequently, following consideration of the first sketch of the forecast chart, some time will need to be spent in vigorous but judicious use of the rubber, adjusting positions, pressures, fronts and isobars here and there to produce a more plausible picture. Following a last appraisal of continuity aspects and the computer product, final amendments to pressure distributions and frontal positions can be made.

3.2 Fronts

This section includes some remarks on frontal characteristics from the practical forecasting point of view. It is important at this stage that the reader has a good appreciation of the typical observational characteristics of mid-latitude synoptic-scale fronts, as described in lectures 2 and 3 of this series.

3.2.1 Warm fronts

The speed of a surface warm front is determined by the speed of the cold air near the surface (just above the friction layer at 900mb), just ahead of the front. The speed will often be different from that of the warm air owing to ageostrophic motions associated with the moving parent depression. With a deepening depression, the effect of the ageostrophic motion is to slow down the rate at which the cold air moves away, and this has the effect of enhancing the rate at which the warm air ascends in the frontal zone, thus increasing the frontal activity. However, ageostrophic effects are difficult to assess subjectively; if necessary, the speed of the warm front is estimated by taking some empirically derived proportion of the component of geostrophic wind perpendicular to the front. The usual proportion is $2/3$ over land and $4/5$ over the sea, but these values can vary according to the degree of ageostrophic motion, and, for the forecast period under consideration (12-36 hours), it is usually preferable to make use of the numerical model's guidance on frontal movement, particularly if the front is a well-marked feature in the predicted fields.

The classical model of a warm front shows the cloud lowering and thickening, the rate of precipitation increasing and the visibility decreasing at a given place as the front approaches, with cessation of precipitation, or a decrease to drizzle only, at the passage of the front. This is, on many occasions, a reasonable approximation to the truth, particularly with fronts moving towards the British Isles from the west or south-west. In detail, however, warm fronts differ considerably from one to another, even in apparently similar synoptic situations. It is therefore difficult to give any general guidance, based on synoptic climatology, to help in the forecasting of warm frontal weather. To obtain the best basis for a forecast,

the forecaster must study the latest observations, including those of hourly rainfall, and then assess the likely developments making full use of available computer products, including the precipitation forecasts.

In addition, the following descriptive remarks may be of some use in attempting to predict warm frontal weather for the British Isles.

Appreciable rain is likely at a warm front if the water content of the warm air is high up to the 800mb level or above and some ascent seems likely. If the warm air is dry above 950mb the front will generally give only drizzle which may be confined to the west. Douglas (1957) remarks that "in many cases the very high humidity goes up to 900mb or only a little higher and the situation is of a marginal type in which definite deductions are impossible. Where information is scarce the older air mass conceptions are sometimes useful. A warm air mass from tropical regions is more rain-producing that one which has previously subsided in the subtropical high at 40° - 50°N and has not been over a really warm sea long enough to have much moisture in it. If an approaching warm front has tropical air behind it, the chances of escaping rain are not high, even in the south-east in Summer".

If the synoptic situation shows that the lower tropospheric air in the warm sector is approaching this country more or less directly from tropical regions (say a general current of air below 700mb from a direction between about south and south-west) it would be prudent to include a forecast of warm front rain. Rainfall amounts tend to be less when the general current of warm air arrives from a direction to the north of south-west.

If recent observations show that tendencies are consistently negative and becoming increasingly so, or if the forecast chart indicates that a substantial decrease of pressure is expected, it would be prudent to expect some increase in the extent, amount and intensity of warm front precipitation. Experience indicates that a warm front often becomes more active when it approaches a pre-existing thermal band lying parallel to it.

On some occasions, as was described in the second lecture of this series, there are multiple bands of precipitation ahead of the surface warm front and almost parallel to it, separated by zones of less intense or no rainfall; the movement of the rain bands may be faster than that of the warm front, and such features are consistent with the "conveyor belt" concept. On other occasions there may be one or more rather larger areas of heavier precipitation, ahead of the surface front moving parallel to the front in a direction away from the low-pressure centre. These areas may be up to 100km or so across; some may be associated with minor waves on the warm front, but many are not.

Orographic effects are often important in the modification of precipitation associated with warm fronts; this appears to be particular true of the mesoscale precipitation areas which often originate within the conveyor belt flow in the warm sector, where the release of potential instability is enhanced by the forced ascent. For further reading on this aspect, see Browning et al. (1974).

3.2.2 Cold fronts

The movement of cold fronts is determined by the speed of the cold air, undercutting the warm air mass, to the rear of the frontal zone. The speed is nearly always at least equal to the geostrophic wind component perpendicular to the front and, especially when pressure is rising in the

cold air and a ridge is building, it may be quite significantly supergeostrophic.

Reference has already been made in this series of lectures to the two main types of cold front, namely those that are active or inactive (in relation to the weather which accompanies them) - ana-cold and kata-cold fronts respectively.

There is usually an extensive area of upper cloud and a substantial band of precipitation to the rear of an ana-cold front. The belt of cloud and precipitation has its major horizontal dimension aligned along the front. In the horizontal direction at right angles to the front the pall of cloud may well extend in a typical case for something like 150km to the rear. When the surface cold front is continuing to move away, the width of the belt of precipitation often seems to be very close to that of the cloud sheet to the rear of the front. In some cases there is a short burst of heavy precipitation (line convection) at the frontal passage, followed by a marked clearance of low cloud which reveals the extensive sheet of upper cloud from which precipitation, often of light (but sometimes moderate) intensity, continues to fall. (associated with the slant-wise ascent above the cold frontal zone).

The weather accompanying kata-cold fronts is different in detail from that associated with ana-cold fronts. Air above the kata-cold frontal zone is descending and this descent usually severely limits the vertical extent of the frontal cloud system. In many kata-cold fronts affecting the British Isles the top of the main frontal cloud mass does not extend much above 3km, although isolated cumuliform tops may extend to higher levels. Any higher medium cloud systems are usually thin and rather patchy. Precipitation amounts are usually small and the precipitation does not normally continue after the frontal passage; it often ceases abruptly at the passage of the surface front.

Some features of ana- and kata-cold fronts have been listed by Sansom (1951), and a selection of these is given in Table 1 (surface features) and Table 2 (upper air features). The seasonal distribution of cold front types for the British Isles as found by Sansom is given in the following Table.

	Winter (Dec-Feb)	Spring (Mar-May)	Summer (June-Aug)	Autumn (Sept-Nov)
Ana-cold	8	5	0	2
Kata-cold	1	3	10	9
Unclassified	3	4	1	4

For an account of the effects of orography on the precipitation associated with cold fronts, see Browning et al. (1975).

3.2.3 Occluded fronts

Warm occlusions and cold occlusions behave in much the same manner as warm fronts and cold fronts, respectively. Warm occlusions are somewhat rare, but are slow-moving systems and can bring prolonged wet (or snowy) weather in some circumstances. Cold occlusions are the normal development resulting from the ascending motion of the warm air mass within the circulation of a polar front depression. Initially the occlusion is related to the low-level circulation and can be satisfactorily analysed by assuming the tip of the occlusion to be coincident with the surface low-

pressure centre, and moving along with it. Gradually however, as the occlusion process continues and the warm air is lifted to higher levels, the significant cloud and weather are more closely allied to the location and movement of the upper vortex than that at the surface; these may not be vertically aligned although, as the system evolves from maturity to its final decaying stages, they may become more coincident. However by this time it is clear from satellite cloud photographs that the typical cloud formation of the cold occlusion is a complex array of cloud bands spiralling around the upper vortex. The movement of these bands, with vertical motions becoming insignificant at this stage, is given by the observed horizontal wind at the cloud level.

With cold occlusions the rules for movement of cold fronts apply and it is often found that the sharper the isobaric trough at the cold occlusion, the more likely it is to be moving with the geostrophic speed, and, as with some cold fronts, some occlusions move at super-geostrophic speed. The majority of occlusions near the British Isles move and behave like cold fronts. With very deep depressions, once the occlusion process commences it is often virtually complete within 24 hours.

In a developing depression the precipitation tends to become more intense near the tip of the warm sector and at the warm front when occlusion occurs. If a secondary depression forms at the point of occlusion (the "triple point") there is usually a considerable area of precipitation which extends on both sides of the occlusion. Near such secondaries the precipitation is probably seldom of purely frontal origin and general low-level convergence associated with the development of the secondary must often be a factor and, at times, may be the dominant one.

3.3 Frontogenesis

It is readily shown that the velocity field is frontogenetic or frontolytic according as the isotherms lie within 45° of the axis of dilatation or not (see Palmén, Newton (1969), for example). In Sawyer's (1954) investigations of the relationship between fronts and frontogenesis, he concluded that: "The large-scale circulation around depressions and anticyclones inevitably contains regions of confluence and when these are associated with a temperature gradient perpendicular to the axis of dilatation frontogenesis results. This frontogenesis leads to a vertical circulation which causes the ascent of warm air and the descent of cold air and the formation of an inclined frontal zone. Synoptic evidence suggests that such frontogenesis is in progress in association with most active fronts, and it seems likely that they owe their characteristic features to it".

This sets a (qualitative) scale on which to look for frontogenesis in the first instance; the velocity and thermal fields should be kinematically favourable before large-scale frontogenesis is forecast. If convergence is also occurring in that area then the chances of frontogenesis are considerably enhanced. If a depression forms in the area, the typical frontal surfaces seem to be established in a few hours. There should always be good physical, kinematical and dynamical reasons before marked frontogenesis is predicted; the basic synoptic-scale processes involved are often quite well represented in numerical model fields and, again, the model's predictions of frontogenesis (or frontolysis) should form the basic guidance on such developments.

There are certain preferred geographical regions for frontogenesis; the best known are near the eastern seaboards of the major continental land masses in mid-latitudes in winter. In such areas the air mass contrasts are often large and pronounced fronts occur. Of direct interest to forecasters in the British Isles is the formation of a strong polar front off the eastern seaboard of North America.

4. Medium range forecasts (2-7 days)

It is convenient to further subdivide the medium range category into (a) 2-3 days and (b) 4-7 days.

4.1 2- to 3-day forecasts

The broad principles used in the production of forecast charts for 2 and 3 days ahead are little different from those for the 12- to 36-hour forecasts. The main differences are that it is not possible to give as much detail as in the short range forecasts and that systematic errors of the numerical models (and the need to make allowances for them) become greater as the forecast period becomes longer. In the preparation of the forecast, the following possible sources of error in the model fields should be borne in mind:

(a) any significant error in the analyses.

(b) any known general deficiency of the model.

(c) any particular deficiency as evidenced by errors in situations of the same general type.

Forecast surface pressure, 500 mb geopotential and 1000-500 mb thickness charts are usually prepared, using the already available 24-hour and 36-hour forecasts as "lead in" to the 2- to 3-day period. A useful check on the continuity and general trend of development within the 3-day sequence of predicted fields can be made by drawing selected frontal systems and/or isopleths (eg 500 mb contours) at 24-hour intervals on one chart.

When the forecast charts have been prepared, there remains the important and often difficult task of inferring the associated weather for the region of interest. This is, at present, an almost entirely subjective process based on the forecaster's experience of the weather associated with similar synoptic types and his knowledge of the physical processes of the weather in the particular situation.

The most useful guidance on the predicted intensity of frontal systems, or on the formation of new fronts must again come from the numerical model; precipitation fields (as produced by the fine-mesh Rectangle for up to 36-hours ahead) are not produced by the Operational (coarse-mesh) Octagon, and heavy reliance must be placed on the predicted horizontal temperature and wind gradients in the identification of frontal features; here again, continuity is an important tool in the prediction of the movement of the major frontal systems. Experience has shown that development and movement of these major baroclinic zones are often quite well

indicated by numerical models in 2- and 3-day forecasts, but the short-wave features such as warm front and cold front waves are often badly mistimed or missed completely.

The degree of detail appropriate to a forecast for 2-3 days ahead varies with the synoptic situation and is largely a matter for subjective judgement. Less precision is generally possible than in, say, 24-hour forecasts, but the forecaster may be confident that more detail can be given in a settled situation than in a mobile one, or when a marked change of type is likely. Some elements can be dealt with more successfully than others. For example, the general level of temperature, which is fairly closely related to the thickness, can be forecast with confidence on many occasions, whereas forecasts of fog or frost which often depend critically on the pressure gradient, present more difficult problems.

Examples of 2-day forecasts for 1200 on 21/1/81 (T+48h from 1200 on 19/1/81) produced by the Operational ECMWF and Met Office (Octagon) models are shown in Figs 4a and 4b . The forecast surface pressure (or 1000 mb height) fields are depicted here together with the 850 mb isotherms at intervals of 3°C (pecked lines). The actual positions (at 1200 on 21/1/81) of the major fronts, depressions and anticyclones over NW Europe and the N Atlantic are superimposed for comparison. The objective surface analysis on which the Octagon forecast was based is shown at Fig 3 . (subjectively analysed frontal positions are superimposed). Note that the general evolution of the flow, including the movement of the main baroclinic regions, has been quite well handled by both models, although the eastward movement of the warm front over the UK is a little slow in the Octagon version. This remark also applies to the strong baroclinic zone in the region of Hudson's Bay . (as evidenced by the thermal gradient at 850mb).

4.2 4- to 7-day forecasts

The 3-day forecast is necessarily the starting point for these extended period predictions out to 7 days ahead (D+7). Experience with numerical model forecasts has shown that it is usually during the period from D+4 to D+6 that the objective prediction, particularly the detail thereof, diverges most rapidly from reality. There are occasions however when the evolution of the major long wave features, including the major baroclinic zones and regions of cyclogenesis, is adequately indicated right out to D+6 or D+7; however, although the predicted fields and their evolution may appear entirely realistic with both long and short-wave features depicted, it is unreasonable on present evidence to place any firm reliance on the precise development and timing of the shorter wave features in the objective products for D+4 and beyond. Weather forecasts for this period should be couched in general terms, with the accent on the weather type to be expected.

Examples of the 6-day forecasts for 1200 on 25/1/81 (T+144h from 1200 on 19/1/81) produced by the ECMWF and Octagon models are shown in Figs 5a and 5b. Again, the actual positions (at

1200 on 25/1/81) of the major fronts are superimposed. It can be seen that the forecast for the N.Atlantic/N.W.Europe region is very good for both models, particularly the ECMWF model. The main long wave features of the circulation here changed only slowly through the forecast period, and this undoubtedly contributed towards the atypically good 144-hour forecasts.

5. Assessment of objective medium-range forecasts

Starting in September 1979, Met O 11 have made once-weekly detailed assessments of the guidance value of the ECMWF medium range product and that of the Meteorological Office's operational 10-level (Octagon) model. These assessments are carried out for two areas, one covering eastern USA, N Atlantic and Europe (a sector north of 30°N, from 90°W to 40°E) and the other, a small subset of the first, covering the UK and Republic of Ireland (49°-61°N, 13°W-4°E). For both the 500 mb and surface forecasts (D+1 to D+7) the overall guidance value of the numerical model fields was assessed. The three guidance value categories used were:-

A - Good guidance
B - Did not lead to any major error
C - Misleading in some important respect

The assessment attempts to take account of the various constituent elements of the weather, as inferred from the predicted pressure distribution; qualitative impressions of temperature, wind (speed and direction), general weather type (including likelihood of precipitation) can all be inferred. In addition the sequence of events indicated by the forecast is taken into account.

Figure 6 shows the percentages of A and C classifications for the two models, for the first year (52 cases) of this assessment project. Fig 7 shows the percentage of occasions when A or B marks were retained up to and including day N (N=1 to 6)

The latter of these two figures reveals that, considering only surface forecasts for the whole area, the ECMWF model's forecast sequence provided reasonable guidance (no C marks) up to and including days 3, 4, 5 and 6 on 90%, 71%, 40% and 25% of occasions respectively; the corresponding figures for the Octagon were 81%, 50%, 40% and 33%. At the surface for the UK area, the corresponding figures were 81%, 62%, 35% and 25% for the ECMWF model compared with 77%, 58%, 46% and 43% for the Octagon.

For further details, including some comments on the contrasting characteristic behaviour of the two models, the reader is referred to Dutton and Hall (1980).

References and further reading

RIDDAWAY R W	1979	The effect on the rainfall of various topography schemes that can be used in the 10-level model. Met O 11 Tech Note No.134 (unpublished)
DOUGLAS C K M	1957	Local weather forecasting. Weather, 12, pp269-274
SANSOM H W	1951	A study of cold fronts over the British Isles. Q J R Met Soc, 77, pp96-120.
SAWYER J S	1954	Some characteristics of fronts and their relation to frontogenesis. Met Res Paper No 896
PALMEN E NEWTON C W	1969	Atmospheric circulation systems. Int Geophys Series, 13, New York Academic Press
BROWNING K A HARROLD T W	1969	Air motion and precipitation growth in a wave depression. Q J R Met Soc, 95, pp288-309
BROWNING K A PARDOE C W HILL F F	1975	The nature of orographic rain at wintertime cold fronts. Q J R Met Soc, 101, pp333-352
Met. Office	1975	Handbook of Weather Forecasting. Chapters 5,13 & 14
DUTTON M J O HALL B A	1980	Subjective assessments of medium-range forecasts produced by ECMWF and Meteorological Office Operational Numerical Models. Met O 11 Tech Note No.146 (unpublished)
BROWNING K A HARDMAN M E HARROLD T W PARDOE C W	1973	The structure of rainbands within a mid-latitude depression. Q J R Met Soc, 99, pp215-231
HARROLD T W	1973	Mechanisms influencing the distribution of precipitation within baroclinic disturbances. Q J R Met Soc, 99, pp232-251
BROWNING K A HILL F F PARDOE C W	1974	The structure and mechanism of precipitation and the effect of orography in a winter-time warm sector. Q J R Met Soc, 100, pp309-330
WICKHAM P G	1978	Rainfall forecasts from the 10-level model. Met O 11 Tech Note No.104
KIRK T H	1974	The use of numerical forecasts. Met Mag, 103, pp14-20

TABLE I. Some characteristic surface features of ana-cold and kata-cold fronts (after Sansom (1951))

Surface features	*Ana-cold front*	*Kata-cold front*
Temperature	Often a large fall which may be sudden - mean temperature drop 3 degrees.	Changes may be very slight and gradual - mean temperature drop < 1 degree.
Relative humidity	High and changes slight.	Decreases and the fall may be of considerable magnitude and quite sharp.
Precipitation	Generally fairly heavy rain at the frontal passage with steady lighter rain for some time (perhaps 2-3 h) behind the front. A comparison by Sansom showed for each frontal passage an average fall of 6.5 mm.	Amounts generally very slight and frequently nil. The precipitation amounted to only 0.8 mm on average and fell immediately before or during the frontal passage. There was very little post-frontal rain.
Wind	Usually a sharp veer accompanied by a sharp decrease in wind speed.	Wind veer may be very gradual and speed changes usually slight.
Pressure field (frequency of occurrence of sharp, average or weak pressure troughs).	Sharp 7 Average 2 Weak 6	2 8 13

TABLE 2. Some characteristic upper features of ana-cold and kata-cold fronts (after Sansom (1951))

Upper features	*Ana-cold front*	*Kata-cold front*
Radio-sonde sounding started in cold air and passing through the frontal layer	No sharp temperature discontinuity. Relative humidities high at all levels. Ascent of warm air led to the high humidities, often saturated conditions, above the front.	A fairly sharp inversion of temperature or isothermal layer with very low humidities at higher levels. The inversion was primarily due to subsidence which was usually occurring in both the warm and cold air masses and the base of the inversion was normally in the cold air.
Wind sounding started in cold air and passing through the frontal layer	The component of wind normal to the front decreased slightly while the component parallel to the front increased rapidly with height. The total backing of the wind from 950 to 400 mb was about 65°. At 500 mb the mean wind direction was inclined at only 16° to the tangent to the front. The mean thermal wind between 950 and 400 mb was almost parallel to the front (actually backed by some 3½°) and corresponded to a thermal gradient of 0.7 degree per 50 km.	The components of wind parallel and normal to the front both increased with height. The total backing of the wind from 950 to 400 mb was only 20°. At 500 mb the mean wind direction was at an angle of 42° to the tangent to the front. The mean thermal wind was inclined some 30° (i.e. veered) across the front and corresponded to a temperature gradient of 0.5 degree per 50 km. (This cross-front thermal wind is an essential condition for an active kata-front and can be readily recognized.)
Relation between the component of wind normal to the front and the speed of the front	The mean speed of the front exceeded at all heights the mean component of wind normal to the front, though the difference was insignificant below 800 mb. Higher up the difference was definite which implied that both warm and cold air masses were ascending.	The mean component of the wind normal to the front exceeded the speed of the front at all levels above the lowest layers, implying that both air masses were generally descending.
Angle between the tangent to the cold front and the mean wind direction in the warm sector some 80 to 240 km ahead of the front	At 700 mb 18° At 500 mb 17°	35° 35°
Average upper wind veer at passage of front	At 700 mb 23° At 500 mb 15°	15° 5°

Fig. 1a. Surface pressure and precipitation forecasts (fine-mesh Rectangle) T+12, 24, 36h from data time 00Z 15/1/81.

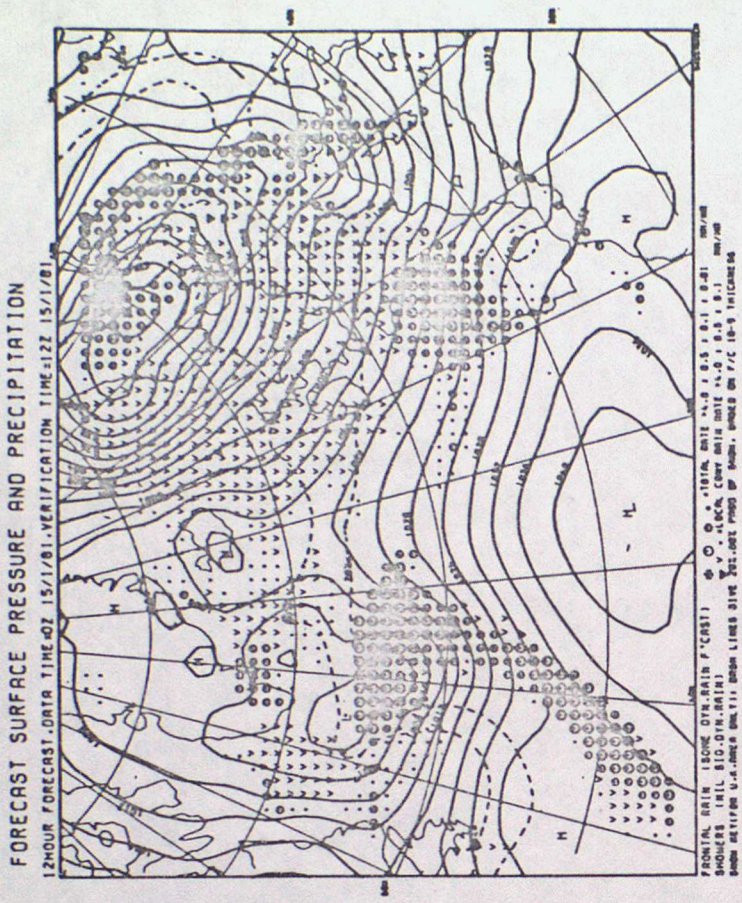

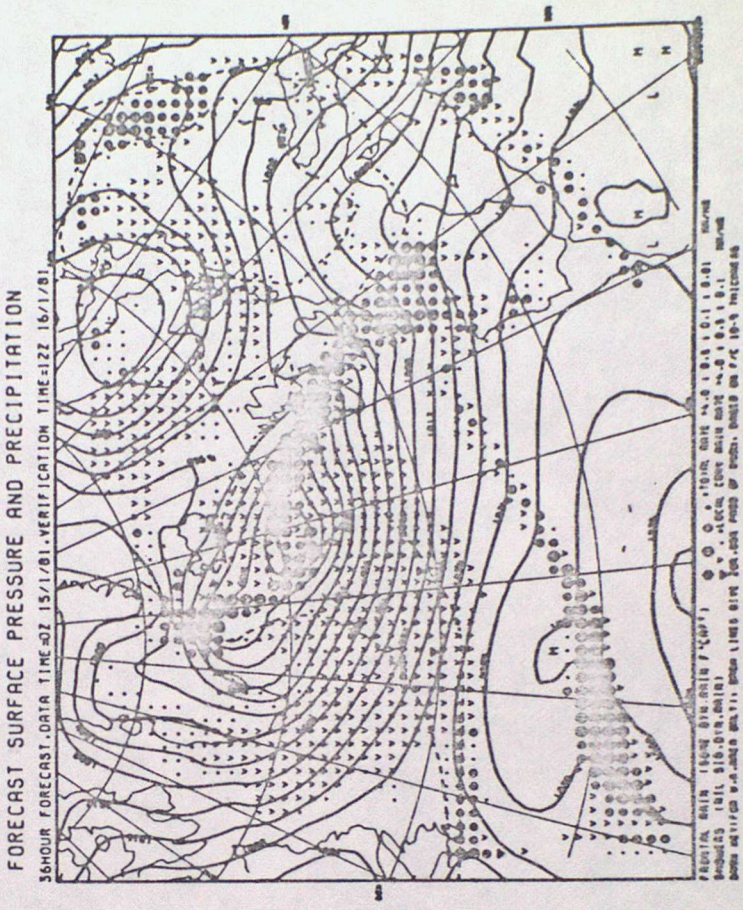

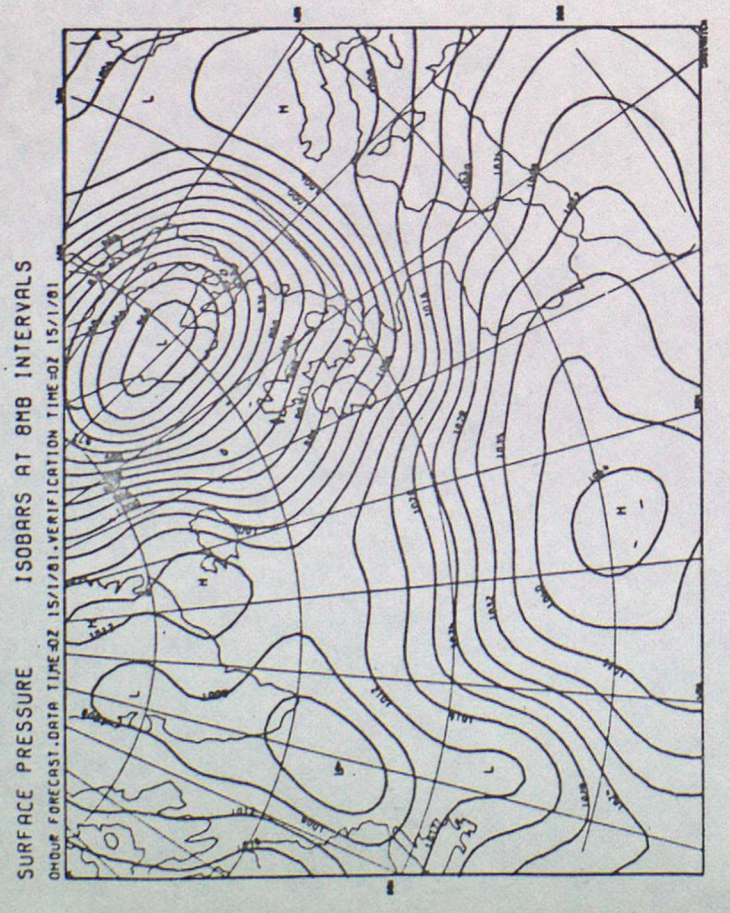

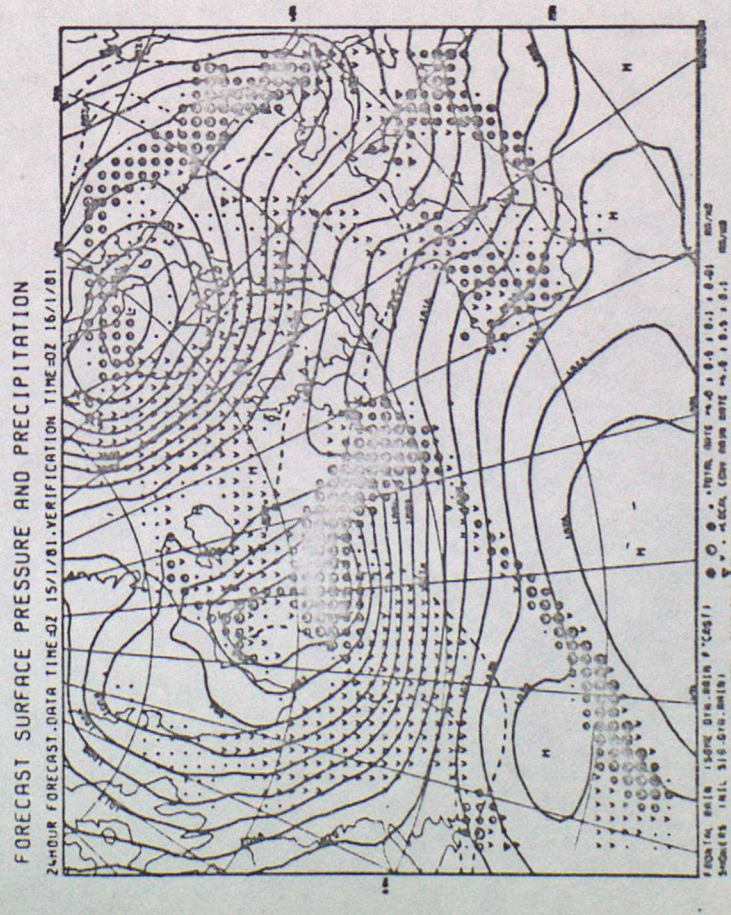

T+0 1200Z 16/1/81

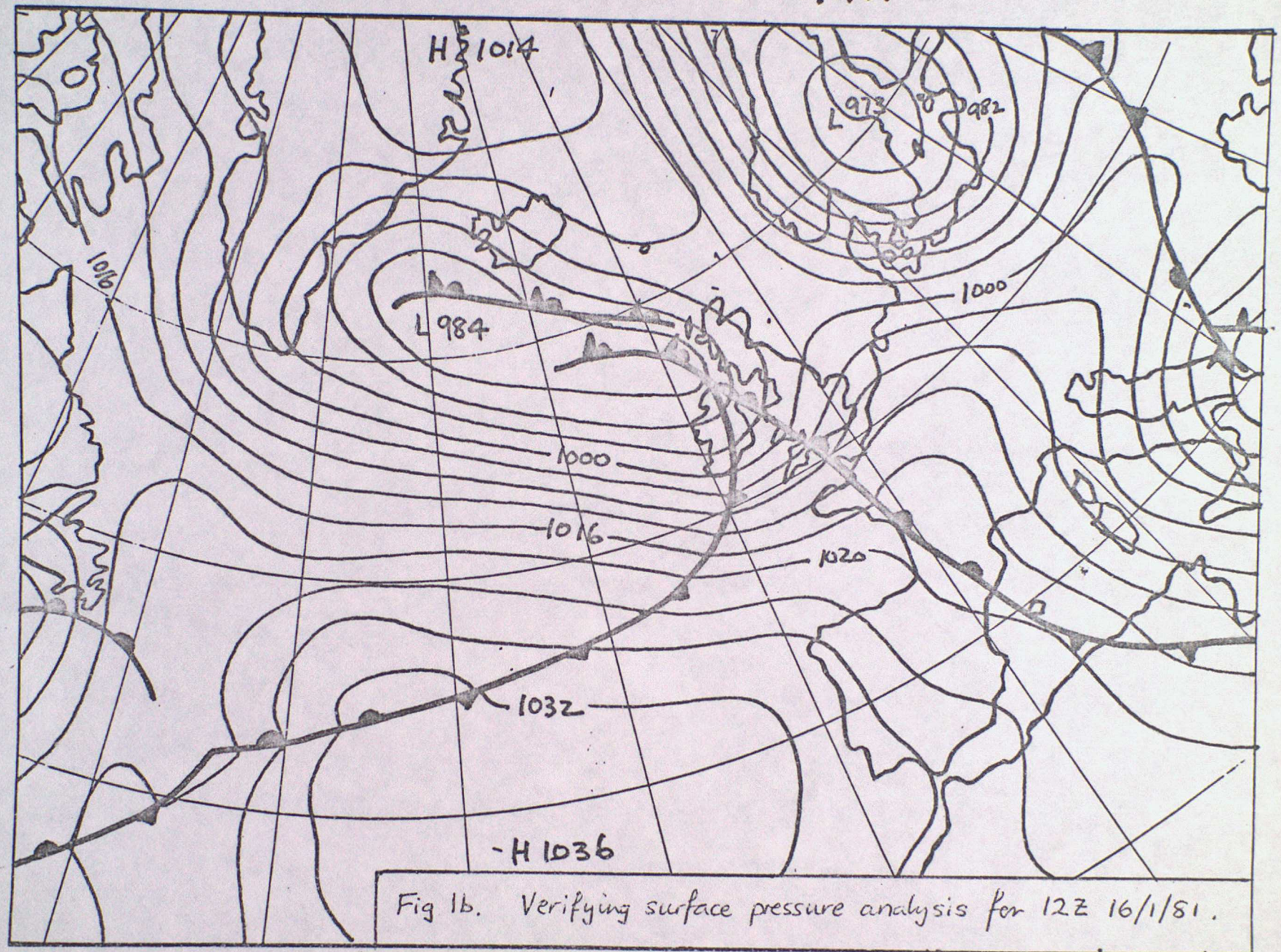

Fig 1b. Verifying surface pressure analysis for 12Z 16/1/81.

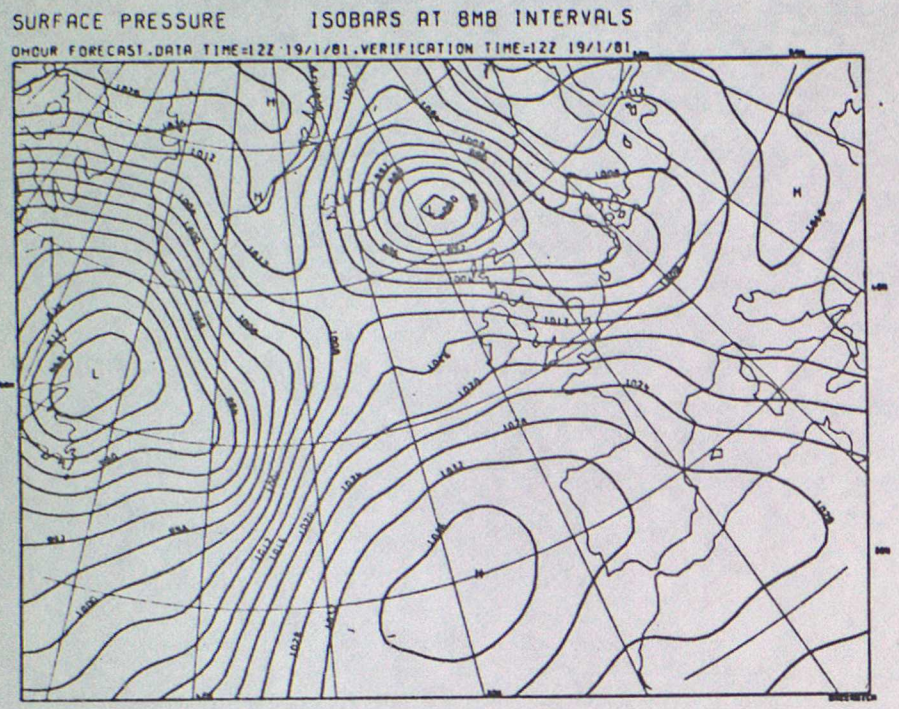

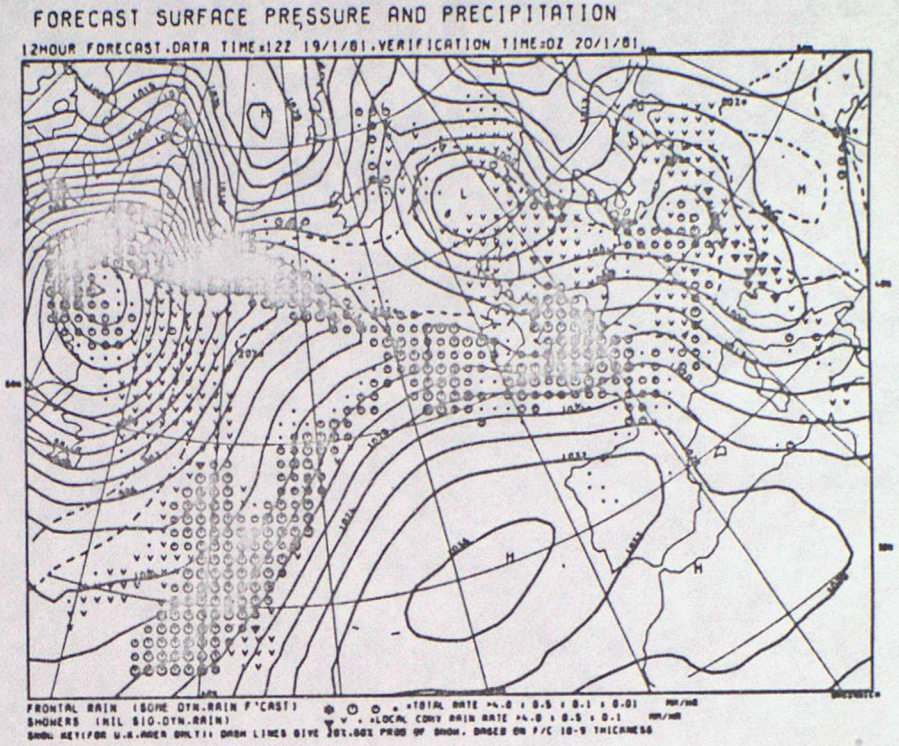

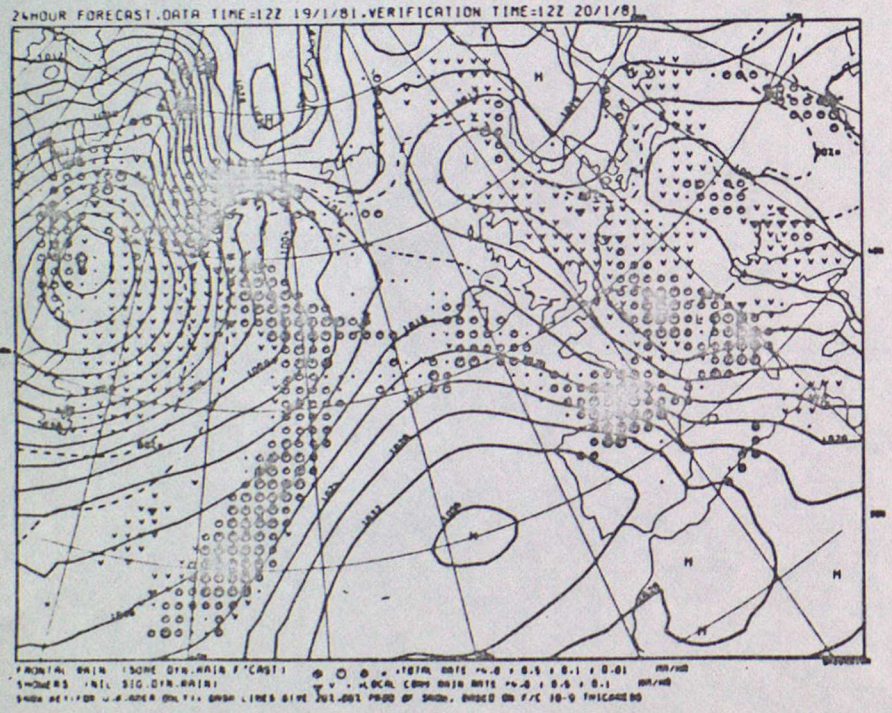

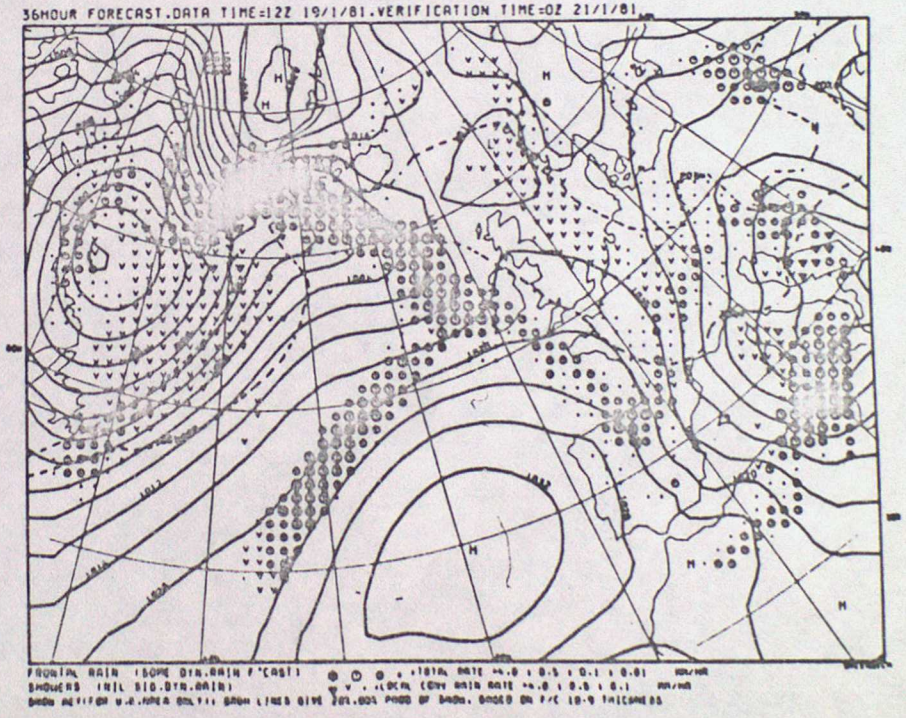

Fig 2a. Surface pressure and precipitation forecasts (fine-mesh Rectangle) T+12, 24, 36h from data time 12Z 19/1/81.

T+0 1200 Z 20/1/81

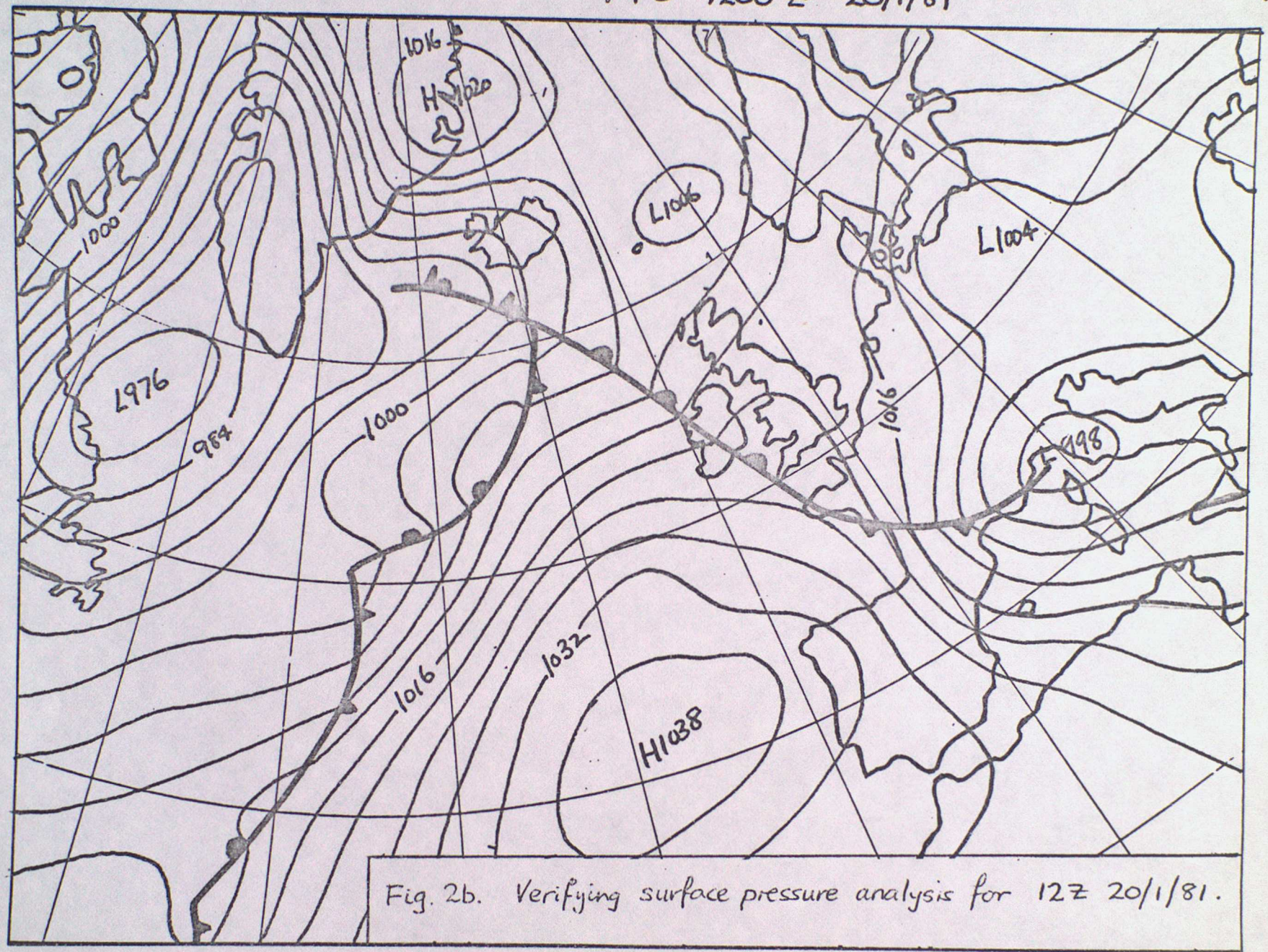

Fig. 2b. Verifying surface pressure analysis for 12Z 20/1/81.

SURFACE PRESSURE (FULL CONTOURS)
VT 12Z 19/01/81 T+0 850 MB CENTIGRADE TEMP. (3C INT)

Fig 3. Objective surface pressure analysis for 12Z 19/1/81
(subjectively analysed fronts superimposed)

CHART 15
CFO

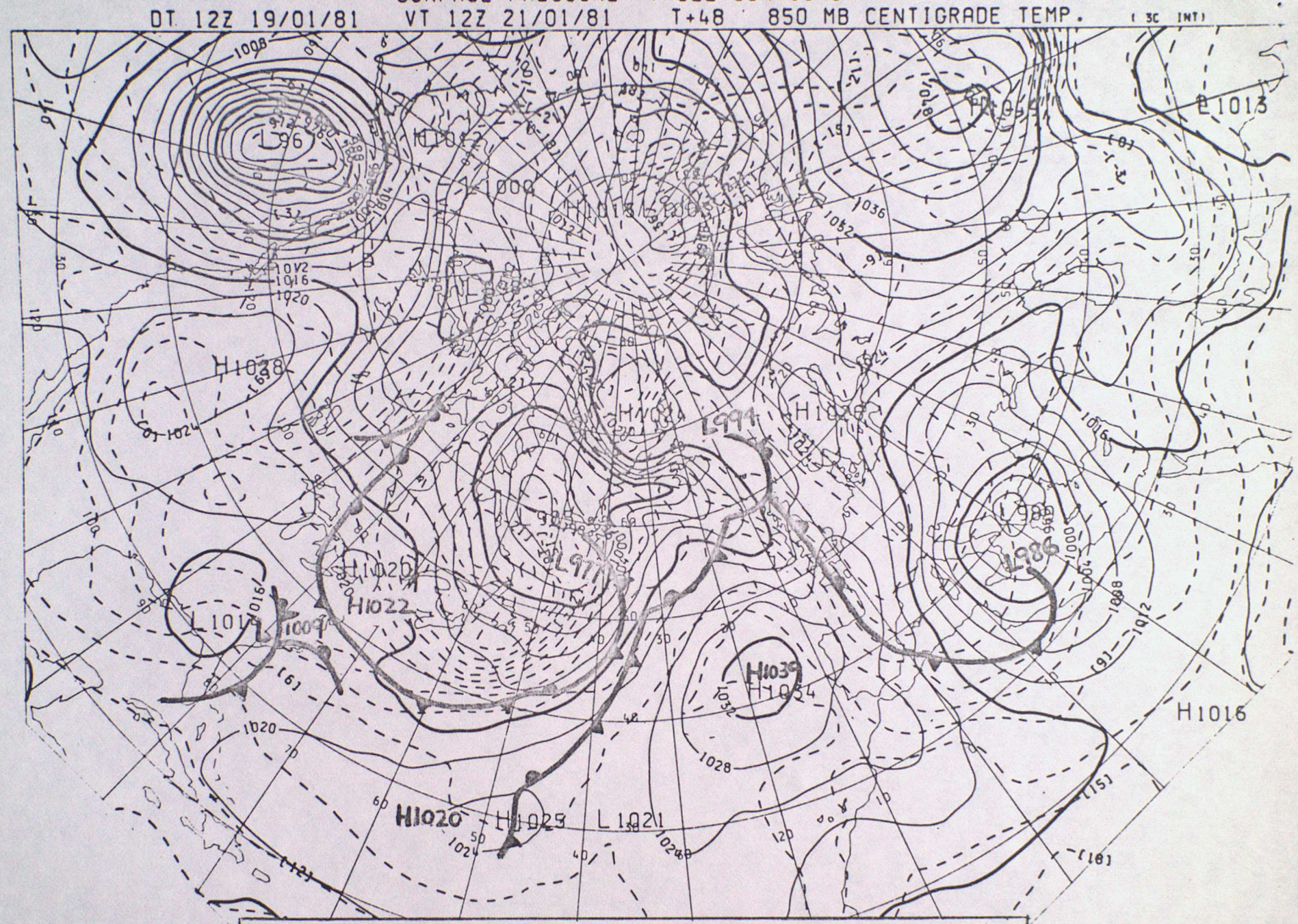

Fig 4a OCTAGON T+48h forecast surface pressure and 850mb isotherms for 12Z 21/1/81.
(verifying frontal analysis superimposed)

CHART 15
CFO

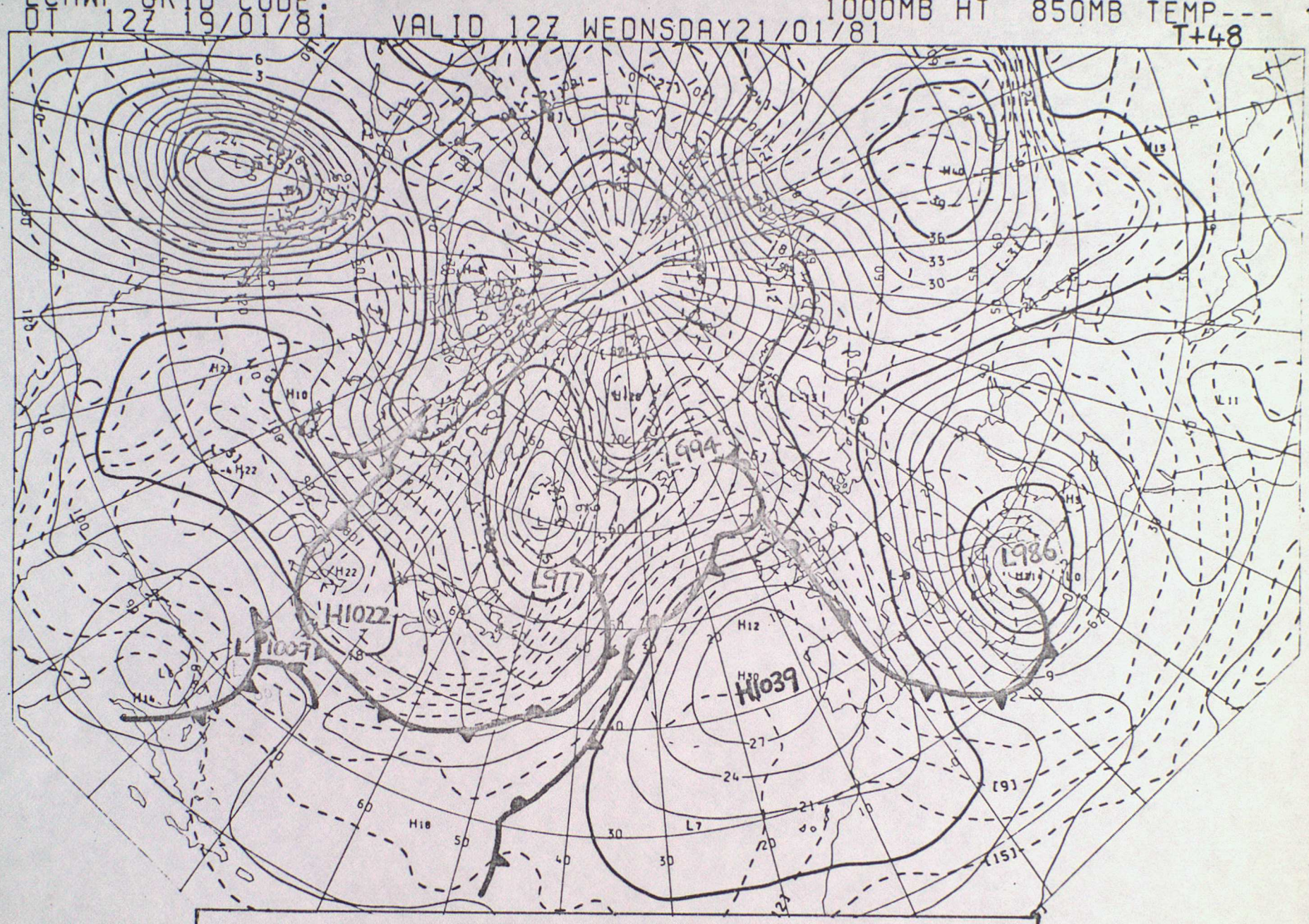

Fig 4b. ECMWF T+48h forecast 1000 mb height and 850 mb isotherms for 12Z 21/1/81.
(verifying frontal analysis superimposed)

CHART 15
CFO

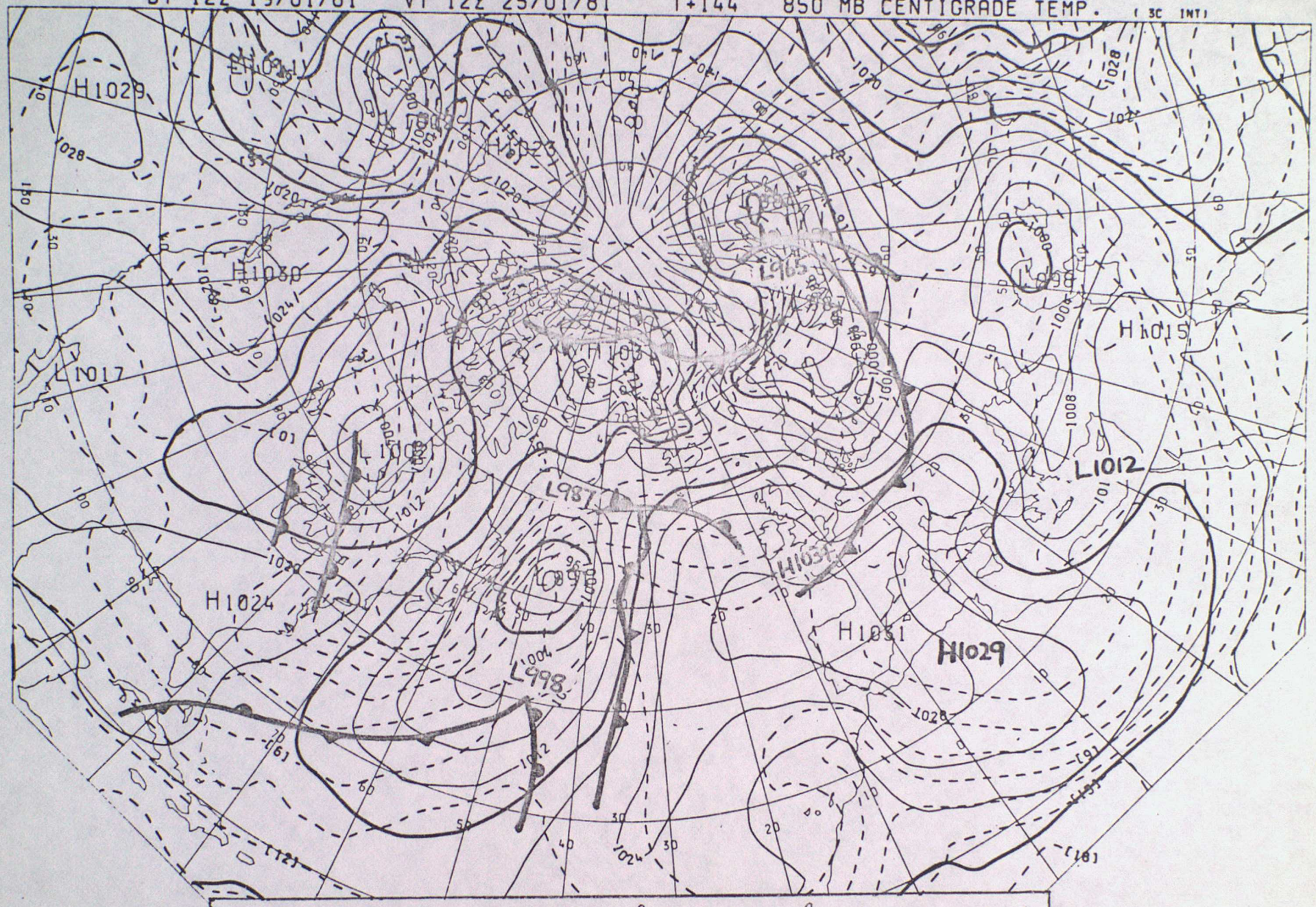

Fig 5a. OCTAGON T+144h forecast surface pressure and 850 mb isotherms for 12Z 25/1/81. (verifying frontal analysis superimposed)

CHART 15
CFO

Fig 5b ECMWF T+144h forecast 1000 mb height and 850 mb isotherms for 12Z 25/1/81 (verifying frontal analysis superimposed)

CHART 15
CFO

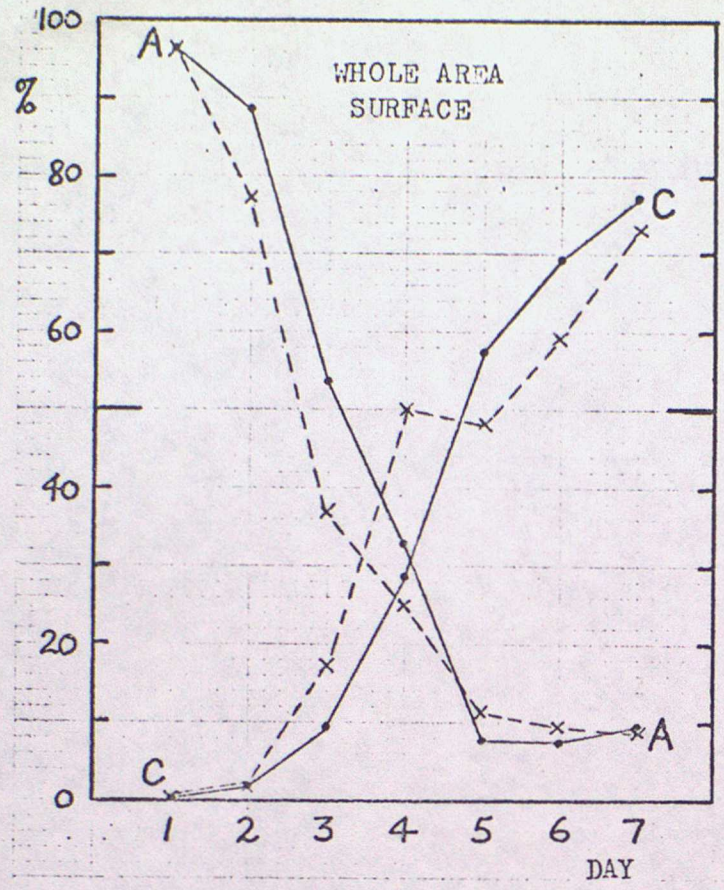

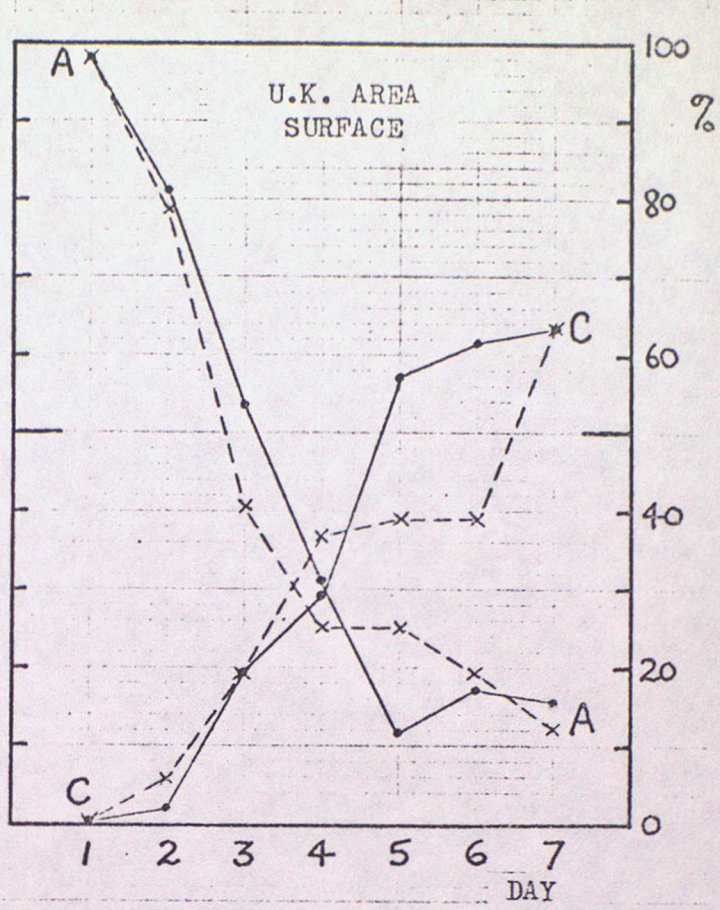

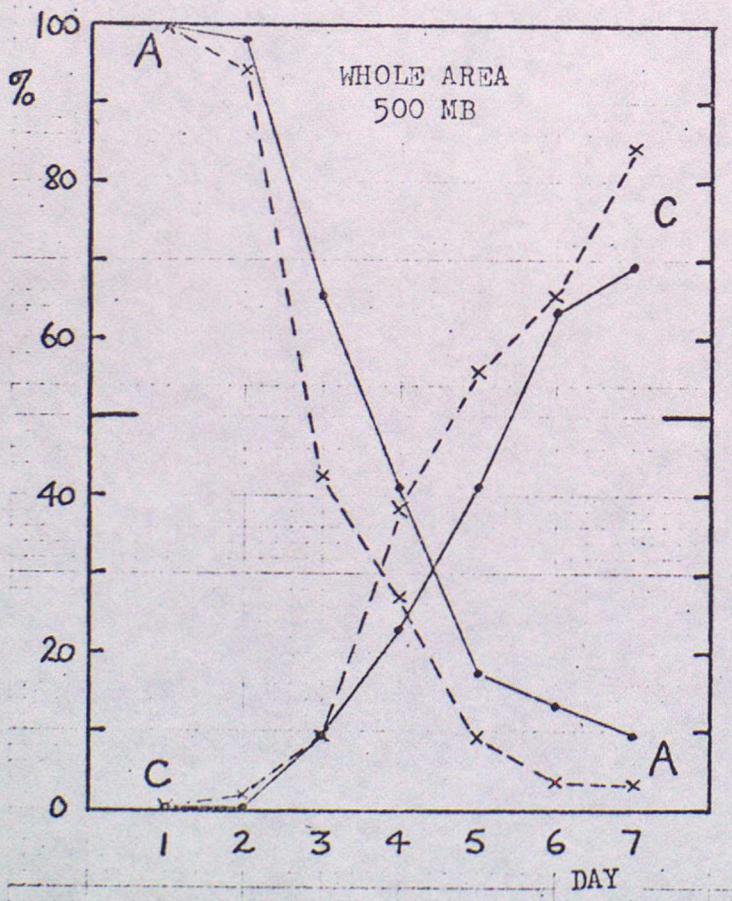

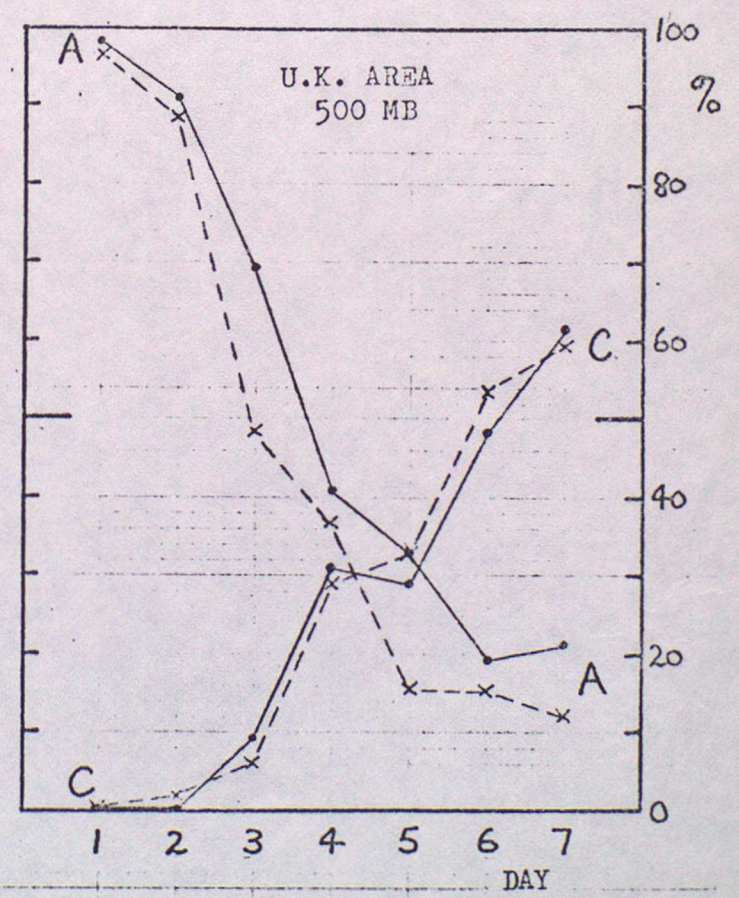

Fig. 6. Percentage of A and C classifications. 3/9/79 to 25/8/80 (whole year).

——•—— ECMWF model

×- - - -× Met O model (32 cases at day 7)

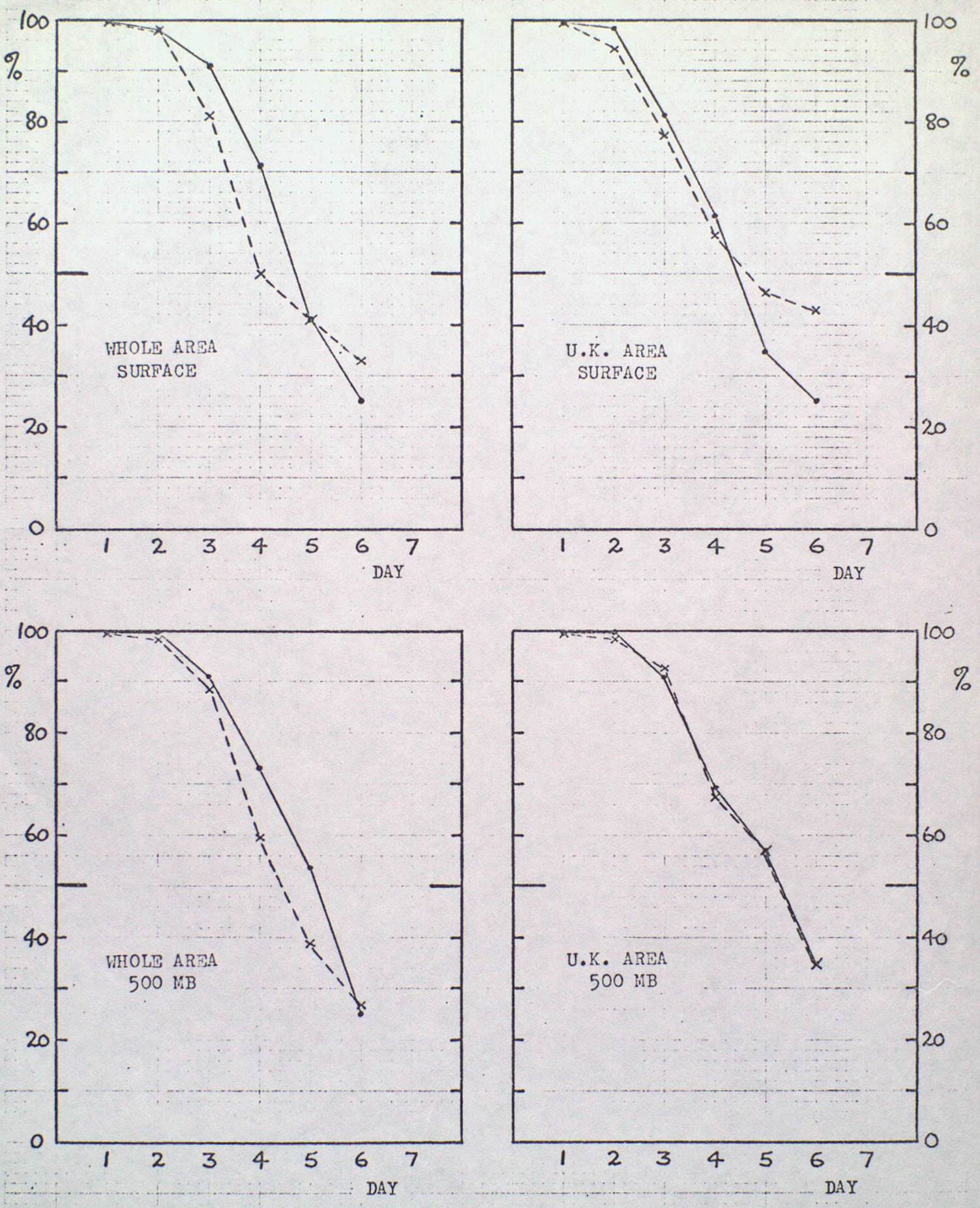

Fig. 7. Percentage of occasions when A/B marks were retained up to and including day N, for the period 3/9/79 to 25/8/80 (whole year).

●——● ECMWF model
×- - -× Met O model

KW

FRONTS IN THE ATMOSPHERE

Lecture Nine - Practical forecasting of frontal phenomena - very short period forecasts

Summary of Lecture by Dr K M Carpenter

1. Two projects were discussed:-

   (a) the use of a fine resolution (10 km) numerical model for local weather forecasting

   (b) the use of radar to provide detailed and extensive observations of surface rainfall.

Numerical models can be used to predict tomorrow's weather using synoptic scale forecasts to force the model through the boundary conditions, or they can be used to make short term forecasts on the basis of detailed initial conditions. (In practice, both are done together). It will take about 3 hours to collect observations, analyse them, calculate initial conditions, make the forecast and disseminate it.

Rainfall analyses based on radar observations can be extrapolated for several hours - usually about 6 hours. It will be possible to collect the radar observations, make analyses of surface rainfall, calculate and deliver a 6-hour rainfall forecast in under 30 mins.

2. Example of a mesoscale model forecast

Tapp, M.C and White, P.W. (1976), Q.J.Roy.Met.Soc. 102, p 277-296
"A non-hydrostatic mesoscale model"

K. M. Carpenter (1979), Q.J.Roy.Met.Soc. 105, p 629-655
"An experimental forecast using a non-hydrostatic mesoscale model"

14 June 1973. An anticyclone moved slowly across the south of England. The mesoscale model forecast started at 04Z using initial conditions derived from a synoptic scale model forecast. Boundary conditions were also taken from the synoptic scale forecast, and were changed during the forecast in line with the synoptic scale evolution. The mesoscale model succesfully forecast the formation and movement of the sea breezes even though it could not resolve

the frontal structure. The mesoscale model used was non-hydrostatic, using the fully compressible primitive equations and height above ground level as the vertical coordinate. (10 levels up to a height of 4 km). The horizontal gridlength was 10 km (over a 61 x 61 grid); the computing time amounted to about 12 mins/hour on the IBM 360/195.

3. Radar network

C.G.Collier (1980) Met. Mag. 109, p 161-177

4 radars are in continuous use:

Hameldon Hill (North-west): completely automatic at a remote site. C-band radar ie wavelength of EM radiation is 5.6 cm and angle of beam is 1°

Clee Hill (West Midlands): C-band radar

Camborne: S-band radar.. 10 cm wavelength and 2° beam

Upavon: S-band radar

Each radar completes one revolution in about 1 minute.

4 elevations are used, typically 0.5°, 1.5°, 2.5° and 4.5°

A complete cycle takes 5 min (exactly)

Data is used every 15 min at present.

At 250 km range, a 1° beam centred at 0.5° observes rain in a layer from 5 km altitude to 9.5 km.

Surface rainfall is inferred from the intensity of the reflected radar beam using

$$Z \propto R^{1.6}$$

Z = intensity of echo

R = surface rainfall rate.

(Nicholass C A and Larke P R (1976) - Met Mag, 105, pp 361 - 381)

A composite analysis of surface rainfall is produced every 15 min on a grid covering most of England and Wales with a resolution of 5 km.

3.1 Objective extrapolation of rainfall

Browning et al (1981) "On the forecasting of frontal rain using a weather radar network" (submitted to Q.J.R Met. Soc).

The full procedure can be described in a number of steps, summarised as follows:-

1. Reduce the data from 128 x 128 5 km grid to 32 x 32 20 km grid.
2. Organise areas of rainfall into a small number of individual clusters.
3. Calculate centroid positions of clusters (without regard to echo intensity).
4. Repeat the process (steps 1-3) for a second analysed rainfall field 15 min earlier.
5. Calculate velocities of individual clusters from the displacement of the centroids over the 15 min period.
6. Extrapolate the movement of the observed clusters (retaining intensity information) using the calculated velocities of the clusters.

3.2 Pathology (radar rainfall)

(a) Bright band The echo from melting snow is more intense than that from either snow or rain. This leads to an anomolously intense signal from the range at which the radar beam intersects the $0^{o}C$ isotherm.

(b) Clutter Echoes from objects other than rain, usually the land or sea surface. This is usually evident at known positions and echoes from these points are ignored routinely. Propogation of EM waves varies slightly so the clutter can be variable and sometimes appears on the rainfall analysis (either stationary or moving erratically).

(c) Anoprop Severe clutter due to the anomolous propogation of radar waves. It occurs commonly in conditions of strong hydrolapse and temperature inversion close to the surface (eg in fog).

(d) Low-level evaporation Some or all of the precipitation measured by the elevated beam may be evaporated in dry air below the level of the beam, leading to overestimates of the surface rainfall.

(e) Low-level intensification If the precipitation is enhanced at low-levels by, for example, orography, the inferred surface rainfall will be underestimated.

(f) Break in coverage, incompatible radar calibration Systematic errors in one radar can cause the inferred rainfall to be quantitatively wrong, or more seriously, it can cause a discontinuity between radars. Where the rain is shallow, or where there is a gap in the radar coverage, misleading gaps will appear in the full rainfall analysis.

(g) Interference Radars can interfere with each other and produce radial lines of spurious echo. (These cannot be mistaken for real precipitation).